Precipitation behavior of different micro-alloyed 0.2 wt% C steels

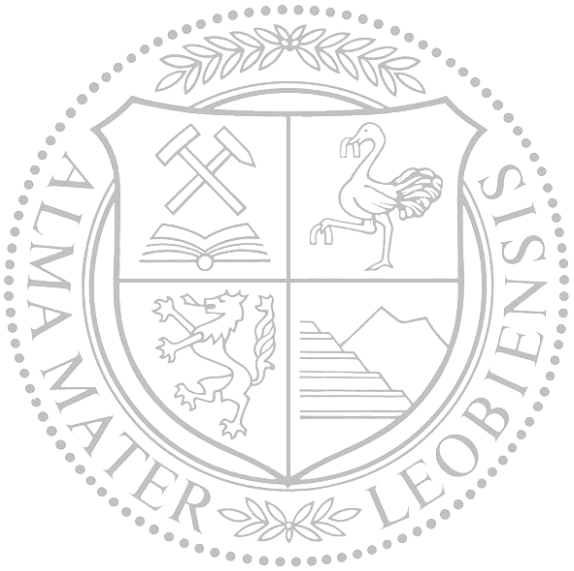

Doctoral thesis

Dipl.-Ing. Matthias Nöhrer

Accomplished at the Department of Physical Metallurgy and Material Testing of the University of Leoben.

Leoben, March 2013

Affidavit

I declare in lieu of oath, that I wrote this thesis and performed the associated research myself, using only literature cited in this volume.

Leoben, April 2013 Matthias Nöhrer

Acknowledgment

Numerous people helped on this doctoral thesis in more than 3 years of work. They are thankfully acknowledged in the following.

I would like to thank Univ.-Prof. Dr. Helmut Clemens for giving me the chance to conduct this thesis at the Department of Physical Metallurgy and Materials Testing.

Most of all, I want to thank my supervisor, Dr. Harald Leitner, who gave me the possibility to realize my scientific ambitions. I am thankful for his cooperative supervision and extensive willingness to support this work, which made my time at work pleasant.

I am thankful for the support of the company voestalpine Stahl Donawitz GmbH, which initiated the idea to this work. Especially, my gratitude goes to Dipl.-Ing. Sabine Zamberger for the fruitful and interesting discussions, which gave me impulses for my research.

To accomplish this thesis and to expand my point of view I want to thank Univ.-Prof. Dr. Ernst Kozeschnik and Dipl.-Ing. Walter Mayer for their simulation calculations and they supported my ambitions to publicize.

I am thankful for the diploma theses of Dipl.-Ing. Dominik Moisi, whose supervision was an interesting and pleasant task and extended my scientific view. All the student co-workers, who supported my experimental work, are acknowledged for their help. Furthermore, I want to thank the staff of the Department of Physical Metallurgy and Materials Testing, who always supported me in a friendly way.

For the great time at the Department, I want to thank my colleagues, especially, the steel group and also the non-scientific staff and the people from the Thin film- and TiAl-group, who provided a friendly, helpful and cheerful environment. A special thanks to Lerchi, Manschi and Stoffal. I am grateful for their friendship and for their support at all situations. I will never forget our incredible trips and the endless hours at the “Admiral”.

Thank you to my parents, my sister and my brother and my whole family as well as my friends for supporting me and providing a relaxing atmosphere.

Contents

1. Introduction

Nowadays the environmental conservation is of great importance for our society. The ambition to protect the environment influences the economic status which should be avoided. Thereby, big challenges arise on the different technologies and consequently on the used materials. In the automotive industry the demand is to create cars with lower fuel consumption. One point to reach this effort is to produce lighter cars, but without degrading the safety. Material-saving is also considered in the pipeline industry to reduce the costs. To work more economically the pressures in such pipes should be increased without amplify the wall thickness and to keep the material and welding costs low. Because of these requirements, materials should be designed with higher strengths connected with good technological performances, for example weldability and formability. Low carbon and alloyed steels are commonly used in such branches since they provide the requested properties and low costs.

A typical way to improve the strength of steels is to increase the carbon content. These results in a decrease in toughness and the technological properties are influenced negatively. In order to increase the mechanical properties without influencing the technological characteristics, micro-alloying elements like Nb, V and Ti are added in small amounts of lower than 0.1 wt%. The effects on the mechanical properties of these elements are indirectly by grain refinement and directly by precipitation strengthening. In the following chapters the different mechanism, which leads to the properties improvement, are explained.

The improvement of common steels with micro-alloying elements has been established since 1930. For the manufactures the effects of the micro-alloying elements were discovered in the 1950's. The first elements which were known to improve the properties of steel in small amounts were V and Ti. Cone [1] described the properties of a 0.18 wt% carbon steel alloyed with 0.08–0.10 wt% V in 1934. In the early years, the strength increase of V alloyed steel was mainly adjudged to the formation of carbides and nitrides, and not to the grain refining ability which was also known [2,3]. At this time investigations of C-Mn forging steels alloyed with 0.1 wt% Ti showed grain refining effects [4], but Ti was less widely used. The first patents which correlate to the effect of Nb in steel, were issued to Becket and Franks in 1939/1941[5–8]. They found that the strength of C-Mn steels alloyed with 0.02–1 wt% Nb increases by grain refinement. Although V and Ti were firstly established as micro-alloying elements, by

the announcement of the production of Nb micro-alloyed steel by the Great Lakes Steel Corporation in 1958 the successful story of micro-alloyed steels started. In the 1960's controlled rolling was developed for commercial production to optimize the effects of the micro-alloying elements and for economical steel production. One of the main application areas for this material was the pipeline market. The new micro-alloyed steel with the material appellation X 60 (420 MPa yield strength) replaced the X 52 (360 MPa yield strength). Basically, the X designated steels have a low C content and a Mn content of less than 2 wt% [9]. With this new steel the material and the welding costs could be reduced due to weight reduction. Increased requirements on pipelines and on automotive applications resulted in the development of steels with a higher strength. In the 1980's the X 70 were developed, which reached a yield strength of 490 MPa by modifying the processing side [10]. The first micro-alloyed steels had a ferritic-perlitic microstructure, which was adjusted by air cooling. To increase the strength, modifications in the microstructure were required which could be achieved by faster cooling rates due to water cooling after hot rolling. This was done by interrupted accelerated cooling (IAC) or interrupted direct quenching (IDQ) [9]. By optimizing the alloys and the thermo-mechanical control process (TMCP) it was possible to design steels with revised mechanical properties. Modern micro-alloyed steels, which are used in pipeline applications and in the automotive industry, reach strength of 690 MPa (X 100). Such steels are produced by controlled thermo-mechanical treatments where a bainitic structure is adjusted. Figure 1 shows the evolution of pipeline steels [11], from ferrite-perlite steels in the early years to thermo-mechanical produced bainite steels with improved properties.

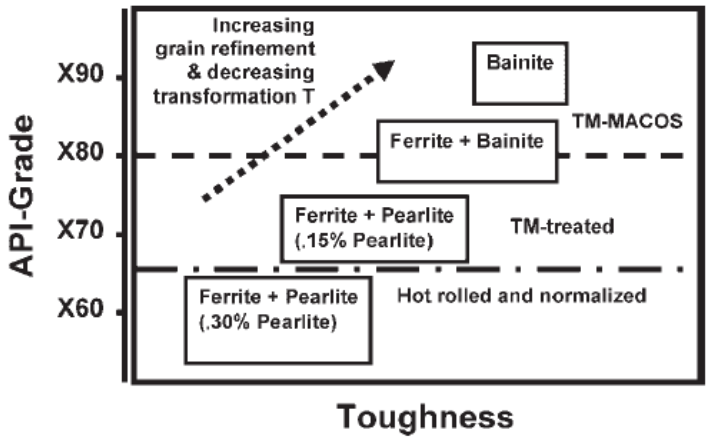

Figure 1: Development of plate steel for pipeline applications: microstructure and mechanical properties (API – American Petroleum Institute; MACOS – accelerated cooling with Mannesmann Cooling System; TM – thermo mechanical) [11].

The historical evolution of micro-alloyed steels shows that they have been investigated for more than 80 years. But the increasing requirements on steels in pipeline and automotive industries demand a deeper understanding of the microstructural evolution during thermo-mechanical processes. Also to predict the microstructure and the properties of such steels, by means of thermodynamic and thermo-kinetic calculations, it is important to understand the microstructural influences and changes. New characterization methods have been developed, which can help to answer open questions and support the simulation. Thus, the aim of the present doctoral thesis is to improve the understanding of the precipitation behavior of micro-alloying elements in C steels. These precipitates have a size of a few nm and therefore the main characterization techniques were transmission electron microscopy (TEM) and atom probe tomography (APT). Details of TEM and APT can be found elsewhere [12–14].

In the following chapters the influence of micro-alloying elements on the microstructure of thermo-mechanical produced steels should be explained and for which type of steels it is meaningful to use these elements. Chapter 2 deals with the different types of micro-alloyed steels. Chapter 3 is divided into five subchapters. In section 3.1 the effects of a thermo-mechanical process on the microstructure is explained. Section 3.2 describes the solubility of micro-alloyed carbides and nitrides which is important because thereby the thermodynamic background for the formation of micro-alloy carbides and nitrides could be interpreted. This is a main part of the papers P1, P2, P3 and P4. Section 3.3 and P 1 and P 2 contain the effect of micro-alloying elements in austenite. An important part for the mechanical properties adjustment is the formation of ferrite, which is described in section 3.4 and also P3 deals with the precipitate formation during the austenite-ferrite transformation. The last section as well as P2 and P4 deal with the effects of micro-alloying elements in ferrite. The main focus of the papers is on the precipitation behavior of the micro-alloying elements. In the final chapter 4 a summary and a contribution to the field are given.

2. Types of micro-alloyed steels

Micro-alloying elements can be added in many steel applications. The used type of micro-alloying elements depends mainly on the used heat treatment and consequently on the final microstructure of the steel. The main effect of Ti is to influence the grain size by TiN precipitation in the melt or in the austenite region. Thereby, the grain size can already be controlled during the solidification [15–17]. At further heat treatments TiN precipitates hardly dissolve and an effect which corresponds to the re-precipitation of Ti precipitates is not distinct. Nb is known as the most effective micro-alloying element. It retards the austenite grain growth and the recrystallization in two ways, on one hand in solid solution by the solute drag effect [18,19] and on the other hand due to Nb precipitates [20–23]. A strengthening effect by precipitation is less distinct. In contrast, by alloying V the precipitation strengthening is more effective [24–27]. The ability of recrystallization and grain growth retardation is lower for V than for Nb alloyed steels [28,29]. This is caused by the lower precipitation behavior of V in austenite [30,31] and also the solute drag effect is less distinct [29]. From these different behaviors it can be seen that it is possible to design the properties of micro-alloyed steels in different ways. In the following section a short overview of the steels in which micro-alloying elements are added is given.

- Conventional micro-alloyed high strength low alloyed (HSLA) steels:
  This kind of steels is alloyed with maximum 0.2 wt% C to avoid a negative influence on the weldability and formability. The microstructure mainly consists of a fine ferritic-perlitic structure to gain good mechanical properties. This structure is achieved by controlling the austenite grain growth and the recrystallization by precipitates. Small austenite grains lead to a fine ferritic-perlitic microstructure because of more nucleation sites for ferrite. The formation and properties of ferrite and perlite can be found elsewhere [32–34]. Further increases of the strength are possible by secondary hardening in the ferrite phase which is mainly realized by alloying with V [24,26,27]. In modern HSLA, which are low and ultra-low carbon steels, the microstructure consists of bainite and martensite, which have remarkable properties. By specific TMCP yield strength of 850 MPa can be achieved. Details of the bainite formation are not explained here and can be found elsewhere [35].

- Quenched and tempered steels:

  As the name implies, the production of quenched and tempered steels consists of two processes, hardening and tempering. At the hardening stage a martensitic structure is formed. To improve the toughness of the material a tempering process follows the hardening. The hardening process usually takes place at 920 to 1050°C and the tempering process at 500°C. Detailed explanations of the production stages can be found elsewhere [36,37]. Typically heat-treatable steels have a carbon content of 0.2 to 0.65 wt%. In this type of steel mainly Nb and V are alloyed because during hardening the Nb and V precipitates partially or completely can dissolve and this can influence tempering [38]. During tempering by accumulation of Nb or V at dislocations the recovery of the martensite is retarded, the tempering resistance is increased and secondary hardening takes place [38,39]. Due to dislocations, the diffusion of the micro-alloying elements is facilitated and the precipitate formation is supported. Thereby, an increase of hardness can be achieved compared to similar steels without micro-alloying elements [40].

- Acicular ferrite steels:

  The acicular ferrite structure is commonly used for pipeline steels with low carbon content. Tanaka [41] reported for an 0.07C - 2.0Mn – 0.6Nb – 0.5 Mo HSLA steel that the microstructure with the best mechanical properties consists of mainly acicular ferrite, which consists of fine non-equiaxed ferrite grains dispersed with cementite and martensite/austenite islands. Acicular ferrite has a similar morphology to low carbon bainite. Both have lath-like ferrite grains with a high dislocation density.

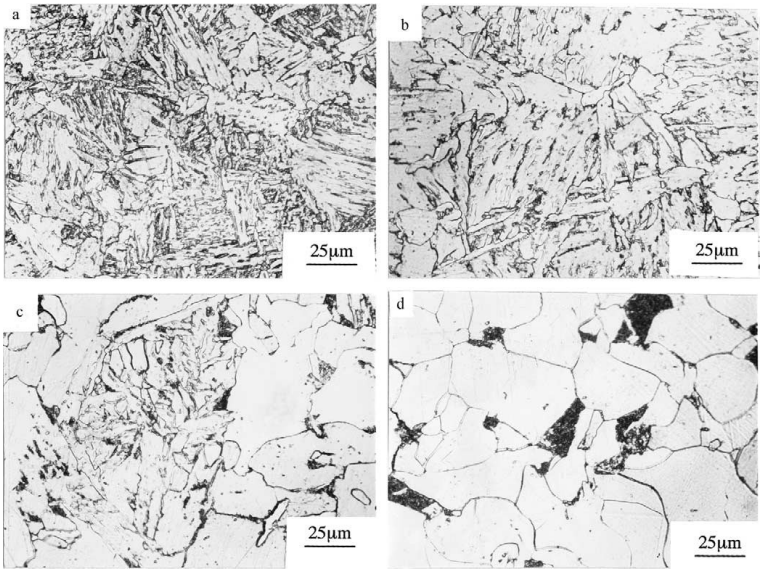

Figure 2: optical micrographs for the microstructure of a 0.045C – 1.94Mn – 0.30Si steel cooled from 950°C to room temperature with different cooling rates. a) 50°C/s, b) 10°C/s, c) 1°C/s, d) 0.1°C/s [42].

Acicular ferrite is produced by a mixture of diffusion and share mode. Growth occurs by the displacement of C and the movement of coherent and semi-coherent austenite-ferrite interfaces [43,44]. This phase is characterized by fine non-equiaxed ferrite, which are randomly distributed and have different grain sizes [42–44]. As mentioned before, the grains of this ferrite have a quite high dislocation density [44]. The transformation of this kind of phase happens in a temperature range higher than the upper bainite during hot rolling. To form acicular ferrite, the cooling rate has to be faster than for the formation of a ferritic-perlitic microstructure [45]. Figure 2 shows the influence of the cooling rate on the microstructure [42]. At fast cooling rates of 50°C/s (a) and 10°C/s (b) the microstructure consists exclusively of acicular ferrite. At a cooling rate of 1°C/s (c) acicular and polygonal ferrite is visible. In picture 2d the material was cooled with 0.1°C/s which leads to a microstructure consisting of polygonal ferrite and perlite. The good mechanical properties of acicular ferrite are related to the assembling of the microstructure. Due to the random distribution of the ferrite grains and their small size, cleavage cracks can be deflected at boundaries [44].

- Dual phase steels:

  Because of the insufficient cold formability of HSLA steels with a ferritic-perlitic structure, which is required for automotive applications, dual phase steels were invented. These steels consist of ferritic-bainitic or ferritic-martensitic microstructure. The production of this steel type is similar to the production of conventional HSLA steels. Also in this case micro-alloying elements are alloyed to control the grain size

and to form finally a fine structure. By precipitation hardening of micro-alloying elements in the ferrite phase the strength of this phase can be improved. To get a ferritic-bainitic/martensitic structure, controlled rolling is required. Two methods are used, interrupted accelerated cooling (IAC) [46–48] and interrupted direct quenching (IDQ) [49].

The alloys which are used in this Doctoral thesis are given in Table 1. Steels with such chemical composition are integrated in the type of conventional HSLA steels and mainly used for wire applications. The basis material is a 0.2 wt% C steel with 1.4 wt% Mn and 0.3 wt% Si. Cr, Ni, Mo, Al and N are added in amounts lower than 0.03 wt%. The difference between the steels is the type and the number of micro-alloying elements. One material is alloyed with 0.05 wt% Nb (Nb-alloy), one with 0.15 wt% V (V-alloy). Another variant contains 0.02 wt% Ti, 0.1 wt% V and 0.04 wt% Nb (Nb-V-Ti-alloy). The Nb- and V-alloys were industrial produced materials and the Nb-V-Ti-alloy was produced in laboratory scale. All of them were provided by the voestalpine Stahl Donawitz GmbH. These compositions were chosen because thereby the precipitation behavior of the micro-alloying elements by oneself and in combination could be examined. The influence of Nb (Nb-alloy) was investigated in ferrite and austenite because in both phases Nb leads to properties improvements [P2]. The precipitation behavior of V was investigated in the ferrite phase [P3][P4] because the influence of V is less in austenite. The precipitation of the Nb, V and Ti combination was investigated in the austenite because in this phase the most important precipitation takes place [P1].

Table 1: Chemical composition (in wt. %) of the investigated micro-alloyed steels.

	C	Si	Mn	Cr	Ni	Mo	Al	Ti	V	Nb	N
Nb-alloy	0.2	0.3	1.4	0.03	0.03	0.01	0.03	0.002	0.001	0.05	0.011
V-alloy	0.2	0.3	1.4	0.03	0.03	0.01	0.03	0.002	0.15	0.0002	0.011
Nb-V-Ti-alloy	0.2	0.3	1.4	0.03	0.03	0.01	0.03	0.02	0.1	0.04	0.011

3. Effects of micro-alloying

3.1 Basics of thermo mechanical processing

For the adjustment of the mechanical properties of steels one important part is to know how the microstructure could be influenced by the heat treatment. A well-established way to optimize the mechanical properties in an economical way is a TMCP [10,44,50,51]. Due to controlled rolling and cooling, the microstructure can be designed in any way with the main aim to achieve a homogeneous fine-grained microstructure. Depending on the different applications, the microstructure can consist of ferrite and perlite, acicular ferrite, bainite, martensite or a multi-phase structure [10,43,51–53]. Figure 3 shows schematically how the microstructure can be influenced by controlled rolling [54].

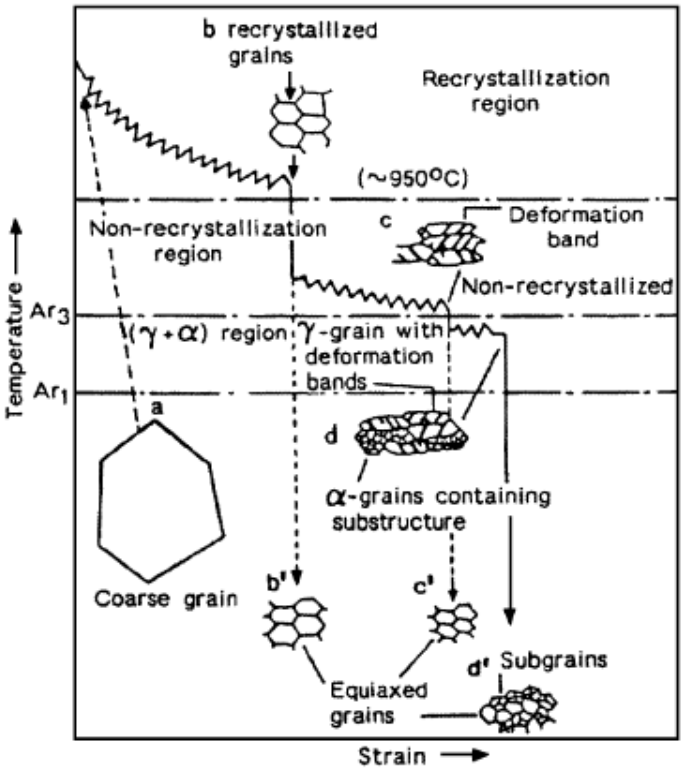

Figure 3: Schematic illustration of changes in microstructure during a virtual thermo-mechanical process [54].

The influences on the structural changes are related to deformation in three regions: Deformation in recrystallization region, in non-recrystallization region and in the gamma-alpha region (figure 3).

1. Deformation in the recrystallization region: In this region the austenite grain coarse (figure 3 marked by **a**). Due to repeated deformation and recrystallization fine recrystallized grain is formed (figure 3 marked by **b**). By this process the austenite is refined, but during cooling these grains would transform into relative coarse ferrite, as shown in figure 3 marked by **b'**.
2. Deformation in the non-recrystallization region: During deformation the fine recrystallized grains from the first region are deformed into elongated, non-recrystallized austenite grains with deformation bands inside (figure 3 marked by **c**). At these deformation bands and at the austenite grain boundaries ferrite nucleates and a fine ferrite grain develops (figure 3 marked by **c'**).
3. Deformation in the gamma-alpha region: In this region proeutectoid ferrite is formed at deformation bands and austenite grain boundaries. By deformation in the proeutectoid ferrite a dislocation substructure is created and also in the austenite grains the formation of deformation bands continuous (figure 3 marked by **d**). During cooling the non-recrystallized austenite grains changes into equiaxed ferrite and the deformed ferrite forms subgrains (figure 3 marked by **d'**).

The formation of deformation bands in austenite is one of the main features of TMCP. Ferrite can nucleate at deformation bands and austenite grain-boundaries which consequently leads to finer ferrite grains [51,55–60]. The microstructure is not only influenced by the deformation, also by the rolling reduction. The higher the rolling reduction is the finer are the resulting ferrite grains. Bakkaloglu [54] showed in his study, on a 0.1C - 1.04 Mn steel micro-alloyed with Nb and V, that with increasing deformation the final average ferrite grain size decreases parabolically. It was also reported that with a finer ferrite grain the impact toughness, the tensile and yield strength increase and the elongation decreases [54]. It should be noted that the determination of the cooling rate influence was also a part in this study. The results showed that with faster cooling rates the ferrite grains are finer and the phase fraction of martensite increases. Thereby, tensile and yield strength increased and impact toughness and elongation decreased. As mentioned before there are two cooling processes established to produce multi-phase structures with higher strength [9]. On the one hand, the IAC, where the material is

accelerated cooled after the last deformation step, to transform the remaining austenite into bainite and martensite [46–48]. On the other hand the IDQ, where after the last deformation step the material is quenched to temperatures above the martensitic start temperature and then by isothermal ageing the remaining austenite transforms into bainite. After this transformation the material is quenched to room temperature [49].

The deformation processes also influences the formation of precipitates, thereby, by deformation bands the nucleation of ferrite and precipitates is facilitated. Precipitates which are favorable formed by deformation are called strain induced precipitates [61–64]. Through the formation of dislocations in the austenite, as well as in the ferrite, nucleation sites are created [65]. By dislocation networks also the diffusion of the precipitate forming elements is accelerated, because along the dislocation cores the element diffusion is facilitated. This kind of diffusion is called pipe diffusion [62,63]. The formation of micro-alloyed carbides, nitrides or carbonitrides is desired because of precipitation hardening. Precipitates which were formed in the austenite do not have a strengthening impact in the ferrite due to the loss of the coherent interface. However, when the precipitates in the austenite are large enough, they can act as ferrite nucleation sites [66–68].

Finally, it should be mentioned that the mechanical properties of steel depend not only on the chemical composition, also on the production parameters, e.g. deformation in the different regions (figure 3), rolling reduction, temperatures, cooling rates etc..

3.2 Solubility of Micro-alloy carbides and nitrides

The mechanical properties of micro-alloyed steels are influenced by the grain growth inhibition by micro-alloying particles and also by precipitation hardening due to them. To exploit these effects for a steel improvement, it is important to understand the dissolution of various micro-alloying carbides and nitrides. The dissolution characteristics of micro-alloying carbides and nitrides are the thermodynamic background for the re-precipitation of such carbides, nitrides and carbonitrides for recrystallization inhibition and precipitation hardening. Basically, the lower the solubility of such precipitates is, the higher is the chemical driving force for their formation. However, the dissolution of the micro-alloying carbides and nitrides was not the focus of this work, but rather the precipitation behavior and to understand the precipitate formation it is important to understand which parameters influence the stability of micro-alloying particles.

The solubility of carbides and nitrides in austenite and ferrite is expressed by the solubility product in terms of the micro-alloying element and carbon and/or nitrogen (in wt%). The dependency of the solubility product by the temperature is expressed by the following Arrhenius relationship,

$$\log k_s = \log[M][X] = A - \frac{B}{T} \qquad 3.1$$

where k_s is the equilibrium constant, [M] is the dissolved micro-alloying element, [X] is the dissolved content of nitrogen and/or carbon, A and B are constants for a given system and T is the absolute temperature in K.

For the solubility product of micro-alloy carbides, nitride and carbonitrides in austenite and ferrite a lot of equations exist [24,30,69–72]. This is caused by the big influence of the micro-alloying amount and also the amounts of N and C. Furthermore, the developed equations apply different alloying systems, where the other elements also influence the solubility product of micro-alloying precipitates. It should also be mentioned that the determination of the solubility product is even more difficult when more than one micro-alloying element is present and when the ratio of carbon and nitrogen changes during dissolving. Although, there are differences in the solubility product equations it is possible to estimate the solubility of the carbides and nitrides. Figure 4 shows a solubility diagram for a fictitious micro-alloyed steel [30]. With such diagrams it is possible to determine the solution temperature of micro-alloy precipitates, when the content of M, C and N of the alloy are known. By means of this information it is possible to generate the boundary between the austenite single and the austenite plus MX phase field. The boundary between these fields corresponds to a constant temperature and consequently to the corresponding constant k_s. The inserting of the [M] and [X] values in equation 3.1 leads to the solubility boundary. That means at any alloy lying left or below the boundary at a given temperature there is only the austenite phase present. For any alloy lying above or to the right of the boundary austenite and MX is present. The solubility diagrams for different micro-alloyed steels look similar. The trend that higher micro-alloying amounts and higher C and N amounts lead to more thermally stable precipitates is given for every micro-alloying element.

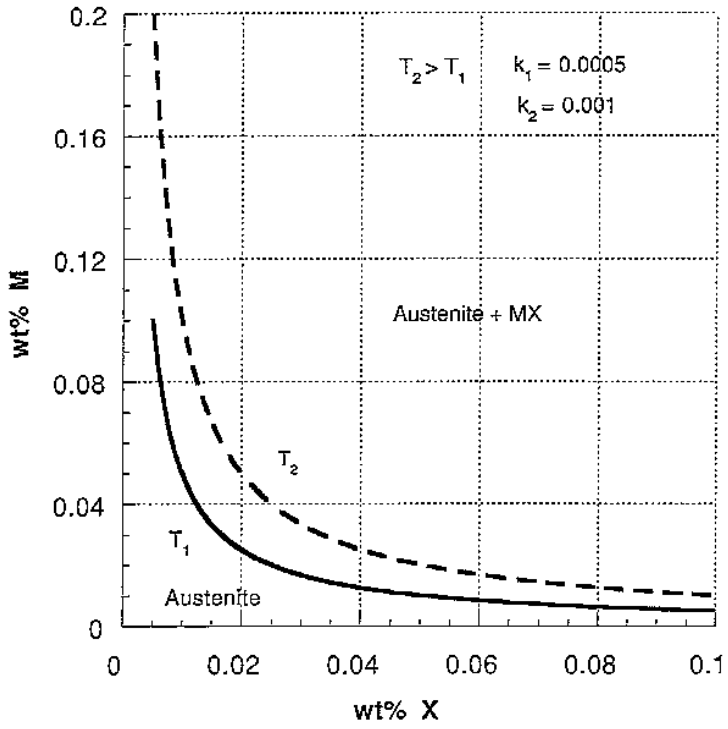

Figure 4: Solubility diagram showing the single phase field of austenite and the double phase field of austenite + MX. The boundary between the fields is given by the equation 3.1 which depends on the temperature and the solubility product [30].

The solubility products do not depend only on the amount of the micro-alloying element and the C and N contents in the alloy, the more important is the type of the micro-alloying element. Figure 5 shows a comparison of the solubility products of different micro-alloying nitrides and carbides in ferrite and austenite [30]. The table reveals that the lower the k_s value is the more stable is the precipitate type. For every micro-alloying element the nitrides are more stable than the carbides in austenite and ferrite. A large difference is observed between Ti nitrides and carbides and between V nitrides and carbides. In the austenite phase the solubility of niobium nitrides and carbides differ less significantly than in ferrite. Another point is that the solubility levels of micro-alloying carbides and nitrides in austenite differs not that strongly. Excluded TiN, which is less soluble, and VC, which is more soluble than the other nitrides and carbides. From figure 5 it is also visible that the carbides and nitrides in ferrite are less soluble than in austenite.

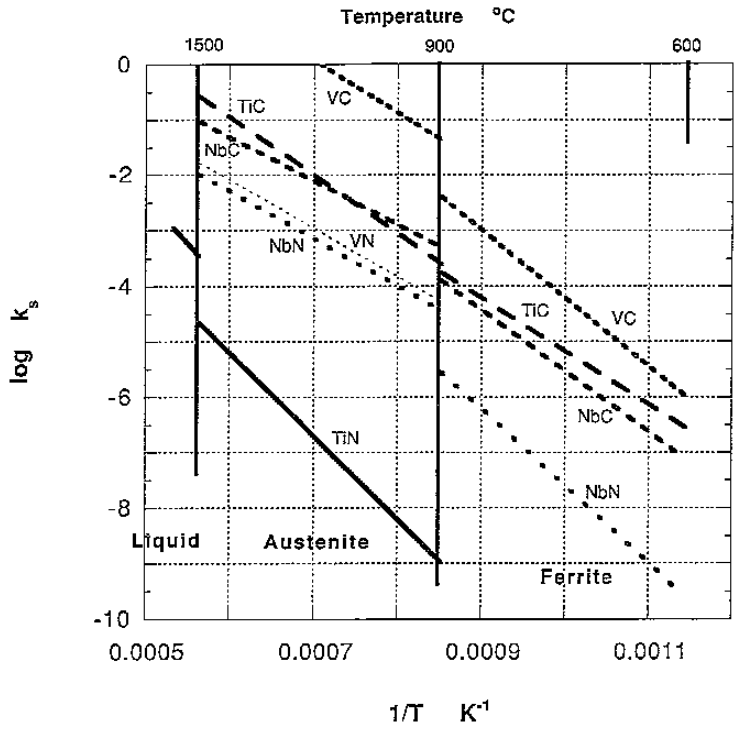

Figure 5: Comparison of the solubility products of the different micro-alloying nitrides and carbides in ferrite and austenite [30].

For complex precipitates, which consist of more than one micro-alloying element, and also for carbonitrides solubility data are rare in literature. The reason for that is the partial dissolution of complex micro-alloying precipitates and the solubility product depends strongly on the composition of the precipitates. Speer et al. [31] reported that the solubility of NbV carbonitrides depends strongly on the Nb, V, N and C contents. The higher the Nb content is the more stable are the NbV precipitates. That is also valid for the solubility behavior of carbonitrides, i.e. the higher the N content of the carbonitrides the more stable the precipitates. [30,31,62,73–76]. Due to the high thermal stability of TiN, it does not dissolve during austenitisation [30]. Thereby, TiN precipitates act as nucleation sides for Nb and V, and complex precipitates are formed where the complete dissolution of the precipitate depends on the part which shows a higher thermal stability [77,78]. Steels alloyed with Nb and Ti form complex TiNb precipitates which dissolve partially. That means that Nb dissolves and TiN remains. The amount of dissolved Nb depends on the solution annealing temperature, with increasing temperature the amount of Nb in the complex TiNb carbonitrides decreases [77,79,80]. However, not only the Nb amount of the precipitates is decreased with higher annealing temperatures, also the C content of the carbonitrides decreases and they become N richer [81,82]. In steels alloyed with Ti and V complex TiV carbonitrides are formed. Pandit et al. [78] showed that the solution behavior is similar to TiNb precipitates. During solution

annealing the amount of V and also of C decreases and a Ti and N rich precipitate remains [83]. There are also applications in which V, Nb and Ti are added. In this case complex (V, Nb, Ti) (C, N) precipitates are formed [15,71,84,85][P1]. During dissolution of this triplex precipitates the TiN part remains and depending on the solution annealing temperature the precipitates consists partially of Nb and V. However, the dissolution behavior is similar to TiNb or TiV carbonitrides, the higher the annealing temperature is the lower is the amount of Nb, V an C of the precipitate [15].

3.3 Micro-alloying effects in austenite

As mentioned in the previous sections, to design a microstructure which achieves good mechanical properties, it is important to know how the material acts at different heat treatments and deforming processes. In the following chapter the influence of the micro-alloying elements on the austenite grain growth, the recrystallization and their precipitation behavior in austenite should be explained.

To produce a homogeneous, fine microstructure, the first process is a solution annealing heat treatment. It is well known that during solution annealing in the austenite region the grain coarsens. To realize a final fine-grained microstructure, a first step is to control the austenite grain size and keep it as small as possible. By adding micro-alloying elements the existence of fine austenite grains can be facilitated. Micro-alloying elements influence the grain growth in two different ways. On the one hand randomly distributed precipitates constrain the movement of the grain boundaries by pinning the grain boundary on particles. This effect is in literature known as the zener drag effect [30,86,87]. The pinning force of the particles depends on their size and the surface energy of the grain boundary [30,87]. For the inhibition of grain growth the amount, distribution and shape of the precipitates are important [87]. Generally, the more and regular distributed the particles are the larger is the inhibition of the grain growth [87]. It is also possible that the grain growth is inhibited by dissolved micro-alloying elements by enrichments at the migration boundary. Depending on the element and the amount of the enrichment the mobility of the boundary is retarded. This behavior is known as the solute drag effect [18,19]. Further, the occupation leads to the formation of grain boundary precipitates, which inhibit the grain growth more effective than randomly distributed precipitates [30,88,89]. For the grain growth inhibition by grain boundary precipitates it is necessary to cool the material down to temperatures were the micro-alloying elements can precipitate. Investigations of this effect showed that Nb is most effective [90]. As described in the section about the solubility of micro-alloying carbide and nitrides the

particle dissolving temperature depends on the micro-alloying type and the amount of the precipitate forming elements. Due to this fact the different micro-alloying elements have more or less influence on the austenite grain size. Generally, the more thermal stable the precipitates are the smaller the austenite grains [91–93]. That means that nitrides are more effective than carbides and Nb and Ti are more effective than V. By considering the different particles in this way TiN is an exception because it is known as the most thermal stable particle, however, due to coarsening of TiN a grain growth inhibition is not pronounced [30]. It is also possible that during solution annealing abnormal grain growth occurs [94]. This can be caused by two effects, on the one hand by segregations of the micro-alloying elements [94,95] and on the other hand due to dissolution of different kinds of micro-alloying precipitates in steels alloyed with more than one micro-alloying element. Fernandez et al. [91] described for a 0.165 wt% C steel micro-alloyed with V, Nb and Ti the start of abnormal grain growth by the dissolution of different micro-alloying precipitates. He reported that at 1100°C and 1050°C and short times VC dissolves and grain growth starts. Solution annealing at 1200°C and short times lead to dissolution of TiC and VN and consequently the grain growth is accelerated. For a longer heat treatment at 1050°C and 1100°C grain growth starts by the dissolution of NbN and VC.

An important part of the thermo-mechanical process is recrystallization of the material. Recrystallization was not investigated in this thesis, but the recrystallization inhibition is one of the main effects of the micro-alloying elements and, hence, this behavior is also described. Recrystallization happens to reduce stored deformation energy by a rearrangement of the deformed microstructure. By adding micro-alloying elements the recrystallization is retarded and deformation bands are available for ferrite nucleation. Because of the important influence of these elements on the recrystallization this effect was investigated by many researchers [19,22,29,89,96–107]. Micro-alloying elements can act in two different ways to inhibit recrystallization. They can influence the recrystallization in solid solution by the so-called solute drag effect or by forming precipitates in the austenite by the so-called precipitation pinning effect [16,54,58,96,100,108].

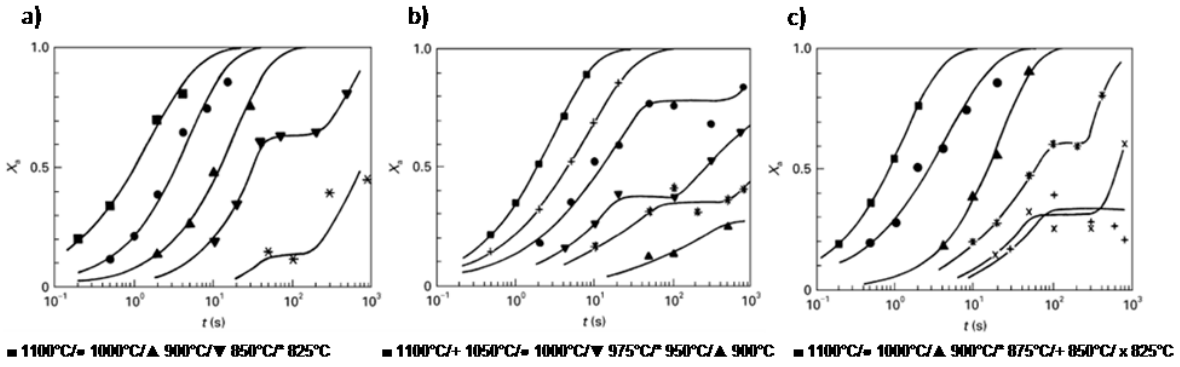

Figure 6: Recrystallized fraction (X_a) versus time. φ=0.35; $\dot{\varphi}$=3.63 $^{s-1}$. a) for a V steel; b) for a Nb steel; c) for a Ti steel [96].

The influence of micro-alloying elements is often determined by so-called precipitation-time-temperature (PTT) diagrams. To explain the effect of the micro-alloying elements on the recrystallization figure 6 is depicted. Figure 6 shows PTT diagrams for steels with different micro-alloying elements, one time alloyed with 0.11 wt% C and 0.043 wt% V (a), one time with 0.11 wt% C and 0.042 wt% Nb (b) and one time with 0.15 wt% C and 0.05 wt% Ti [96]. On the y-axis the recrystallized fraction is plotted and on the x-axis the time. For the construction of the diagram the material was deformed with a natural strain of φ=0.35 and a strain rate of $\dot{\varphi}$=3.63 $^{s-1}$ at different temperatures. After deformation the grade of recrystallization depending on the time was determined. For all three steels it is obvious that a higher deformation temperature leads to a faster recrystallization. At lower deformation temperatures a plateau is formed. That means that the recrystallization is stopped. This inhibition is explained by the formation of strain induced precipitates. The beginning and the end of the plateau have been identified as the start and finish of precipitation. Due to the formation of precipitates the grain boundaries are pinned and the recrystallization is quasi stopped. Comparing the diagrams in figure 6 reveals that Nb is most effective to retard the recrystallization. The retardation by Nb particles is already observed at 1000°C. For the V and Ti steel recrystallization retardation is observed at 850°C. Medina [96] also gives an explanation for this behavior. In the Ti steel nitrides are formed close to the solidification temperature. They are not responsible for the retardation because they are too large, but strain induced TiC precipitates inhibits the recrystallization. However, TiC are formed in a lower temperature range in austenite, hence, Ti do not have a high influence on the recrystallization inhibition [30]. In the V and in the Nb steel due to the strain nitrides and carbides are formed which inhibits the recrystallization. In the V steel mainly VN and in the Nb steel mainly $NbC_{0.7}N_{0.2}$ are formed. For V the effect on the recrystallization depends on the N content, because VN is mainly formed in austenite range and VC is formed in ferrite [30]. As a

consequence of this V micro-alloyed steels with hardly N, do not have a large influence on the recrystallization behavior [30].

It is obvious from the section about recrystallization inhibition that the formation of micro-alloyed carbides and nitrides is an important part to realize a final fine grained microstructure. The following section describes the precipitation behavior of micro-alloying elements in austenite. The precipitation of V, Nb and Ti in austenite was explained partially in the previous part about the recrystallization. Basically, the formation of the micro-alloying precipitates correlates with their solubility. That means the lower the solubility of micro-alloyed carbide or nitride is the higher is the driving force to form such precipitates. A requirement for this is the presence of enough precipitate forming elements in solid solution. Nb is known as the most effective element to inhibit recrystallization and austenite grain growth by forming precipitates. The formation of Nb in austenite is well known and discussed in literature [20–22,61,62,74,100,109,110]. Similar to V and Ti, the Nb nitrides have a lower solubility than the carbides which means that nitrides are formed earlier than carbides. In industrial used steels mainly Nb carbonitrides are formed. The precipitation of micro-alloying elements in austenite happens mainly by heterogeneous nucleation at grain boundaries or dislocation structures, whereat by deformation processes strain induced precipitates are formed. Independent of the formation and the forming element the micro-alloying precipitates have a NaCl type f.c.c structure [30,111–113]. The formation of strain induced Nb carbonitrides is well described by Dutta and Sellars et al. [57,58,106]. They reported that the formation of the Nb(C, N) is facilitated by the deformation induced dislocations, which act as nucleation sites. By the dislocations networks also the growth is faster because the diffusion of Nb is easier by pipe diffusion along dislocation cores [23,61,62,74,109].

Table 2: Average radius of gyration, composition of the particles, the C/N ratio and the phase fraction of the particles in martensite or bainite in the Nb-alloy after different deformations and dwell times at 700°C determined using APT data [P2].

φ	Time [min]	Phase	Rg [nm]	Nb [at%]	C [at%]	N [at%]	Fe [at%]	C/N	Phase fraction [10^{-4}%]
0.05	5	martensite or bainite	0.72±0.16	35.49±2.40	2.11±0.28	8.90±0.39	52.19±2.23	0.24	1.5
	10	martensite or bainite	0.84±0.43	22.45±0.56	5.34±0.37	5.01±0.19	64.88±0.59	1.07	3.4
0.2	5	martensite or bainite	0.57±0.17	32.46±2.05	3.66±0.55	6.95±0.09	55.58±1.59	0.53	1.9
	10	martensite or bainite	1.02±0.35	38.22±2.06	5.69±0.73	11.43±0.46	42.43±1.46	0.50	0.64
0.7	5	martensite or bainite	0.75±0.35	27.10±0.57	6.54±0.20	6.93±.25	57.50±0.75	0.94	3.4
	10	martensite or bainite	0.68±0.25	31.87±0.53	4.25±0.30	4.80±0.22	56.91±0.73	0.89	3.4

Investigations which were performed in this doctoral thesis did not show this trend. The results of the study about the precipitation behavior of Nb in austenite at 700°C are summarized in table 2 [P2]. An increase in the precipitate phase fraction is apparent with higher true strains, but an accelerated precipitate growth cannot be observed, because the sizes of the precipitates are nearly the same. After a true strain of φ= 0.05 and a dwell time of 5 min the precipitates phase fraction is $1.5x10^{-4}$% and the precipitate size is 0.72±0.16 nm. In contrast to that, after a true strain of φ= 0.7 and a dwell time of 5 min the precipitates phase fraction increased to $3.4x10^{-4}$% and the precipitate size is nearly the same with 0.75±0.35 nm. The results imply that at a higher true strain the dislocation density increases and thereby the number of Nb precipitates, which results in an increase of the precipitate volume fraction [P2]. However, the distribution of the strain induced precipitates depends on the assembling of the dislocations. Because of the heterogeneous distribution also the precipitates are heterogeneously assembled [89][P2]. Furthermore, the result from this study show that with longer dwell times the chemistry of the Nb carbonitrides changes from N rich into C rich (table 2). This is caused by the consumption of the N in solid solution and consequently C accumulates at existing N rich Nb carbonitrides [P2]. Without deformation the nucleation of Nb precipitates in austenite occurs heterogeneously at austenite grain boundaries [30,74]. The formation of Ti precipitates in austenite depends mainly on the N content. After solution annealing TiN is still precipitated because of their thermal stability and consequently no Ti is in solid solution to from strain-induced precipitates [114]. These TiN particles are formed in the melt and when the steel is solidified the particles mainly exhibit a size where they have no influence on the austenite grain size during heat treatment. Therefore, this precipitates do not have a significant impact on the grain growth inhibition [16,30,97]. In the case of more Ti than N in the alloy TiC particles can be formed. These particles have a higher solubility than TiN and dissolve during solid solution [30,114]. This behavior leads to the formation of strain induced TiC which retard recrystallization [72,114]. V is known as the most effective micro-alloying element for precipitation hardening, by forming VN, VC and V(C, N) in ferrite [25–27,76]. Due to the high solubility of VC only VN can be formed in the austenite phase [30,96,115]. The formation of VN in austenite is supported by deformation [96], and by a higher N content. The higher the N content is the more stable are the VN precipitates [24]. It is obvious that the different micro-alloying elements are added when different requirements should be achieved. To accomplish different requirements which are not possible by one micro-alloying element, several elements can be alloyed. The combination of the individual elements results in the formation of precipitates with a complex chemistry. The formation of

them, their chemistry and the assembling depends strongly on the solubility of the individual micro-alloying elements. The solution annealing temperature controls the dissolution of the complex micro-alloying precipitates and only partial dissolution can happen which leads to limited re-precipitation for recrystallization inhibition. However, Hillert and Steffansson [116] developed a model for the formation of complex stoichiometric precipitates by considering the change of the free energy. In steels alloyed with Nb and V complex NbV carbonitrides are formed [31,78,117–119]. Because of the lower solubility of Nb carbonitrides than V carbonitrides the first formed precipitates consist of Nb. Nb carbonitrides are formed at 1200°, at this temperature V is completely soluble in austenite. By the combination of Nb and V the activity coefficient of C and N is decreased and thus the solubility of VN increases and also the incubation time for VN. At lower temperatures, of about 1000°C, V accumulates at existing Nb precipitates, thereby complex NbV carbonitrides are formed [78,118].

By alloying of Nb and Ti in steel complex NbTi carbonitrides are formed [80,81,120–124]. It is assumed that the dissolution temperature of NbTi carbonitrides is comparable to the dissolution temperature of TiN [81]. Because of the high dissolution temperature during solution annealing NbTi precipitates dissolve only partially. The higher the solution annealing temperature is the more Nb is in solid solution because only the Nb part dissolves [77,82]. After reheating the undissolved TiN and (Nb, Ti) (C, N) act as nucleation sites for dissolved micro-alloying elements. For instance, Nb nucleates at the Ti rich precipitates and forms a Nb-rich part. This heterogeneous nucleation is preferred due to the decrease of the barrier energy for nucleation. Depending on the formation temperature of the NbTi precipitates the Nb and Ti content is different. At lower temperatures in the austenite region the precipitates are Nb richer and at higher temperatures Ti richer [77,80–82].

By alloying Ti and V in steel complex TiV carbonitrides are formed [83,125,126]. Such as the precipitation of NbTi carbonitrides, TiN does not dissolve during the solution annealing, only V dissolves. Also in this case the TiN particles act as nucleation sides for V, and at lower temperatures, close to the A_{e3} temperature, V accumulates at TiN. In this way (Ti, V) (C, N) precipitates are formed composed of a TiN-rich core and a VC-rich shell [83,126].

Steel alloyed with Nb, Ti and V forms complex NbTiV carbonitrides [71,84,85][P1]. From literature is well known that at higher temperatures, above 900°C, mainly (Ti, Nb) (C, N) are formed. The formation of such precipitates is similar to the formation of TiNb precipitates in steels only alloyed with Ti and Nb. Below 900°C due to deformation small strain induced (Nb, Ti, V) C carbides can be formed [85]. A main part of this doctoral thesis was to

investigate the evolution of strain induced complex NbTiV carbonitrides [P1]. In literature detail investigations about the chemistry of complex NbTiV carbonitrides are not available, especially the C and N behavior. In this work it could be shown that during isothermal aging at 900°C Nb and V accumulate at existing TiN precipitates and they form a shell around the TiN. Figure 7 shows an APT measurement of this work where the elemental maps for the precipitates in martensite are illustrated. The one dimensional concentration profiles of the precipitates in this figure depict that deformation leads to the formation of NbVTi carbonitrides. The larger precipitate (figure 7b) has a C to N ratio of nearly 1:1 and the smaller precipitate (figure 7c) a C to N ratio of nearly 2:3. Which leads to the assumption that smaller precipitates are N-richer than coarsen. Ti is slightly increased, but it seems that strain induced Ti clusters facilitate the nucleation of Nb and V [P1].

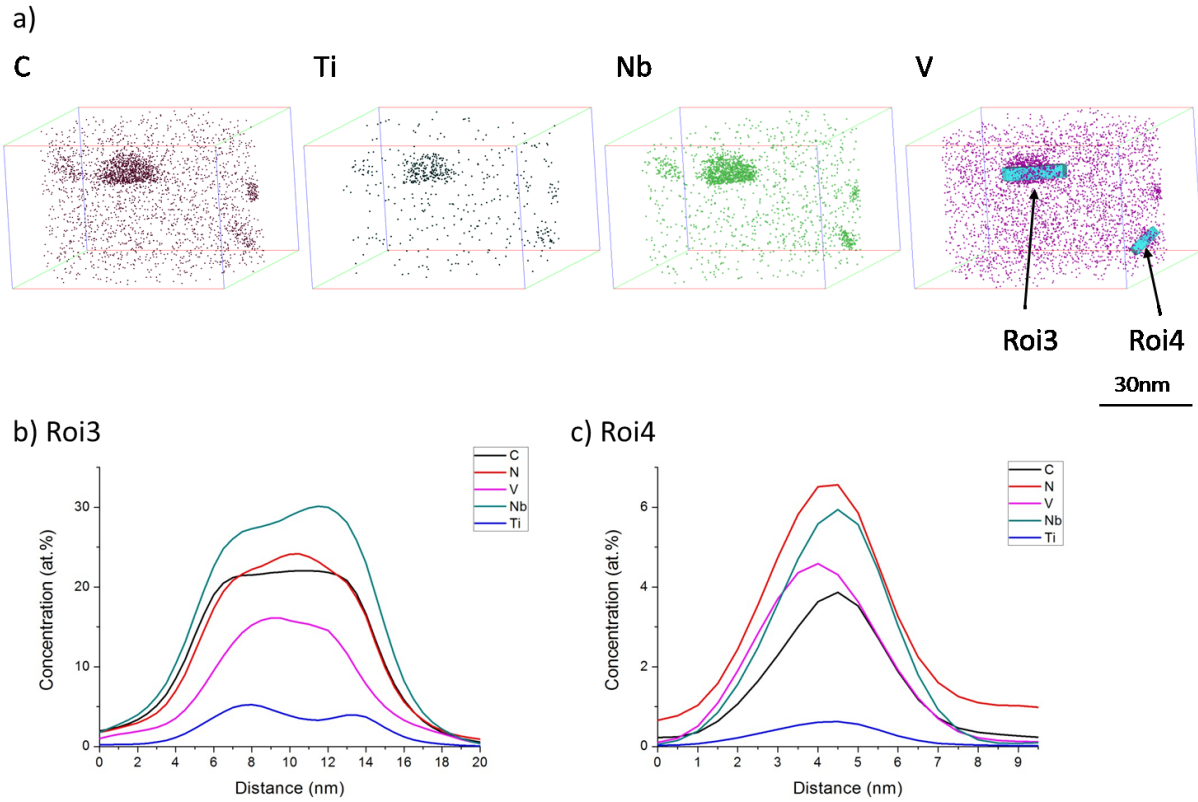

Figure 7: a) Three-dimensional elemental map for precipitates in martensite after a deformation of φ=0.7 and a dwell time of 5 min at 900°C in the Nb-V-Ti-alloy, showing the C, Ti, Nb and V distribution; b) one dimensional concentration profile of Roi3 in a); c) one dimensional concentration profile of Roi 4 in a) [P1].

3.4 Micro-alloying effect on the austenite-ferrite transformation

By the formation of different phases, especially ferrite, the mechanical properties are specified. Therefore, it is important to know the influences on the austenite-ferrite (γ-α) transformation. The formation of small sized ferrite grains depends mainly on the nucleation

possibilities. The ferrite nucleation takes place at austenite grain boundaries, dislocation structures or adequate sized precipitates [51,55–57,65,68]. However, the growth of ferrite depends on the composition of the alloy and if the different elements are precipitated or in solid solution. During γ-α transformation the elements can be redistributed because of different solubilities in austenite and ferrite. Furthermore, the grain boundary motion can be influenced by the dragging of elements in solid solution and by precipitates which constrain the γ-α interface movement.

The γ-α transformation is retarded by pinning of the γ-α interface within the austenite existing precipitates. To influence the transformation, these precipitates have to be small-sized (nm range) and homogenously distributed. These ability corresponds mainly to Nb and V precipitates [24,30,52,59,67,113]. In carbon steels the γ-α transformation is strongly influenced by C. Due to the higher solubility of C in austenite than in ferrite, C has to diffuse into the austenite phase during the transformation [32,33]. Further elements, which are added to improve the properties of low alloyed steels, also have different stabilizing impacts on the austenite or ferrite phase. In typical micro-alloyed steels mainly the Si and Mn contents are raised. Because Mn has the ability to decrease the red shortness and facilitate the weldability and formability and Si act as deoxidant [36]. Other elements are mainly added in small amounts and the content depends on the used application. These elements also have an influence on the γ-α transformation. Mn depresses the transformation similar as Ni, N and C, they are known as austenite stabilizer [36,127,128]. Si accelerates the transformation as well as Cr, Al, Ti, Mo and V, they are known as ferrite stabilizer [36,127]. Although, lower contents of alloying elements do not have a large impact on the phase stabilization the transformation can be reduced by solute drag effect. Thereby, the velocity of the γ-α interface is reduced by impurity occupation of the grain boundary [18]. Cahn [18] reported that the solute drag effect depends on the grain boundary velocity and the diffusivity of the dragged element. The faster the grain boundary is the more effective are elements which diffuse easier. In the present thesis the distribution of the alloying elements in ferrite and austenite was investigated to determine the influence of the phase composition on the precipitate chemistry. Figure 8a depicts an APT elemental map of a γ-α interface showing the V atoms. The upper part where the V atoms are less is ferrite and the lower part where more V exists corresponds to austenite. By a one dimensional profile, depicted in figure 8b, c and d, the element distribution across the γ-α interface is examined, with the result that V, C, Mn, Al, P and Cr are enriched at the interface. This fact leads to the assumption that these elements have an impact on the γ-α interface velocity. The distribution of the elements reveals that V, Mn and C

are redistributed because the amount of these elements is higher in austenite than in ferrite [P3].

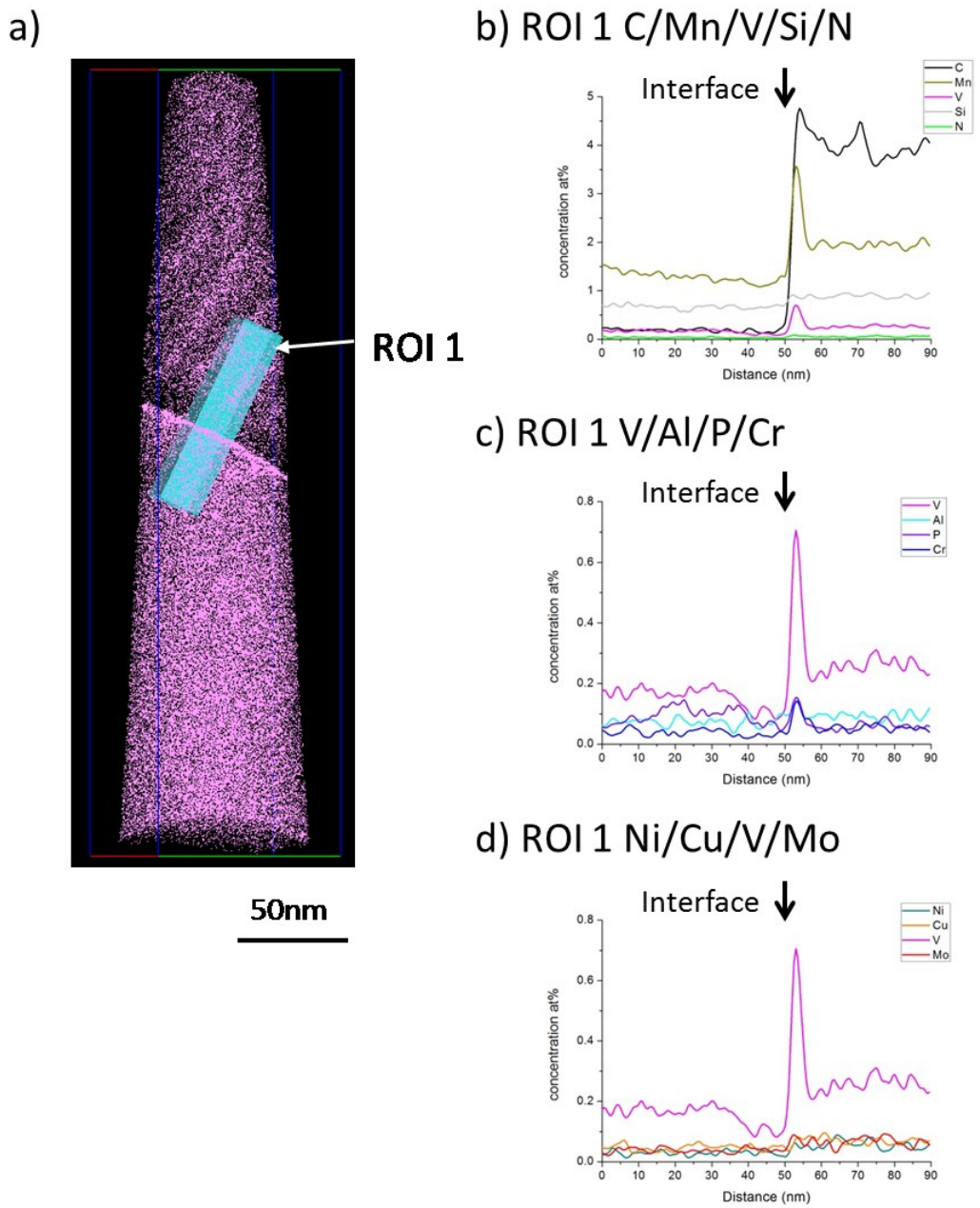

Figure 8: a) Three-dimensional elemental map of an interface in the V-alloy, showing the V distribution. For a detailed investigation of the interface, by a concentration profile, a box (ROI 1), box size of 20 x 20 x 90 nm^3, marked by an arrow) was positioned. b) one dimensional concentration profile of C, Mn, V, Si and N, c) one dimensional concentration profile of V, Al, P and Cr, d) one dimensional concentration profile of Ni, Cu, V and Mo.

By the γ-α transformation not only a redistribution of the elements is observed. During the transformation precipitation occurs at the γ-α interface. Precipitates which are formed by this way are called interphase precipitates. Typical elements which form such precipitates are V, Nb and Mo [129–140], but V is known as the most effective because a small V amount in

steel is required to form distinctive interphase precipitates [135]. Figure 9 shows a dark field TEM image of VC interphase precipitates in ferrite in a 0.3 wt% V steel [139]. By visual inspection the periodical sheet arrangement of the VC is visible. It is also visible that the distance between the sheets is not constant. That happens because the intersheet space of the carbides depends on the velocity of the γ-α transformation and this is affected by the continuous cooling rate, the isothermal transformation temperature and the chemical composition [141–145]. According to these studies and many more the intersheet space depends also on the diffusion of the element that constitutes the interphase precipitates [137,138,140]. The formation process for the interphase precipitates is in literature described differently. Two main theories exist, on the one hand the so-called ledge mechanism and on the other hand the solute depletion model.

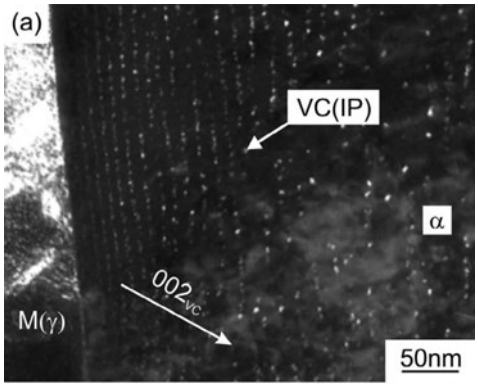

Figure 9: dark field TEM image of VC interphase precipitates in grain boundary ferrite in a 0.3 wt% V steel [139].

Davenport and Honeycomb [135] proposed at first the formation of interphase precipitates by the ledge mechanism. Figure 10a shows schematically how the ledge mechanism works [135]. The model assumes that the nucleation and growth of VC on γ-α interface can happen with regular or irregular heights. The precipitation occurs on planar, low energy, semi-coherent, immobile interfaces. The interfaces are formed by the passage of high energy ledges, which are moving too fast to act as nucleation site [131]. By the lateral mobile ledges austenite transforms into ferrite and this results in a macroscopic motion of the planar γ-α interface normal to the direction of the ledge migration. The height of the mobile and for the γ-α transformation responsible interface is equal to the distance between the precipitation sheets. To explain the formation of interphase precipitates at incoherent and often curved γ-α interfaces, a new model was proposed by Ricks and Howell [133]. This model is known as the quasi ledge mechanism or bowing mechanism and is schematically shown in Figure 10b. In this model the γ-α interface is pinned by the interphase precipitates. New ledges are formed

by bowing of the interface between widely spaced particles. Subsequent precipitation repins the interface and force the ledge to move sideways. In both models V diffuse to the immobile interfaces and by reaching sufficient amount of V precipitation occur [131,132,135–138]. By considering of this formation model one of the main drawbacks is to produce an explanation for the observed variation of the intersheet space with temperature and the steel composition. A complete different forming process, which gives a credible explanation to this question, was first proposed by Roberts [146]. This model based on the diffusion control of V in solid solution and is shown in Figure 10c [147]. He assumed that V carbonitrides were formed directly behind a migrating interface and the growth happens by the depletion of V in the ferrite. By further studies it could be shown that the precipitation occur directly at the interface [148]. A quantitative description of the solute depletion model due to Lagneborge and Zajac [149] considers a ferrite grain growth controlled by C diffusion into austenite. The formation of the V(C, N) precipitates is controlled by the V diffusion. By V diffusion as well as V dragging by the interface the γ-α boundary enriches in V, whereat a region is formed with a higher V content and precipitation can happen. This process occurs during the migration of the interface. Thereby it is important that the V diffusion is fast enough to follow the interface [138,150][P3]. By the solute depletion model also the formation of fibers can be explained. Analysis of the fiber formation showed that the velocity of the γ-α interface is important. When the interface migration is slow enough fibers are formed. The most effective element to slow down the interface is Mn [127,147,148].

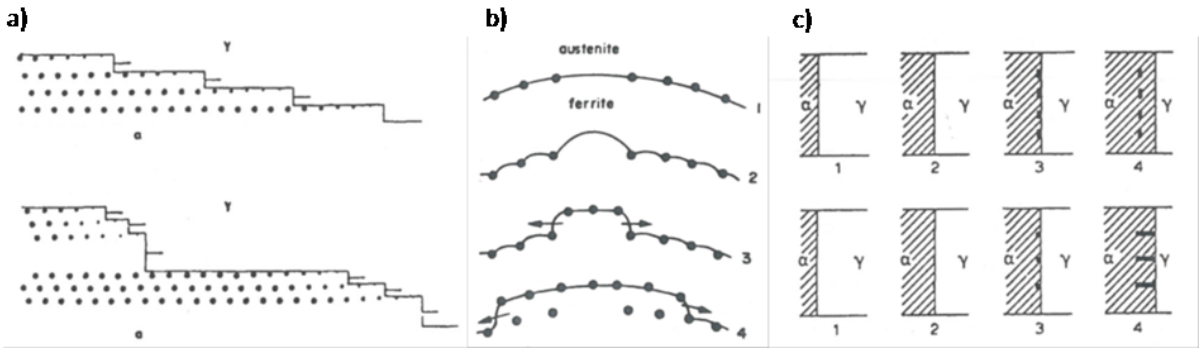

Figure 10: schematic depiction of the nucleation and growth of carbides at the α/γ; a) representing the ledge mechanism, at the top the regular ledge heights, at the bottom the irregular ledge heights [135]; b) representing the bowing mechanism; c) representing the solute depletion model[147].

Till this day none of these models are established as the only one to explain the formation of interphase precipitates. In the frame of this doctoral thesis the differences between interphase precipitates and randomly distributed precipitates in ferrite was examined to improve the understanding of the formation process of the interphase precipitates [P3]. In literature the

early stages of these precipitates are described as V_4C_3[135]. Information about the chemistry of the interphase precipitates in combination with the area in which they are formed is not available.

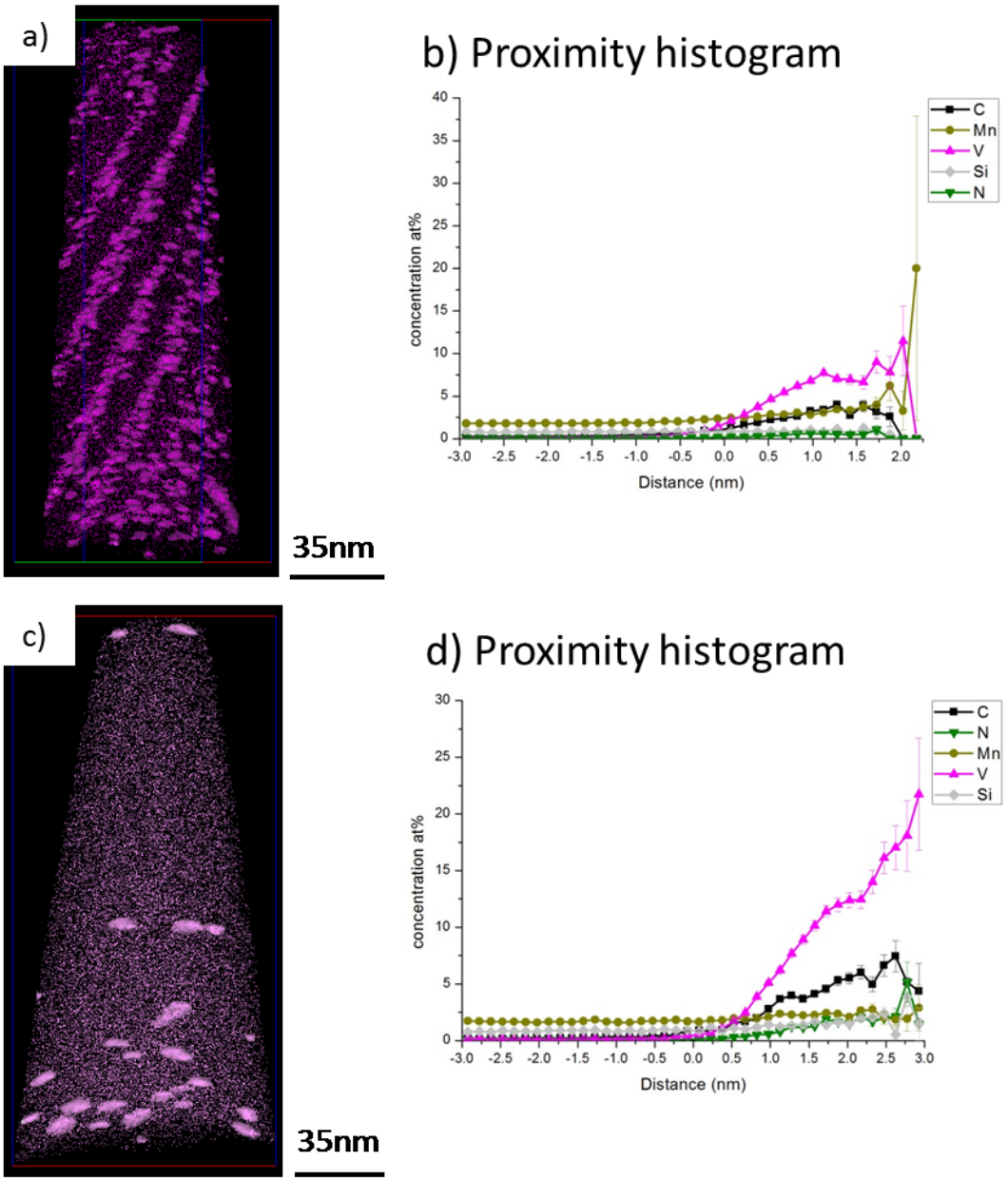

Figure 11**:** a) Three dimensional elemental map of the interphase precipitates in ferrite formed at 700°C showing the V atoms and isoconcentration surfaces with 1.2 at% V which show the interphase precipitates laterally, b) Proximity histogram of C, Mn, V, N and Si, c) three dimensional elemental map of randomly distributed precipitates in ferrite formed at 700°C showing the V atoms and isoconcentration surfaces with 1.2 at%, d) Proximity histogram of C, Mn, V, N and Si. Both in the V-alloy [P3].

Figure 11a and b shows V interphase precipitates with the corresponding proximity histogram and figure 11c and d illustrates randomly distributed V precipitates with the corresponding proximity histogram. It could be shown that the randomly formed precipitates are enriched in C and N (figure 11d). In contrast the interphase precipitates showed a higher amount of C and Mn (figure 11b). It is assumed that the difference in the chemistry resulted from the site in

which they were formed. The randomly formed precipitates occur in ferrite which consisted mainly of 0.05 at% C, 0.68 at% Si, 0.03 at% N and 1.51 at% Mn. The interphase precipitates were formed at the γ-α interface (figure 8), whereas C, Mn and V are higher than in ferrite [P3].

3.5 Micro-alloying effects in ferrite

The formation of interphase precipitates happens mainly in proeutectoide ferrite, which means in temperature regions above 700°C [139,151]. At lower temperatures the interphase precipitates is commonly found to be incomplete and random precipitation from supersaturated ferrite after the γ-α transformation takes over. The precipitates which were formed in ferrite have a strengthening effect on the material [30,52,113,152]. Mainly Nb and V of the micro-alloying elements form precipitates in the ferrite and V is known as the most effective element to form precipitates which improve strengthening. Ti is hardly in solid solution to form effective secondary precipitates in ferrite. It is reported that precipitates which were formed in austenite do not have a strengthening impact because of the incoherent interface to the ferritic matrix [63,153]. In the ferrite formed Nb and V precipitates have a NaCl f.c.c structure, such as the precipitates formed in the austenite. These precipitates exhibit a Baker-Nutting orientation relationship $(001)_{\alpha}$ // $(001)_{V(C, N) \text{ or } Nb(C, N)}$, $[001]_{\alpha}$ // $[011]_{V(C, N) \text{ or } Nb(C, N)}$ with ferrite [112]. Figure 12 illustrates Nb precipitates in ferrite characterized and identified by TEM [P2]. The Nb(C, N) are illustrated in figure 12a as dark dots in the TEM bright field image and as bright appearing dots in the corresponding dark field image (figure 12b). To create the dark field image, the marked precipitate diffraction reflex $(0\bar{2}0)$ in figure 12c was used. From the diffraction pattern the b.c.c structure of the ferrite and the NaCl type f.c.c structure of the Nb(C, N) can be seen. Based on figure 12c the Baker-Nutting orientation relationship $[001]_{\alpha}$ // $[011]_{Nb(C, N)}$ was identified. Figure 12d shows a representative EDX-spectrum of the precipitates in ferrite. In the spectrum, Nb is clearly detected, the dominant Fe peak stems from the surrounding ferritic matrix. Estimation about the C and N fraction is not possible [P2].

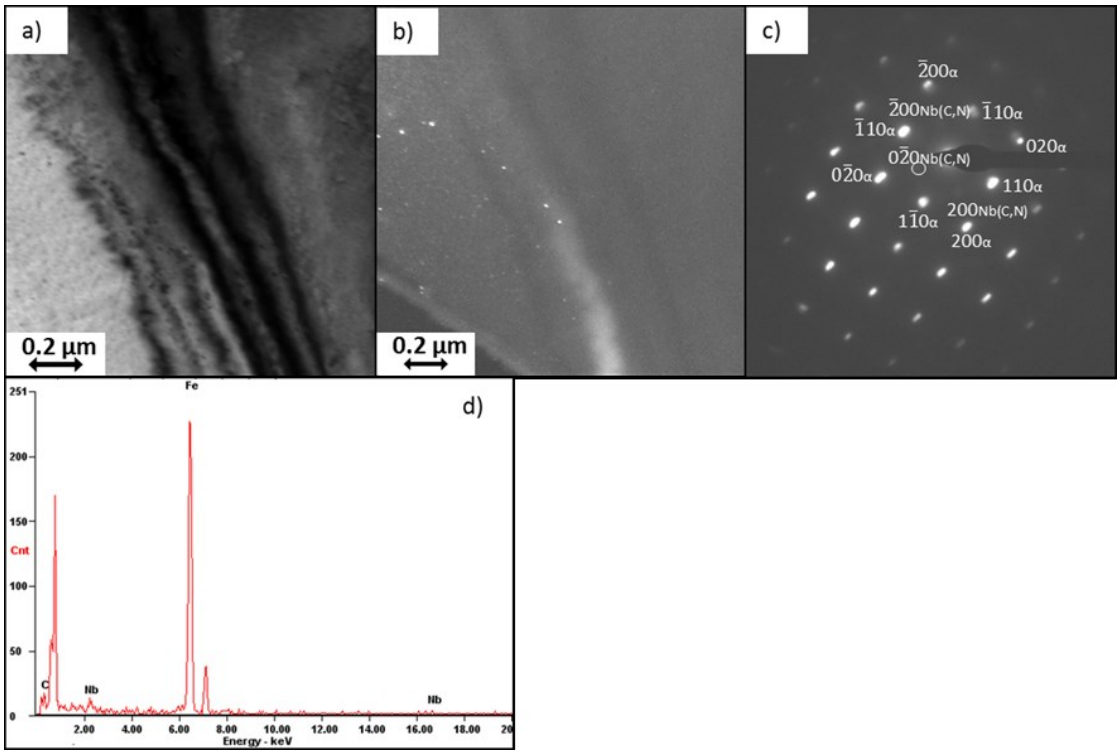

Figure 12: TEM bright field image of a Nb alloyed 0.2 wt% C steel (a), TEM dark field image (b) of the ferrite phase in the material after deformation of φ=0.7 at 700°C and a dwell time of 10min. (c) shows the selected area diffraction pattern of the ferrite phase and the Nb precipitates in (a) with the orientation relationship $[001]_{\alpha}$ // $[011]_{Nb(C,N)}$, (d) is representative energy dispersive X-ray spectrum from the particles [P2].

The nucleation of V or Nb precipitates can happen homogenously or heterogeneously. By homogenous Nb precipitation monatomic platelets are formed [154]. The carbides, nitrides and carbonitrides of the transition metals which are formed homogenously from ferrite are predicted to be coherent in their early stages. During growth the precipitate-ferrite interface becomes semi-coherent [113]. Heterogeneous nucleation can be facilitated by a deformation process to form strain induced precipitates on dislocations in ferrite, like in austenite [65]. As already mentioned by a higher dislocation density the diffusion of the precipitate forming element is accelerated and consequently the precipitate formation [23,61,74,109]. The investigation of the formation of strain induced precipitates in ferrite was an essential topic in this doctoral thesis [P2][P4]. By these studies the evolution of V and Nb precipitates were evaluated, especially the change of the C- and N-content of the carbonitrides. Figure 13 shows the evolution of strain induced V precipitates after a true strain of φ=0.7 at 600°C examined by APT [P4]. After short dwell times of 60s (figure 13a) small V clusters are visible and with longer dwell times those clusters grow (figure 13b and c).

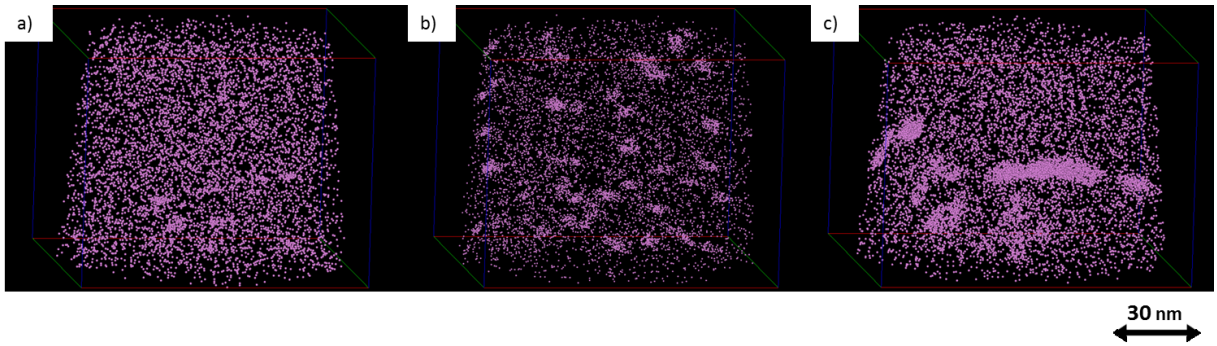

Figure 13: Three dimensional elemental maps of the particles in ferrite after a deformation of φ=0.7 at 600°C for different dwell times in the V-alloy, showing the distribution of the V atoms. a) 60 s, b) 300 s, c) 7200 s [P4].

Table 3: Average radius (spherical particles), composition of the particles, the C/N ratio and the phase fraction of the particles in ferrite after a deformation of φ=0.7 and different dwell times and temperatures in the V-alloy determined APT data [P4].

Temp [°C]	Time [s]	r [nm]	V [at%]	C [at%]	N [at%]	Fe [at%]	Mn [at%]	C/N	Phasefr. [%]
700	60	0.98±0.29	59.34±8.74	2.10±1.40	4.24±1.43	39.12±14.59	1.76±0.30	0.50	0.0650
	300	1.34±0.58	37.49±5.67	4.41±0.35	3.37±0.10	52.87±5.37	1.42±0.31	1.31	0.0908
	7200	3.13±1.76	25.92±6.20	9.44±2.47	2.52±0.52	60.04±9.81	1.52±0.21	3.75	0.1294
600	60	0.69±0.29	52.00±6.80	1.28±0.17	5.66±1.46	39.40±11.60	1.70±0.40	0.23	0.0080
	300	1.02±0.49	35.97±6.29	2.84±1.43	5.44±0.98	53.22±7.75	1.99±0.52	0.52	0.1192
	7200	1.24±0.53	43.97±9.31	3.31±0.11	3.38±0.52	47.31±10.02	1.52±0.29	0.98	0.1034

The investigations of the evolution of V strain induced precipitates were done for 600°C and 700°C. Table 3 reveals the results of this study and exhibits the evolution of size, chemistry and precipitate phase fraction [P4]. The APT analysis showed that the early stages of the precipitates are N rich and with longer dwell times the C content increases. For 700°C the C/N ratio changes from 0.50 after 60s dwell time to 3.75 after 7200s dwell time. The reason for this behavior is the lower solubility of nitrides in ferrite than of carbides. Hence, the formation of nitrides is benefited, but due to low availability of N in the material for the further growth, C accumulated at already existing N rich V precipitates. At 600°C the evolution is similar but not as fast, which is obvious because after a dwell time of 7200s a C/N ratio of 0.98 is examined and for 700°C a C/N ratio of 3.75. [P4]. Generally, the results revealed that the precipitate evolution at the higher temperature (700°C) is faster than at the lower temperature (600°), which means that also the precipitate growth and the increase of the precipitate phase fraction is faster. This is especially obvious after short dwell times. After

60s the particle size of the V precipitates at 700°C is 0.98 nm and the phase fraction 0.065% and at 600°C the particles had a size of 0.69 nm and a phase fraction of 0.008%. The reason for this behavior is also the faster diffusion of V at 700°C than at 600°C. Because of the lower diffusion of V than C or N, this element is responsible for the precipitation evolution. A similar behavior is detected for homogenously nucleated precipitates. By their growth also due to limited N the composition of the V carbonitrides changes from N into C rich [24,26,155]. Further studies of V precipitates revealed that V carbonitrides in ferrite are N richer than carbonitrides with the same size in austenite. This is caused by the lower solubility of V precipitates in ferrite than in austenite [155]. N does not only enhance the formation of the precipitates. By higher N content the VN and V(C,N) are more disperse and uniform distributed than VC and the precipitation coarsening is reduced [26,113,155].

Table 4: Average radius of gyration, composition of the particles, the C/N ratio and the phase fraction of the particles in ferrite at 700°C in the Nb-alloy after different deformations and dwell times determined using APT data [P2].

φ	Time [min]	Phase	Rg [nm]	Nb [at%]	C [at%]	N [at%]	Fe [at%]	C/N	Phase fraction [10^{-4}%]
0.05	5	ferrite	1.01±0.66	24.6±0.68	7.15±0.17	8.44±0.56	56.56±0.75	0.85	2.6
	10	ferrite	Could not be detected						
0.2	5	ferrite	0.86±0.39	22.13±0.36	3.32±0.13	6.03±0.36	65.70±0.38	0.55	5.6
	10	ferrite	0.8±0.22	17.18±0.54	8.46±0.27	5.38±.37	67.11±0.64	1.57	4.4
0.7	5	ferrite	1.02±0.47	15.99±0.57	4.46±0.22	4.81±0.28	72.22±0.76	0.93	7.5
	10	ferrite	1.99±0.68	10.36±0.21	5.24±0.13	3.71±0.16	78.12±0.30	1.41	10

For the formation of Nb precipitates a similar behavior is known, but fewer studies have been carried out because of the lower strengthening impact of Nb precipitates by secondary hardening. A summary of the investigations which were done in course of this thesis are shown in table 4 [P2]. They revealed that the change of the chemistry is similar to that for V. In the early stages the Nb precipitates are N rich and with longer dwell times C enriches. For a true strain of φ=0.2 and 0.7 this behavior was examined, in both cases the C/N ratios changes from N to C rich (φ=0.2/5min the C/N ratios is 0.55 and after dwell time of 10 min 1.57; φ=0.7/5min the C/N ratios is 0.93 and after dwell time of 10min 1.41). The higher N amount at the early stages is caused by the lower solubility of NbN and during growth due to the limited amount of N, the carbonitrides enriches in C [154]. The investigations further revealed that Nb precipitates which are formed at the same time in ferrite (table 4) and in austenite (table 2) are larger and have a higher C content in ferrite. It is assumed that this is due to the lower solubility of Nb precipitates in ferrite than in austenite and the diffusivity of Nb in ferrite is higher than in austenite. By the faster growth of the Nb precipitates in ferrite, the available N is earlier consumed and C is used for the growth.

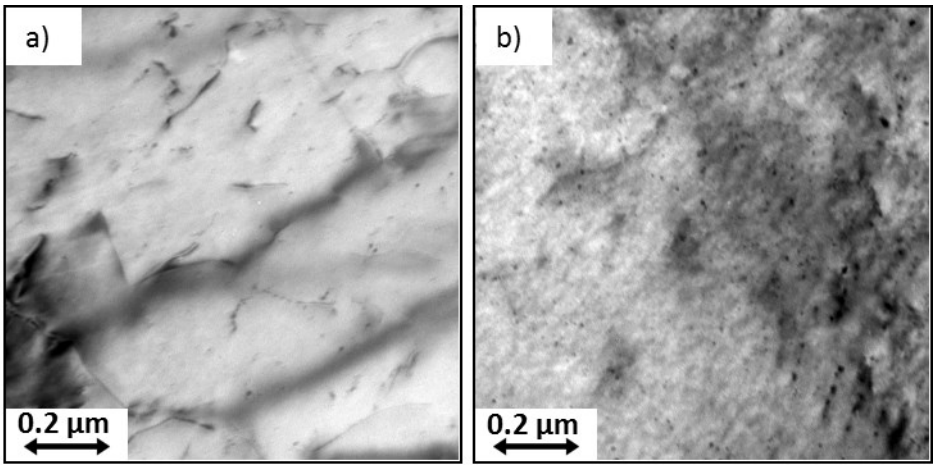

Figure 14: TEM bright field image of the ferrite phase for the Nb-alloy deformed at 700°C at a strain rate of 0.1 s^{-1} with different strains and isothermal holding: a) φ=0.05 / 10min, b) φ=0.7 / 10min [P2].

Investigations about the influence of the true strain revealed that with higher true strains the Nb precipitate volume fraction increases [P2]. In literature such a behavior is also reported, but there it is assumed that because of the higher true strain the incubation time is reduced, the diffusion is accelerated by pipe diffusion and the precipitates grow faster [23,74,109]. In this work [P2] the Nb precipitate phase fraction increase is caused by the increase of the number of precipitates and not the accelerated growth. Already by comparing the TEM images in figure 14 (figure14a for a true strain of φ=0.05 and a dwell time of 10min, and figure 14b for a true strain of φ=0.7 and a dwell time of 10min) it is visible that more particles exist at the condition deformed with a higher true strain. This assumption is also supported by the APT data in Table 4. After a true strain of φ=0.05 and a dwell time of 5min the precipitate phase fraction was 2.6×10^{-4} and after a true strain of φ=0.7 and the same dwell time the precipitate phase fraction was 7.5×10^{-4} but the Nb precipitate size was nearly the same with R_g is 1.01 nm respectively 1.02 nm.

4. Publications and Summary

[P1] Publication A: M. Nöhrer, S. Zamberger, H. Leitner

Strain-induced precipitation behaviour of a Nb-Ti-V steel in the austenite phase field

Steel research international, online published 28 February 2013

TEM and APT were used to investigate the precipitation behavior of a Nb (0.041 wt%), V (0.11 wt%) and Ti (0.018 wt%) micro-alloyed steel influenced by a deformation process in the austenite region. After solution annealing at 1250°C the entire Nb and V amounts are in solid solution. The thermic stable TiN precipitates do not dissolve and Ti is not in solid solution. These TiN precipitates act as nucleation sites for Nb and V during the cooling process to deformation temperature. By this way precipitates with a TiN rich core and a V-rich shell are formed. Nb is nearly homogenously distributed over the precipitate. After deformation, strain induced precipitates occur, which consist mainly of Nb, V and small amounts of Ti. Smaller strain induced precipitates have a higher N than C-content, with growth the C-content increases.

[P2] Publication B: M. Nöhrer, W. Mayer, S. Zamberger, E. Kozeschnik, H. Leitner

Influence of deformation on the precipitation behaviour of Nb(CN) in austenite and ferrite

Submitted to **Metallurgical and Materials Transactions A**, April 2013

The evolution of Nb precipitates in low-alloy steel at 700°C, influenced by different deformation strains, is studied by APT and TEM. The results show that, with increasing deformation, also the volume fraction of the precipitates increases. The strain-induced dislocations act as nucleation sites for Nb precipitates. The chemistry of the Nb carbonitrides changes with longer dwell times after the deformation. In the early stages of the precipitates they are N rich and the larger the precipitates grow, the higher is their C fraction. The precipitation analysis in austenite and ferrite showed that Nb precipitates grown in ferrite are larger with a higher C fraction compared to the precipitates growing in the austenite at the same condition. The investigations also revealed that the volume fraction of Nb carbonitrides grown in ferrite is higher than that in the austenite phase.

[P3] Publication C: M. Nöhrer, S. Zamberger, S. Primig, H. Leitner

Atom probe study of V interphase precipitates and randomly formed V precipitates in ferrite

Submitted to **Micron**, April 2013

APT and TEM were used to analyze the precipitation reaction in V micro-alloyed steel after a thermo-mechanical process in the austenite and the ferrite phase. It was observed that only in the ferrite phase precipitates were formed, whereupon two different types were detected. Thus, the aim was to examine the difference between these two types. The first type was randomly formed precipitates from V supersaturated ferrite and the second type V interphase precipitates. The arrangement of the particles was different and also the chemical composition. The randomly formed precipitates were enriched in C and N, the interphase precipitates showed an enrichment of C and Mn. It was assumed because of the different nucleation site in which they were formed the chemistry is different. The randomly formed precipitates were formed in a ferrite matrix consisting mainly of 0.05 at% C, 0.68 at% Si, 0.03 at% N, 0.145 at% V and 1.51 at% Mn. The interphase precipitates were formed in a region with a higher C, Mn and V content.

[P4] Publication D: M. Nöhrer, W. Mayer, S. Zamberger, E. Kozeschnik, H. Leitner

Precipitation behavior of strain-induced V precipitates in ferrite at different temperatures in a 0.2 wt% carbon steel

Submitted to **Steel research international**, April 2013

The evolution of strain induced V precipitates at two different temperatures (600°C and 700°C) in ferrite was studied via APT and TEM. The experimental results are compared with simulation data, which was calculated by means of MatCalc. The study reveals that V carbonitrides are formed independently from the formation temperature. The early stages of the precipitates have a higher N content than C. With longer dwell times the C to N ratio changes from nitrogen rich to carbon rich. At 700°C formation temperature the growth of the precipitates and the change from higher N to higher C occurs faster than at 600°C. Due to the faster growth the V content in solid solution decreases earlier. The simulated data fitted well with the experimental result which leads to the assumption that simulation is a useful tool to predict microstructural changes.

Summary

The aim of the present thesis was to gain knowledge about the precipitation behavior and evolution of micro-alloying elements in a 0.2 wt% C steel. Micro-alloying elements are used in many different applications to improve the mechanical properties without influencing the technological properties. Although, the effects of these elements have been known since 1930 and the influences on the microstructure of steels are well established new application areas and manufacturing processes require a deeper understanding of these effects. Also the prediction of the microstructure by thermo dynamical simulation is a big challenge where a deeper understanding of the microstructural evolution is essential. The combination of APT and TEM generate an ideal way to investigate the behavior of micro-alloying elements in steel because of their ability to gain information in an nm size range. Due to the affinity of micro-alloying elements to form nitrides, carbides and carbonitrides APT is adequate to detect the behavior of C and N in the precipitates. TEM and EDX measurements give less information about the C and N behavior, but by these methods the distribution-, number density-, size of precipitates and the type of nucleation can be analyzed. Consequently, the precipitation behavior was mainly analyzed by APT and TEM.

The main investigations were done on steel alloyed one time with V, one time with Nb and one time with Nb, V and Ti. At the material alloyed with 3 micro-alloying elements the precipitation behavior in austenite was investigated. This work [P1] revealed that after deformation strain induced precipitates occurred. They consisted mainly of the micro-alloying elements Nb and V and the C/N ratio was 1:1. In this precipitates the Ti content was slightly increased whereby it was assumed that Ti is in low amounts in solid solution and small strain induced TiN acted as nucleation sites for Nb and V. At undissolved TiN particles during isothermal aging in the austenite phase a V, Nb and C shell was detected [P1]. A study [P2] of strain induced Nb carbonitrides showed that with longer dwell times after deformation the C/N ratio of the particles changed from N to C rich. That happened because of the limited amount of N for precipitation. When the entire N was consumed C was used for the growth of the Nb(C, N) particles and the C content enriches. The investigations also revealed that Nb(C, N) which were formed at the same time in ferrite and austenite were larger and had a higher C content in ferrite. This was mainly caused by faster growth due to the lower solubility of Nb carbides, nitrides and carbonitrides in ferrite and on the other hand due to the higher diffusivity of Nb in ferrite. By means of APT and TEM it was detected that with higher true

strain the Nb precipitate phase fraction increases due to a higher number of precipitates and not by accelerated particle growth [P2]. In V micro-alloyed steel during the γ-α transformation V interphase precipitates were formed. The formation of this precipitates is discussed differently in literature. Two main theories exist, the ledge mechanism [131,132,135] and the solute depletion model [146,149]. For clarification which process is responsible for the interphase precipitation further investigations should be done. However, the results in this work [P3] showed that the γ-α interface enriches in V, Mn and C by formation of a depletion zone in the ferrite region which supports the solute depletion model. Comparison of the interphase precipitates and the randomly distributed precipitates indicated that the interphase precipitates were enriched in Mn and V and the randomly distributed precipitates were enriched in C and N. It was assumed that the difference resulted from the region in which they were formed and the interphase precipitates were formed in a region with a much higher Mn, V and C content than the randomly formed precipitates [P3]. In the course of this doctoral thesis also the formation of V strain induced precipitates in ferrite was investigated and compared with simulation calculations [P4]. The results revealed that the early stages of the V precipitates were N rich and with longer dwell times the C content increased. This was also observed by Nb precipitates and can be explained by the same way, due to the N depletion by precipitation. Furthermore, the investigations showed that the precipitate evolution in ferrite at higher temperatures was faster than at lower temperatures because of the higher diffusivity of V. The comparison of the experimental and simulation results showed that the tendency of the evolution of the precipitate size and chemistry and the V depletion in ferrite solid solution for the different temperatures are equal and the current simulation models are useful tools to predict the microstructure evolution [P4].

Micro-alloying elements are investigated for many years, but deeper understanding is necessary to improve the properties of micro alloyed steels. On the scientific site the clarification of the precipitation process of interphase precipitates is a big challenge. Also the behavior of micro-alloying elements in steels with higher C content requires further investigations because of the unusual use of micro-alloying elements in this field till today. Nowadays, the challenges for manufactures are the specific adjustment of microstructures to achieve the required properties of such steels. Thereby not only the influence of the micro-alloying elements is important also the control of the microstructure due to cooling. By improved knowledge of the influence of the micro-alloying elements on the phase transformation also controlled cooling is easier to handle and a more efficient way to produce heavy-duty steels is possible.

5. Bibliography

[1] E.F. Cone, Steel (1934) 41.

[2] H. Neumeister, H.J. Wiester, Stahl Und Eisen 65 (1945) 36.

[3] J. Strauss, F.F. Franklin, Metals Handbook, ASM, Cleveland, OH, 1948.

[4] G.F. Comstock, Transformation ASM 28 (1940) 608.

[5] F.M. Becket, R. Franks, US Patent No. 2,158,651, 1939.

[6] F.M. Becket, R. Franks, US Patent No. 2,158,652, 1939.

[7] F.M. Becket, R. Franks, US Patent No. 2,194,178, 1940.

[8] F.M. Becket, R. Franks, US Patent No. 2,264,355, 1941.

[9] A.J. DeArdo, M.J. Hua, K.G. Cho, C.I. Garcia, Materials Science and Technology 25 (2009) 1074.

[10] C. Ouchi, ISIJ International 41 (2001) 542.

[11] M.K. Graff, H.G. Hillenbrand, P.A. Peters, Accelerated Cooling of Steel, TMS-AIME, Warrendale, PA, 1986.

[12] M. von Heimendahl, Einführung in Die Elektronenmikroskophie, Vieweg, Braunschweig, 1970.

[13] D.B. Williams, C.B. Carter, Transmission Electron Microscopy, Springer, New York, 2009.

[14] M.K. Miller, A. Cerezo, M.G. Hetherington, G.D.W. Smith, Atom Probe Field Ion Microscopy, Oxford University Press Inc., Oxford, 1996.

[15] S.G. Hong, H.J. Jun, K.B. Kang, C.G. Park, Scripta Materialia 48 (2003) 1201.

[16] S. Yannacopoulos, M.C. Chaturvedi, Canadian Metallurgical Quarterly 27 (1988) 163.

[17] S.F. Medina, M.I. Vega, M. Gómez, P.P. Gómez, ISIJ International 45 (2005) 1307.

[18] J.W. Cahn, Acta Metallurgica 10 (1962) 789.

[19] L. Bäcke, ISIJ International 50 (2010) 239.

[20] K. Banks, A. Koursaris, F. Verdoorn, A. Tuling, Materials Science and Technology 17 (2001) 1596.

[21] N. Maruyama, R. Uemori, M. Sugiyama, Materials Science and Engineering A 250 (1998) 2.

[22] S. Vervynckt, K. Verbeken, P. Thibaux, Y. Houbaert, Materials Science and Engineering A 528 (2011) 5519.

[23] S.F. Medina, A. Quispe, P. Valles, J.L. Banos, ISIJ International 39 (1999) 913.

[24] R. Lagneborg, T. Siwecki, S. Zajac, B. Hutchinson, The Scandanavian Journal of Metallurgy (1999).

[25] Y. Li, J.A. Wilson, D.N. Crowther, P.S. Mitchell, A.J. Craven, T.N. Baker, ISIJ International 44 (2004) 1093.

[26] Y. Li, J.A. Wilson, A.J. Craven, P.S. Mitchell, D.N. Crowther, T.N. Baker, Materials Science and Technology 23 (2007) 509.

[27] M.M.A. Bepari, Materials Science and Technology 6 (1990) 338.

[28] S.F. Medina, A. Quispe, Steel Research 67 (1996) 257.

[29] S.F. Medina, J.E. Mancilla, ISIJ International 36 (1996) 1063.

[30] T. Gladman, The Physical Metallurgy of Microalloyed Steels, The Institute of Materials, The University Press, London, 1997.

[31] J.G. Speer, J.R. Michael, S.S. Hansen, Metallurgical Transactions A 18A (1987) 211.

[32] R.W.K. Honeycombe, R.F. Mehl Medalist, Metallurgical Transactions A 7A (1976) 915.

[33] R.W.K. Honeycombe, Metal Science 29th Hatfield memorial lecture (1980) 201.

[34] G. Gottstein, Physikalische Grundlagen der Materialkunde, 2nd ed., Springer Verlag, Berlin Heidelberg New York, 2001.

[35] H.K.D.H. Bhadeshia, Bainite in Steels, The Institute of Materials, London, 1992.

[36] H.J. Bargel, G. Schulze, Werkstoffkunde, 8th ed., Springer Verlag, Berlin Heidelberg New York, 2004.

[37] G.R. Speich, W.C. Leslie, Metallurgical Transactions 3 (1972) 1043.

[38] I.M. Robertson, Materials Science and Technology 9 (1993) 1031.

[39] F.B. Pickering, in: HSLA Steels Technology & Applications, American Society for Metals, Philadelphia, PA, 1984, pp. 1–31.

[40] B.D. Jana, A.K. Chakrabarti, K.K. Ray, Materials Science and Technology 19 (2003) 80.

[41] T. Tanaka, International Metals Reviews 26 (1981) 185.

[42] M. Zhao, K. Yang, F. Xiao, Y. Shan, Materials Science and Engineering A 355 (2003) 126.

[43] J.L. Lee, M.H. Hon, G.H. Cheng, Journal of Materials Science 22 (1987) 2767.

[44] M.C. Zhao, K. Yang, Y. Shan, Materials Science and Engineering A 335 (2002) 14.

[45] M. Zhao, T. Hanamura, H. Qiu, K. Nagai, Y. Shan, K. Yang, ISIJ International 45 (2005) 116.

[46] M. Thompson, M. Ferry, P.A. Manohar, ISIJ International 41 (2001) 891.

[47] A.B. Cota, D.B. Santos, Materials Characterization 44 (2000) 291.

[48] A. Yoshi, M. Fujioka, Y. Watanabe, K. Nishioka, H. Morikawa, ISIJ International 32 (1992) 395.

[49] C. Zhou, R. Priestner, ISIJ International 36 (1996) 1397.

[50] H. Asahi, A. Yagi, M. Ueno, Metallurgical and Materials Transactions A 29A (1998) 1375.

[51] A.K. Panda, P.K. Ray, R.I. Ganguly, Materials Science and Technology 16 (2000) 648.

[52] M. Cabbibo, A. Fabrizi, M. Merlin, G.L. Garagnani, Journal of Materials Science 43 (2008) 6857.

[53] A. Ghosh, S. Das, S. Chatterjee, B. Mishra, P. Ramachandra Rao, Materials Science and Engineering A 348 (2003) 299.

[54] A. Bakkaloglu, Materials Letters 56 (2002) 200.

[55] H. Beladi, I.B. Timokhina, S. Mukherjee, P.D. Hodgson, Acta Materialia 59 (2011) 4186.

[56] S.C. Hong, K.S. Lee, Materials Science and Engineering A 323 (2002) 148.

[57] M.R. Hickson, P.J. Hurley, R.K. Gibbs, G.L. Kelly, P.D. Hodgson, Metallurgical and Materials Transactions A 33A (2002) 1019.

[58] P.D. Hodgson, M.R. Hickson, R.K. Gibbs, Scripta Materialia 40 (1999) 1179.

[59] G. Chen, W. Yang, S. Guo, Z. Sun, Journal Of University Of Science And Technology Beijing 14 (2007) 36.

[60] X.Q. Yuan, Z.Y. Liu, S.H. Jiao, L.Q. Ma, G.D. Wang, ISIJ International 46 (2006) 579.

[61] B. Dutta, E.J. Palmiere, C.M. Sellars, Acta Materialia 49 (2001) 785.

[62] B. Dutta, E. Valdes, C.M. Sellars, Acta Metallurgica Et Materialia 40 (1992) 653.

[63] E.V. Pereloma, B.R. Crawford, P.D. Hodgson, Materials Science and Engineering A 299 (2001) 27.

[64] S.F. Medina, A. Quispe, ISIJ International 36 (1996) 1295.

[65] T. Furuhara, T. Maki, Materials Science and Engineering A 312 (2001) 145.

[66] J.-Y. Cho, D.-W. Suh, J.-H. Kang, H.-C. Lee, ISIJ International 42 (2002) 1321.

[67] S.C. Hong, S.H. Lim, H.S. Hong, K.J. Lee, D.H. Shin, K.S. Lee, Materials Science and Engineering A 355 (2003) 241.

[68] S.F. Medina, M. Gomez, J.J. Chaves, P.P. Gomez, P. Adeva, Materials Science Forum 500-501 (2005) 371.

[69] R. Radis, E. Kozeschnik, Modelling and Simulation in Materials Science and Engineering 20 (2012) 1.

[70] S. Shanmugam, M. Tanniru, R.D.K. Misra, D. Panda, S. Jansto, Materials Science and Technology 21 (2005) 883.

[71] K. Inoue, N. Ishikawa, I. Ohnuma, H. Ohtani, K. Ishida, ISIJ International 41 (2001) 175.

[72] Z. Wang, X. Mao, Z. Yang, X. Sun, Q. Yong, Z. Li, Y. Weng, Materials Science and Engineering A 529 (2011) 459.

[73] R.C. Sharma, V.K. Lakshmanan, J.S. Kirkaldy, Metallurgical Transactions A 15A (1984) 545.

[74] J.S. Park, Y.S. Ha, S.J. Lee, Y.K. Lee, Metallurgical and Materials Transactions A 40A (2009) 560.

[75] J. Peng, S. Wang, Y. Dong, L. Liu, Y. Zhou, E. Chen, Journal of Iron and Steel Research, International 15 (2008) 19.

[76] R. Stasko, H. Adrian, A. Adrian, Materials Characterization 56 (2006) 340.

[77] R.M. Poths, R.L. Higginson, E.J. Palmiere, Scripta Materialia 44 (2001) 147.

[78] A. Pandit, A. Murugaiyan, A.S. Podder, A. Haldar, D. Bhattacharjee, S. Chandra, R.K. Ray, Scripta Materialia 53 (2005) 1309.

[79] X. Zhuo, X. Wang, W. Wang, H.-G. Lee, Journal Of University Of Science And Technology Beijing 14 (2007) 112.

[80] S.G. Hong, K.B. Kang, C.G. Park, Scripta Materialia 46 (2002) 163.

[81] H.R. Wang, W. Wang, Journal of Materials Science 44 (2008) 591.

[82] S.Q. Yuan, G.L. Liang, Materials Letters 63 (2009) 2324.

[83] M. Balart, C.L. Davis, M. Strangwood, Scripta Materialia 50 (2004) 371.

[84] S. Shanmugam, M. Tanniru, R.D.K. Misra, D. Panda, S. Jansto, Materials Science and Technology 21 (2005) 165.

[85] J.-G. Jung, J.-S. Park, J. Kim, Y.-K. Lee, Materials Science and Engineering A 528 (2011) 5529.

[86] N. Maazi, N. Rouag, Journal of Crystal Growth 243 (2002) 361.

[87] E. Nes, N. Ryum, O. Hunderi, Acta Metallurgica 33 (1985) 11.

[88] D.N. Crowther, B. Mintz, Materials Science and Technology 2 (1986) 1099.

[89] S.S. Hansen, L.B. Vander Sande, M. Cohen, Metallurgical Transactions A 11A (1980) 387.

[90] R.D. Doherty, D.J. Srolovitz, A.D. Rollett, M.P. Anderson, Scripta Metallurgica 21 (1987) 675.

[91] J. Fernández, S. Illescas, J.M. Guilemany, Materials Letters 61 (2007) 2389.

[92] K. Banerjee, M. Militzer, M. Perez, X. Wang, Metallurgical and Materials Transactions A 41A (2010) 3161.

[93] M. Hamada, Y. Fukada, Y. Komizo, ISIJ International 35 (1995) 1196.

[94] O. Flores, L. Martinez, Journal of Materials Science 32 (1997) 5985.

[95] D. Chakrabarti, C.L. Davis, M. Strangwood, Materials Science and Technology 25 (2009) 939.

[96] S.F. Medina, Journal of Materials Science 32 (1997) 1487.

[97] S.F. Medina, M. Chapa, P. Valles, A. Quispe, M.I. Vega, ISIJ International 39 (1999) 930.

[98] S.F. Medina, C.A. Hernandez, Acta Metallurgica 44 (1996) 165.

[99] S.F. Medina, A. Quispe, ISIJ International 41 (2001) 774.

[100] S. Vervynckt, K. Verbeken, P. Thibaux, M. Liebeherr, Y. Houbaert, ISIJ International 49 (2009) 911.

[101] B. Mintz, R. Abushosha, J.J. Jonas, ISIJ International 32 (1992) 241.

[102] S.F. Medina, A. Quispe, M. Gomez, Materials Science and Technology 17 (2001) 536.

[103] L. Ma, Z. Liu, S. Jiao, X.-Q. Yuan, D. Wu, Journal of Iron and Steel Research, International 15 (2008) 31.

[104] N. Maruyama, G.D.W. Smith, Materials Science and Engineering A 327 (2002) 34.

[105] M. Gomez, S.F. Medina, Materials Science Forum 500-501 (2005) 147.

[106] H. Gao, Z. Xie, Y. Yu, Y. Fang, J. Wang, B. Sun, ISIJ International 49 (2009) 546.

[107] A.I. Fernández, P. Uranga, B. López, J.M. Rodriguez-Ibabe, ISIJ International 40 (2000) 893.

[108] O. Kwon, A. Deardo, Acta Metallurgica Et Materialia 39 (1991) 529.

[109] B. Dutta, C.M. Sellars, Materials Science and Technology 3 (1987) 197.

[110] M.G. Burke, L.J. Cuddy, J. Piller, M.K. Miller, Materials Science and Technology 4 (1988) 113.

[111] P. Liu, Phase Analysis in Steel Using Analytical Transmission Electron Microscopy, First, Sandvik Materials Technology, Sandviken, 2004.

[112] R.G. Baker, J. Nutting, Precipitation Processes in Steels, London, 1959.

[113] T.N. Baker, Materials Science and Technology 25 (2009) 1083.

[114] P.S. Bandyopadhyay, S. Kundu, S.K. Ghosh, S. Chatterjee, Metallurgical and Materials Transactions A 42A (2010) 1051.

[115] P. Maugis, M. Goune, Acta Materialia 53 (2005) 3359.

[116] M. Hillert, L.I. Staffansson, Acta Chemica Scandinavica 24 (1970) 3618.

[117] S.W. Thompson, G. Krauss, Metallurgical Transactions A 20A (1989) 2279.

[118] W. Liu, X. Zhu, X. Wang, X. Xiong, Materials Science Forum 654-656 (2010) 114.

[119] C.P. Reip, S. Shanmugam, R.D.K. Misra, Materials Science and Engineering A 424 (2006) 307.

[120] H.J. Jun, K.B. Kang, C.G. Park, Scripta Materialia 49 (2003) 1081.

[121] A.I. Fernández, P. Uranga, B. López, J.M. Rodriguez-Ibabe, Materials Science and Engineering A 361 (2003) 367.

[122] A.J. Craven, K. He, L.A.J. Garvie, T.N. Baker, Acta Materialia 48 (2000) 3857.

[123] M. Charleux, W.J. Poole, M. Militzer, A. Deschamps, Metallurgical and Materials Transactions A 32A (2001) 1635.

[124] H. Zou, J.S. Kirkaldy, Metallurgical Transactions A 23A (1992).

[125] M.J. Balart, C.L. Davis, M. Strangwood, Materials Science and Engineering A 284 (2000) 1.

[126] M. Prikryl, A. Kroupa, G.C. Weatherly, S.V. Subramanian, Metallurgical and Materials Transactions A 27A (1996) 1149.

[127] P.R. Wilyman, R.W.K. Honeycombe, Metal Science 16 (1982) 295.

[128] J. Odqvist, M. Hillert, J. Agren, Acta Materialia 50 (2002) 3211.

[129] S. Mukherjee, I.B. Timokhina, C. Zhu, S.P. Ringer, P.D. Hodgson, Acta Materialia 61 (2013) 2521.

[130] H. Kestenbach, S.S. Campos, E.V. Morales, Materials Science and Technology 22 (2006) 615.

[131] H.I. Aaronson, M.R. Plichta, G.W. Franti, K.C. Russell, Metallurgical Transactions A 9A (1978) 363.

[132] R.W.K. Honeycombe, in: International Conference on HSLA Steels 1985, 1985, pp. 243–250.

[133] R.A. Ricks, P.R. Howell, Acta Metallurgica 31 (1983) 853.

[134] A. Barbacki, R.W.K. Honeycombe, Metallography 9 (1976) 277.

[135] A.T. Davenport, R.W.K. Honeycombe, Proceedings of the Royal Society of London A 322 (1971) 191.

[136] A.T. Davenport, F.G. Berry, R.W.K. Honeycombe, Metal Science Journal 2 (1968) 104.

[137] P. Li, J.A. Todd, Metallurgical Transactions A 19A (1988) 2139.

[138] P. Li, J.A. Todd, Metallurgical Transactions A 19A (1988) 2139.

[139] G. Miyamoto, R. Hori, B. Poorganji, T. Furuhara, ISIJ International 51 (2011) 1733.

[140] T. Murakami, H. Hatano, G. Miyamoto, T. Furuhara, ISIJ International 52 (2012) 616.

[141] A.D. Batte, R.W.K. Honeycombe, The Journal of Iron and Steel Institute 211 (1973) 284.

[142] S. Zajac, T. Siwecki, M. Korchynsky, Proc. Int. Symp. Low Carbon Steels for the 90's (1993) 139.

[143] J.M. Gray, R.B.G. Yeo, Transactions of the American Society of Metals 61 (1968) 255.

[144] G.L. Dunlop, C.-J. Carlsson, G. Frimodig, Metallurgical Transactions A 9A (1978) 261.

[145] N.K. Balliger, R.W.K. Honeycombe, Metallurgical Transactions A 11A (1980) 421.

[146] W. Roberts, Hot Deformation Studies on a V-microalloyed Steel, Stockholm, 1978.

[147] D.V. Edmonds, Journal of The Iron and Steel Institute (1972) 363.

[148] F.A. Khalid, D.V. Edmonds, Materials Science and Technology 9 (1993) 384.

[149] R. Lagneborg, S. Zajac, Metallurgical and Materials Transactions A 32A (2001) 39.

[150] R. Okamoto, J. Ågren, Acta Materialia 58 (2010) 4791.

[151] J.G. Lenard, M. Tajima, ISIJ International 735 (1995) 1509.

[152] M.M.A. Bepari, Metallurgical Transactions A 21A (1990) 2839.

[153] M.D.C. Sobral, P.R. Mei, H.-J. Kestenbach, Materials Science and Engineering A 367 (2004) 317.

[154] M. Perez, E. Courtois, D. Acevedo, T. Epicier, P. Maugis, Philosophical Magazine Letters 87 (2007) 645.

[155] F. Perrard, C. Scott, ISIJ International 47 (2007) 1168.

6. Publications

6.1 Publications included into this Thesis

Paper A:

Strain-induced precipitation behavior of a Nb-Ti-V steel in the austenite phase field

M. Nöhrer, S. Zamberger, H. Leitner

Steel research international, online published 28 February 2013

DOI: 10.1002/srin.201200257

Paper B:

Influence of deformation on the precipitation behavior of Nb(CN) in austenite and ferrite

M. Nöhrer, W. Mayer, S. Zamberger, E. Kozeschnik, H. Leitner

Submitted to **Metallurgical and Materials Transactions A**, April 2013

Paper C:

Atom probe study of V interphase precipitates and randomly formed V precipitates in ferrite

M. Nöhrer, S. Zamberger, S. Primig, H. Leitner

Submitted to **Micron**, May 2013

Paper D:

Precipitation behavior of strain-induced V precipitates in ferrite at different temperatures in a 0.2 wt% carbon steel

M. Nöhrer, W. Mayer, S. Zamberger, E. Kozeschnik, H. Leitner

Submitted to **Steel research international**, May 2013

6.2 (Co)Supervised Diploma Thesis

Einfluss der Mikrolegierungselemente Nb und V auf den Vergütungsstahl 42CrMo4

Dominic Moisi, finished in October 2012

7. Paper A

Strain-induced precipitation behavior of a Nb-Ti-V steel in the austenite phase field

M. Nöhrer, S. Zamberger, H. Leitner

Steel research international, online published 28 February 2013

DOI: 10.1002/srin.201200257

www.steel-research.de

steel research international

FULL PAPER

Strain-Induced Precipitation Behavior of a Nb–Ti–V Steel in the Austenite Phase Field

Matthias Nöhrer,* Sabine Zamberger, and Harald Leitner

The precipitation behavior of a Nb (0.041 wt%), V (0.11 wt%), and Ti (0.018 wt%) micro-alloyed steel influenced by a deformation process in the austenite region has been investigated by transmission electron microscopy and atom probe. After solution annealing at 1250 °C, nearly the entire Nb and V amount is in solid solution. Ti does not go into in solid solution and stays stable as TiN precipitates. During the cooling process to deformation temperature, these TiN precipitates act as nucleation sites for Nb and V. Precipitates with a TiN rich core and a V-rich shell are formed. Nb is homogenously distributed over the precipitate. After deformation, strain induced precipitates occur, which consist mainly of Nb, V, and only a little Ti. Smaller strain induced precipitates have a higher N-content than C, with growth the C-content increases.

1. Introduction

As a consequence of the increasing requirements in the automotive industry and in pipeline applications, it is necessary to improve the mechanical properties of steels. By increasing the carbon content, it is possible to increase the strength, but carbon has a negative impact on technological properties like weldability and formability. To improve the mechanical properties of low and medium carbon steels without influencing the technological properties negatively, micro-alloying elements, like Ti, V, and Nb are added. These elements influence the austenitic grain size and the recrystallization behavior. Furthermore, they cause precipitation strengthening by carbide, nitride, and carbonitrides formation.[1] Ti has mainly an influence on grain refinement, by TiN precipitation in the melt or in the austenite region.[2–4] V is mostly added for precipitation hardening. The V particles can precipitate at interphase boundaries during the austenite–ferrite transformation or in ferrite region. The precipitation process can be facilitated by deformation.[5] During deformation, the dislocation density increases which generate more nucleation sites for the V-precipitates. The most effective V-precipitates for precipitation hardening are VC and V(C, N).[1,6] Nb is the most important micro-alloying element, as it inhibits austenite grain growth and austenite recrystallization by the formation of NbC and Nb(C, N) precipitates.[7–9] However, Nb also has a strong effect on the austenite grain growth when it is in solid solution by the so-called solute drag effect.[10] It additionally increases the strength by precipitation hardening, because of fine distributed precipitates in the ferrite phase. Basically, to obtain fine ferrite grains, fine austenite grains are required.[11,12] To achieve these fine austenite grains, undissolved precipitates or precipitates which form in the austenite are necessary. The latter ones preferentially nucleate on grain boundaries, sub-grain-boundaries, interfaces, dislocations, or vacancies.[1,13,14] Precipitates which were formed in austenite do not increase the strength by precipitation hardening.[5,15] A further consequence of these particles is that the potential for precipitate formation in the ferrite decreases.[1,16]

The combination of the individual micro-alloying elements results in the formation of carbonitrides with a complex chemistry. The formation of these precipitates, their chemistry and assembling depends on the solubility of the different micro-alloying elements. The different micro-alloying carbides and nitrides are variable stable. In the following order the precipitates from the highest to the lowest stability in austenite are arranged: TiN > NbN > VN > NbC > TiC > VC. This solubility behavior also influences the formation of complex precipitates. At different solution annealing temperatures different amounts of precipitates dissolve and be available for precipitation at the further heat treatment. A model for the

[*] M. Nöhrer, H. Leitner
Christian Doppler Laboratory for Early Stages of Precipitation, Department of Physical Metallurgy and Materials Testing, Montanuniversität Leoben, Franz-Josef-Straße 18, A-8700 Leoben, Austria
Email: matthias.noehrer@unileoben.ac.at
S. Zamberger
Voestalpine Stahl Donawitz GmbH & Co KG, Kerpelystraße 199, A-8700 Leoben, Austria

DOI: 10.1002/srin.201200257

steel research international

www.steel-research.de

formation of complex stoichiometric precipitates, by considering the change of the free energy, was developed by Hillert and Staffansson.[17] Steels alloyed with Nb and V form complex NbV carbonitrides.[18] These complex carbonitrides occur in a temperature range between 800 and 1100°C. By adding Nb to V steel, the activity coefficient of C and N decreases, thereby the solubility of VN increases. Further it is reported that Nb carbonitrides earlier precipitates than V precipitates because of the lower solubility in austenite. Nb precipitates may form at 1200°C. At this temperature V is completely soluble in austenite. At lower temperatures, of about 1000°C the solubility of V decreases and it diffuses into the Nb precipitates. Thereby complex NbV carbonitrides are formed.[18] Another effect is that the precipitation incubation time is delayed at temperatures below 900°C.[7] Steels alloyed with Nb and Ti form complex NbTi carbonitrides. The temperature range in which these complex carbonitrides occur is between 800 and 1200°C. TiN is known as the most stable micro-alloying precipitate. It is assumed that the dissolution temperature of these precipitates is comparable to pure TiN.[19] When the material is reheated to 1200°C, the complex carbonitrides dissolve partially. As higher the solution annealing temperature as lower is the amount of Nb in the complex TiNb carbonitrides, because only the Nb part dissolves.[20,21] However, after reheating the undissolved TiN and (Nb, Ti) (C, N) act as nucleation sites for precipitates. At the Ti rich precipitates Nb rich precipitates nucleate, they form a cap part at the Ti rich precipitates. It is assumed that the heterogeneous nucleation is preferred, due to the decrease of barrier energy for nucleation. The barrier energy is the energy which is needed to create a precipitate/matrix interface. By adding Ti into Nb alloyed steels the incubation time for NbC is increased.[22] A reason for this behavior is that the amount of Nb in solution is lower when Ti is alloyed because not the entire Nb is in solution after solution annealing. Furthermore it is reported, that during isothermal heat treatments at lower temperatures in the austenite region, the precipitates are Nb-rich and at higher temperatures the carbonitrides are Ti-rich. [19–22] Steels alloyed with Ti and V form complex TiV carbonitrides. Their precipitation sequence starts with TiN at higher temperatures, which act as nucleation sides for the precipitation of VC at lower temperatures. At temperatures between 850 and 1100°C precipitates of the type (Ti, V) (C, N) are obtained. It is also reported that these TiV carbonitrides might have a Ti and V concentration gradient with a V-rich shell and a Ti-rich core.[23,24] By using the Hillert–Staffanson equilibrium, it is suggested that the phase separation of (Ti, V) (C, N) precipitates into TiN-rich and VC-rich regions may occur at temperatures close to the A_{e3} temperature in the austenite phase field.[25] The precipitation behavior of complex carbonitrides is also influenced by deformation processes. Through deformation dislocations, deformation bands, and sub-grain structures develop which act as nucleation sides and accelerates the precipitation process in the material.[18,27] The precipitation behavior of steels alloyed with Nb, V, and Ti are less frequently discussed in literature. It is known that NbTiV complex carbonitrides occur, but it is also reported that in such alloys not only triplex precipitates are formed. Various authors found duplex precipitates such as TiV, NbV, and TiNb carbonitrides.[25–31] However, all these precipitates have been reported to form in a ferritic matrix.

Thus, this work focuses on the precipitation behavior of a Ti–Nb–V steel in the austenite after deformation, especially on the influence of Ti on the precipitation behavior of Nb and V. Due to the stable TiN precipitates Nb and V can nucleate easier at these precipitates. Because of depletion of Nb and V in the matrix these elements have a lower influence on the solute drag effect and on the precipitation hardening effect. By understanding the effect of Ti on the precipitation behavior on the other elements it is easier to improve such steels. The precipitates were characterized by transmission electron microscopy (TEM) and atom probe tomography (APT).

2. Experimental

The nominal chemical composition of the Nb–V–Ti steel is shown in Table 1. Figure 1 shows the applied heat treatment and deformation procedure. Deformation was done under uni-axial compression in a servo hydraulic "Servotest TMTS" machine. The specimens were heated by furnace heating and the temperature was controlled by thermocouples. For that, cylindrical samples with a diameter of 30 mm and a height of 50 mm were used. After austenitization at 1250°C for 30 min, the specimens were cooled to 900°C, with a cooling rate of 3°C s^{-1}. After a dwell time of 8 min at 900°C, the samples were deformed with a deformation φ of 0.7 and a deformation rate $\dot{\varphi}$ of 0.1, which leads to a deformation process of 7 s. After

Nb–V–Ti-steel	C	Si	Mn	V	Nb	Ti	N
wt%	0.2	0.28	1.39	0.11	0.041	0.018	0.013
at%	0.92	0.55	1.40	0.12	0.024	0.021	0.043

Table 1. Chemical composition of the steel.

www.steel-research.de

steel research international

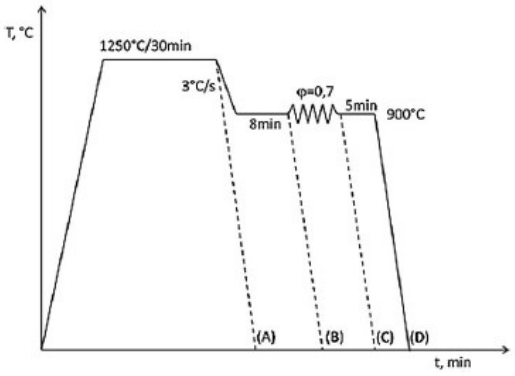

Figure 1. Schematic representation of the heat treatment used for the study of the behavior of micro-alloying elements. A–D indicates the specimen types which were investigated.

deformation, an isothermal sequence of 5 min was added. At the end of this sequence, the material was water quenched. The specimens were investigated after the whole heat treatment (D in Figure 1), after the austenitization process (A), before (B) and after deformation (C). The samples for the microstructural characterization were cut parallel to the deformation direction. To analyze the types and chemistry of precipitates during the thermo-mechanical treatment, the material was investigated via TEM and APT. The thin foils for the TEM investigations were made by mechanical thinning. After that, the samples were prepared by electro-polishing in a Tenu–Pol 5. For the TEM investigations, a TEM Philips CM12 was used. Qualitative energy dispersive X-ray spectroscopy (EDS) was used to identify the chemical composition of the precipitates. For the preparation of the atom probe samples, a standard two-stage electro polishing procedure was used.[32] The atom probe measurements were carried out in voltage mode on a LEAP 3000X HR from Cameca, using a pulse fraction of 20% and a pulse repetition rate of 200 kHz at a sample temperature of 60 K. In the atom probe analysis, V was detected as V^{2+} (25, 25.5), V^{3+} (17) and also as VN^{2+} (32.5, 32). Nb was detected as Nb^{2+} (46.5), Nb^{3+} (31), Nb^{4+} (23.25) and also in combination with N, NbN^{2+} (53.5) and NbN^{3+} (35.66). Ti was detected as Ti^{2+} (24) and Ti^{3+} (16). For the determination of the chemical composition of the atom probe specimens the IVAS 3.4.3 tool decomposition analysis was used. To improve statistics in case of the micro-alloying elements in solid solution, several atom probe measurements were made per condition. These measurements do not only represent the content of micro-alloying elements in solid solution, they also reveal the distribution of the elements. An important parameter for the distribution of the elements in the entire material is the standard deviation because it describes the homogeneity of the material. For determination of clustering of V and Nb in one atom probe measurement, frequency distribution analyze were done.[33] The parameter μ is graduator for the distribution of the alloying elements in a material in a range of 0–1.0 indicates that the element is homogenously distributed while 1 indicates a fully heterogeneous distribution.

3. Results

3.1. Condition after Solution Annealing (A)

After solution annealing at 1250 °C for 30 min, these specimens were water-quenched to room temperature. In order to examine the precipitates after the solution annealing, TEM was used. It should be noted that all present precipitates were identified via TEM-EDS analysis. Figure 2a shows a representative TEM bright field image of this

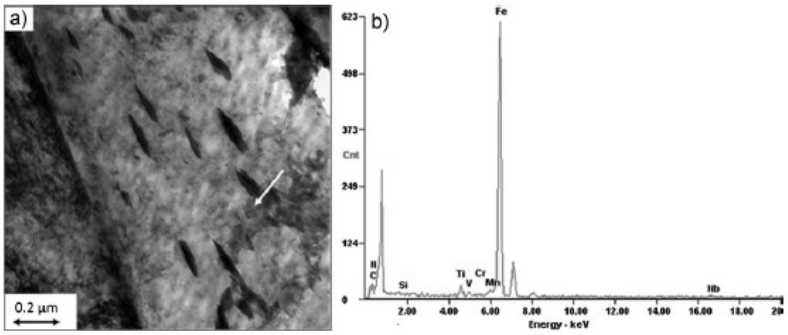

Figure 2. a) TEM bright field image of TiN precipitate (marked by the arrow) in a martensitic matrix after solution annealing (A), b) corresponding EDS spectrum of this precipitate.

steel research international

www.steel-research.de

	V	Nb	Ti
After solution annealing (A)	0.130 ± 0.007	0.035 ± 0.007	0.002 ± 0.002
After deformation (C)	0.131 ± 0.010	0.015 ± 0.002	0
After isothermal heat treatment (D)	0.116 ± 0.004	0.015 ± 0.001	0.002 ± 0.003

The data sets were determined via APT and are given in at%.

Table 2. Micro-alloying elements in solid solution after solution annealing (A), deformation (B), and the isothermal heat treatment (D).

condition. In Figure 2a, a martensitic/bainitic structure can be seen which is due to the rapid quenching from solution annealing temperature. Inside the laths, dark elongated regions are clearly visible. These regions were identified by EDS as Fe-rich carbides. However, the present work does not focus on these types of precipitates. Additionally, Figure 2a shows a Ti-rich precipitate inside the laths, which is marked by an arrow. The corresponding TEM-EDS spectrum of the Ti-precipitate is shown in Figure 2b. The size of such precipitates is in the range of 50–70 nm. They exhibit a cubic shape. The shape and the presence of such precipitates at this condition indicates that the precipitate in Figure 2b is a TiN particle.[1] These precipitates are frequently found in this condition. For determination of the content of the micro-alloying elements in solid solution in this solution, atom probe investigations were conducted. Table 2 shows the fraction of micro-alloying elements in solution and also the corresponding standard deviations. APT measurements revealed a concentration of 0.13 at% ± 0.007 of V and 0.035 at% ± 0.007 of Nb. Almost no Ti is in solution, the measured content is 0.002 at% ± 0.002. The standard deviation of Nb and V is marginal which means that Nb and V are homogenously distributed in the material.

3.2. Condition before Deformation (B)

After the solution annealing for 30 min at 1250 °C these specimens were cooled to deformation temperature at 900 °C with a cooling rate of 3 °C s^{-1}, followed by a 8 min isothermal holding time. Figure 3a shows a bright field TEM image of this condition. Again a martensitic/bainitic lath structure can be seen. However, it seems that during cooling to 900 °C and subsequent isothermal annealing for 8 min, spherical precipitates have formed. These precipitates are marked by arrows in Figure 3a. Their size is in a range of 20–70 nm. A typical EDX spectrum of such precipitates indicates that they are enriched in Nb, V, and Ti (Figure 3b). Thus, it is supposed that these precipitates are carbonitrides.[28] The lath boundaries are decorated by a carbon film which appears dark in Figure 3a. Again, Fe-rich carbides can be found in this condition.

3.3. Condition after Deformation (C)

The influence of deformation on the precipitation behavior in this condition can be seen in Figure 4. Figure 4a shows a bright field TEM image with martensitic/bainitic laths. The

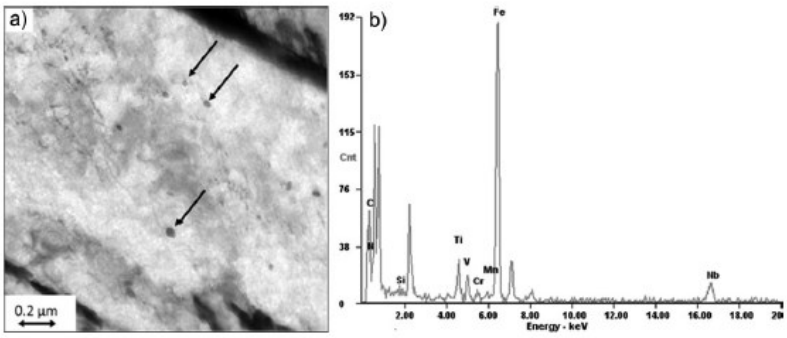

Figure 3. a) TEM bright field image of NbVTi-precipitates (marked by arrows) in a martensitic matrix before deformation (B), b) representative EDS image of the precipitates in this condition.

www.steel-research.de

steel research international

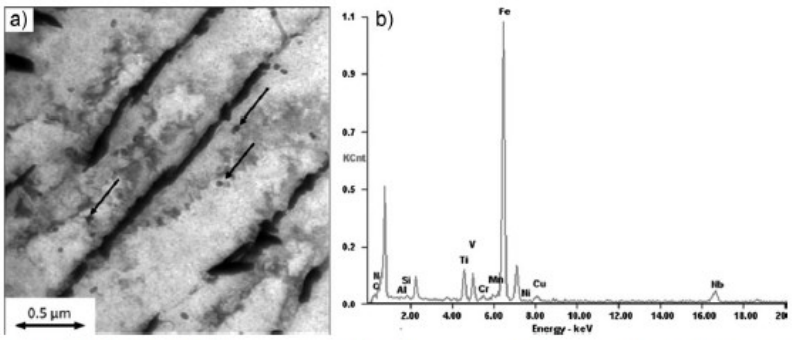

Figure 4. a) TEM bright field image of NbVTi-precipitates (marked by arrows) in a martensitic matrix after deformation (C), b) representative EDS image of the precipitates in this condition.

lath boundaries are covered with a carbon film, which appears as dark features in the TEM image. Inside the laths spherical precipitates (marked by arrows in Figure 4a) can again be found. In this condition, the precipitates exhibit a size in the range of 20–70 nm. The TEM-EDS spectrum in Figure 4b shows that they are enriched in Nb–V–Ti and, thus, it is supposed that they are of same type than before deformation.[28] Figure 5 shows the three dimensional reconstruction of the atomic positions of Nb and V after deformation and subsequent water-quenching. Visual inspection does not give any evidence of clustering of the carbide- and nitride-forming elements Nb and V. Analyses of the atom probe measurements by using the frequency distribution analysis[33] indicate that the micro-alloying elements are homogenously distributed. By using a block size of 1000 atoms, V has a μ value of 0.0619 and Nb of 0.0214. This might indicate that no additional precipitation or clusters are formed during deformation. Table 2 shows the fraction of micro-alloying elements in solid solution and the standard deviation of the concentrations. After deformation, about 0.131 at% ± 0.010 of V and 0.015 at% ± 0.002 of Nb are in solid solution, Ti was not detected here. Also in this condition, the mean concentration and the standard deviation show that the micro-alloying elements are in homogenously distributed.

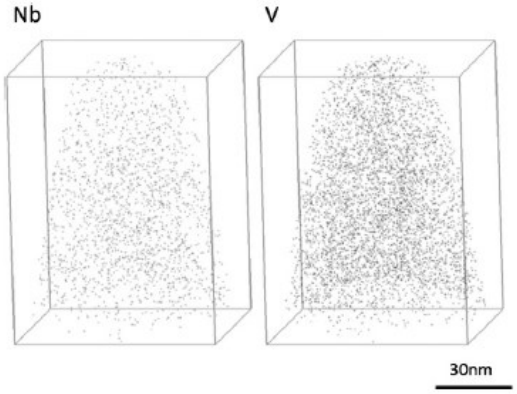

Figure 5. Three-dimensional reconstruction of a sample after deformation (C). The atom map shows the distribution of the Nb and V atoms.

3.4. Condition after Deformation and Subsequent Isothermal Heat Treatment (D)

In order to find out which precipitates occur in the austenitic field after deformation, an isothermal heat treatment at 900°C for 5 min was conducted after deformation, followed by water quenching the specimen. Figure 6a shows a bright field TEM image of this condition. The matrix exhibits a martensitic/bainitic structure. The microstructure contains several precipitates. Figure 6b shows the corresponding TEM-EDS spectrum of the precipitate which is marked by an arrow in Figure 6a. Based on the EDS analysis, it is assumed that the detected particle is a Nb–V–Ti precipitate. These particles have a size from 5–100 nm, exhibit spherical shapes, and are frequently found in the material. Figure 6c shows a TEM bright field image of another type of particles which precipitate in the material. The TEM-EDS spectrum of this precipitate illustrates that this particle only contains Nb and V. Compared to the precipitates which contain Ti, these precipitates are only frequently found. Figure 7a shows a three-dimensional reconstruction of the atomic positions of C and N and the carbide and nitride forming elements Ti, Nb, and V. It can be seen that the analyzed volume contains a (Nb, V, Ti) (C, N) particle. For a detailed investigation of the partially observed precipitate, a one dimensional concen-

steel research international

www.steel-research.de

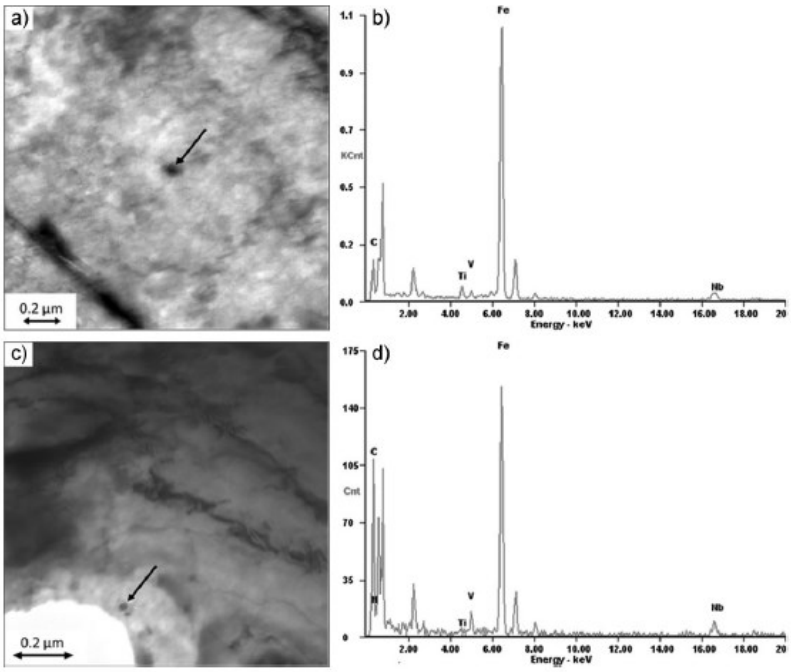

Figure 6. a and c) TEM bright field image of precipitates (marked by arrows) after isothermal heat treatment (D), a) shows a TiVNb precipitate and c) shows a NbV precipitate, b) corresponding EDS image of the precipitate in **Figure 5a**, d) corresponding EDS image of the precipitate in Figure 5c.

tration profile which contains the bainitic matrix and the precipitate was generated. In Figure 7a, this box is marked by Roi1 (region of interest 1) which is provided for the one-dimensional concentration profile. The box has a size of $4 \times 4 \times 20\,nm^3$. Figure 7b reveals that the precipitate has a core–shell assembling. The core is rather enriched in Ti, N, and C and the shell is rather enriched in V. Also Nb, N, and C show higher concentrations in the shell, but their enrichment is not as significant as that of V. At this condition, also a Fe-carbide was detected, which is illustrated in Figure 7a. For a detailed analysis, a box (Roi2) with a size of $5 \times 5 \times 25\,nm^3$ was arranged across this carbide. Figure 7c shows the one-dimensional concentration profile of Roi2 along its axis. It is supposed that the carbide is a Fe_3C carbide, because of the ratio of Fe and C, which is nearly 3:1. Furthermore, the micro-alloying elements are not enriched in the carbide, but their content is in the same order of magnitude as in the bainitic matrix at this condition. Figure 8a shows another three-dimensional reconstruction of the atomic positions of Nb, V, Ti, and C. The analyzed volume contains some (Nb, V, Ti) (C, N) precipitates, which have a maximum size of 20 nm and a elliptical shape. All detected precipitates have a MX stoichiometry (M is V or Nb or Ti; X is C and/or N), independent of their size. The precipitates were analyzed in more detail according to their size. For that, boxes labeled Roi3 and Roi4 with a size of $4 \times 4 \times 20\,nm^3$ were positioned across the precipitates and subsequently one-dimensional concentration profiles were generated. Figure 8b shows the one-dimensional concentration profile of Roi3. The precipitate contains the elements C, N, Nb, V, and Ti, but the Ti content is significantly lower compared to the other elements. The qualitative stoichiometric ratio of these carbonitrides is $(Nb_{0.57}V_{0.35}Ti_{0.08})$ $(C_{0.50}N_{0.50})$. Figure 8c shows the one-dimensional concentration profile along the axis of Roi4.This shows that the main micro-alloying elements in the precipitate are Nb and V. The Ti content of the particle is very low. The stoichiometric ratio of these triplex carbonitrides is $(Nb_{0.55}V_{0.40}Ti_{0.05})$ $(C_{0.33}N_{0.66})$, i.e., both analyzed precipitates exhibit the same stoichiometric ratio of Nb, V, and Ti, but the ratio of C and N differs. The C:N ratio of the smaller precipitate is 2:3, however the C:N ratio of the bigger precipitate is 1:1.

The content of the micro-alloying elements in solid solution as derived by APT measurements is also listed in Table 2. It can be seen that after deformation and subsequent isothermal heat treatment their contents are

steel research international

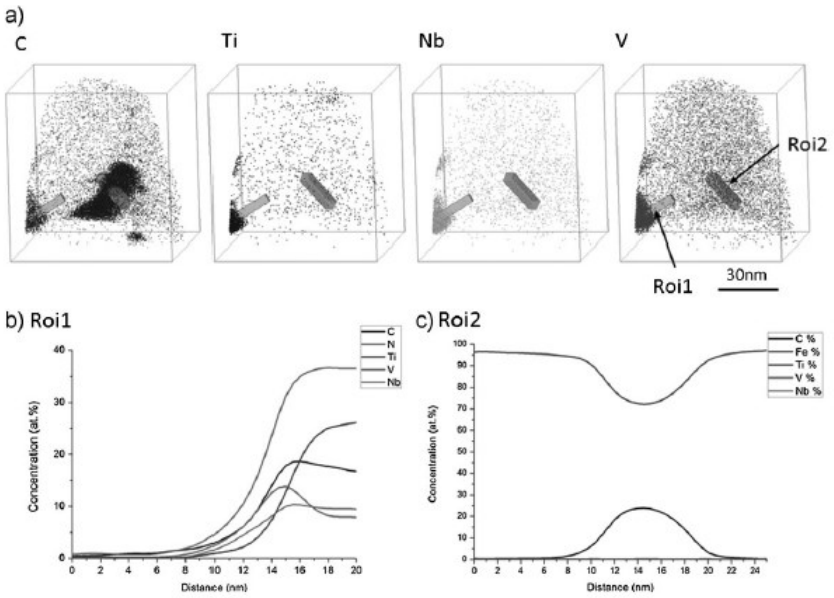

Figure 7. a) Three-dimensional reconstruction of a sample after isothermal heat treatment (D). The atom map shows the distribution of the C, Ti, Nb, and V atoms. For a detailed investigation by concentration profiles, two boxes (Roi1 and Roi2) were positioned, Roi1 has a box size of $4 \times 4 \times 20\,nm^3$ and Roi2 has a box size of $3 \times 3 \times 10\,nm^3$. b) One-dimensional concentration profile of the Roi1 in a), c) one dimensional concentration profile of the Roi2 in a).

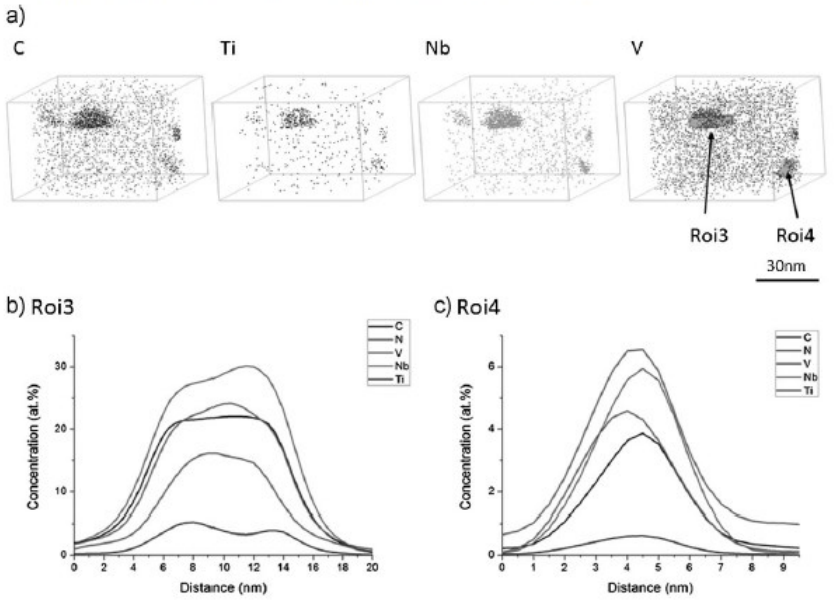

Figure 8. a) Three-dimensional reconstruction of a sample after isothermal heat treatment (D). The atom map shows the distribution of the C, Ti, Nb, and V atoms. For a detailed investigation by concentration profiles, two boxes (Roi3 and Roi4) were positioned, Roi3 has a box size of $4 \times 4 \times 20\,nm^3$ and Roi4 has a box size of $3 \times 3 \times 10\,nm^3$. b) One-dimensional concentration profile of the Roi3 in a), c) one-dimensional concentration profile of the Roi4 in a).

steel research international

www.steel-research.de

0.116 at% ± 0.004 V, 0.015 at% ± 0.001 Nb, and 0.002 at% ± 0.003 Ti. The proportion of the mean concentration and the standard deviation shows that Ti is in homogeneously distributed.

4. Discussion

For the analysis of the micro-alloying elements in solid solution and the precipitation behaviors the conditions after solution annealing at 1250°C, after deformation at 900°C and subsequent isothermal heat treatment at 900°C APT and TEM was used. Additionally, the condition before deformation was analyzed by TEM. According to the nominal composition in Table 1 the investigated alloy contains 0.12 at% V, 0.024 at% Nb, and 0.021 at% Ti.

The precipitation behavior of Ti–Nb–V micro-alloyed steel in the austenite was investigated by APT and TEM. A main point was the influence of the deformation on the precipitation evolution in austenite and the interaction between the different micro-alloying elements.

After the first step of the heat treatment, the solution annealing (A), the atom probe measurements (Table 2) revealed a concentration of 0.13 at% V, 0.024 at% Nb, but almost no Ti was detected (0.002 at%). It is well known from literature that TiN precipitates do not dissolve at solution annealing temperatures of 1250°C.[1] Thus, TiN precipitates, primary from the alloy production, did not dissolve during annealing and consequently a very low amount of Ti is in solid solution. Such undissolved Ti-precipitates after the solution annealing, were found by TEM (Figure 2). However, V and Nb exhibit higher values than the nominal composition. A reason for that might be found in an inhomogeneous distribution of the micro-alloying elements.

After cooling to deformation temperature only precipitates which contains Ti, Nb, and V were found (Figure 3). This means that during the cooling process from solution annealing temperature to deformation temperature, the undissolved Ti-rich precipitates act as nucleation sites for Nb and V. For the formation of precipitates at heterogeneous nucleation sides less energy is required than for homogenously precipitation. The kind of precipitates which are formed depends on the elements in solid solution and their energy of formation. Table 3 shows the adopted free energies of formation in austenite for the different single carbide and nitride phases. In accordance with this table at first TiN precipitates should be formed, because the free formation energy is the least of the micro-alloying precipitates. But nearly no Ti went into solution during the solution annealing at 1250°C, hence only few TiN or either TiC could be formed. NbN and NbC also have a low free energy of formation, and because of the amount of Nb in solid solution Nb-precipitates should be formed at first during the cooling to 900°C and at 900°C. The highest free energy of formation has VC and then VN, which means that V-precipitates will be formed at lower temperatures. The formation of the V precipitates at 900°C is also supported by already existing precipitates like Ti- or Nb-precipitates which are formed at higher temperatures. Because of the formation of the precipitates due to homogenous precipitation or heterogeneous precipitation at grain boundaries, sub-structure, dislocations, or already existing precipitates, the amount of Nb and V in solid solution will decrease. Table 3 also indicates that the formation of nitrides of each micro-alloying element is favorable than the formation of carbides because of the lower free energy of formation. This behavior was also reported by other authors.[7,17–19,21,22,27,33]

After deformation (C), most of the V is still in solid solution with 0.131 at%, on the other hand the Nb content in solid solution decreased to 0.015 at% Ti could not be detected at this state (Table 2). This indicates that Nb formed precipitates during the thermo-mechanical treatment. Although the precipitates consist of Ti, Nb, and V, there is only a significant decrease of Nb in solid solution as revealed by ATP. The change in the V-concentration in solid solution seems to be too small in order to detect this by APT. Other researchers[35] also reported VN precipitates of this type, but such precipitates were not found in the present investigations.

Finally, the condition after deformation and subsequent isothermal holding was investigated (D). As Table 2 shows,

Phases	ΔG [J mol^{-1}]	ΔG at 900°C [kJ mol^{-1}]
VC	$-101\,630 + 7.90T$[37]	−92.4
VN	$-217\,040 + 87.34T$[37]	−114.6
NbC	$-139\,000 + 2.3T$[37]	−136.3
NbN	$-147\,010 - 247.7T + 30.3T \ln T$[38]	−186.4
TiC	$-184\,640 + 11.00T$[37]	−171.7
TiN	$-221\,560 - 238.2T + 30.3T \ln T$[38]	−250.8

Table 3. Free energies of formation of VC, VN, NbC, NbN, TiC, and TiN in austenite.

steel research international

the V content in solid solution decreased to 0.116 at%, while the Nb content is still 0.015 at% and is, thus, unchanged compared to the previous condition. That leads to the assumption that V-rich precipitates have formed. Such precipitates were found by APT, they nucleated on Ti-rich precipitates (1D concentration profile in Figure 7b). This profile reveals that the core is mainly enriched in Ti, N, and C and that there is a shell which is mainly enriched in V. Nb is homogenously distributed over the precipitate. The C to N ratio is 1:2 across the precipitate. There is only a slight decrease of C- and also of the N-concentration from the outside to the inside of the precipitate. The structure of the precipitates with a TiN core and shell consisting of V and Nb was already reported by Baker et al.[34] and Shanmugam et al.[28] Dutta et al.[27] reported for Nb micro-alloyed steels that due to the deformation process the precipitate formation and coarsening is accelerated. At the dislocations the nucleation of precipitates is preferred due to pipe diffusion which accelerates the growth. After the isothermal heat treatment at 900°C for 5 min, small precipitates occurred, which are found only in this condition. The formation of these precipitates seems to be facilitated by the deformation process. TEM in combination with EDS-analysis suggests that these precipitates are enriched in Nb and V, but it is not clear if these precipitates are carbides, nitrides, or carbonitrides (Figure 6c and d). Atom probe revealed that these strain induced precipitates are of the NbV carbonitride type (Figure 8a–c) and that they exhibit an elliptical shape with a size of 8–20 nm.

In the present work, only strain induced triplex precipitates, consisting of (Ti, Nb, V) (C, N), could be identified. The analyzed triplex carbonitrides have a MX chemical composition. The stoichiometric ratios of Nb–V–Ti of the precipitates are similar, but the C to N stoichiometric ratio is different. For the smaller precipitates, C:N is 1:2 and for the bigger one 1:1. That leads to the assumption that for the nucleation process N, is more important than C and for the growing process, C is more important than N. Wang et al.[36] reported that in a steel with 0.047 wt% C, 83 ppm wt% N and 0.109 wt% Ti in a temperature range of 875–950°C, strain induced TiC precipitates occur. The atom probe showed that they contain small amounts of Ti. This might indicate that small Ti nitrides, carbides, or carbonitrides are formed initially which act as nucleation sites for Nb and V. For growth, Nb and V are responsible, because there is more Nb and V than Ti in solid solution. Because of the diffusion conditions, especially the diffusion coefficients of C, N, Ti, V, and Nb in austenite, shown in Table 4 indicates that Ti, V, and Nb are responsible for the growth of complex micro-alloyed precipitates. The reason for this is, that the diffusion coefficient of C and N is with $90\,563 \times 10^{-12}\,m^2\,s^{-1}$ respectively $28\,241 \times 10^{-12}\,m^2\,s^{-1}$ approximately 10^5 times faster than Ti, V, or Nb, and hence the pivotal process is the diffusion of the micro-alloying elements to the precipitates.

	D at 900°C in austenite[1] [$m^2\,s^{-1}$]
C	9.0563×10^{-12}
N	2.8241×10^{-12}
Ti	9.7622×10^{-17}
V	4.2902×10^{-17}
Nb	2.39×10^{-17}

Table 4. Diffusion coefficients of C, N, Ti, V, and Nb at 900°C in austenite.

5. Conclusions

During heat treatment different effects occur, which influences the forming process of strain induced precipitates.

1. Nb and V are more or less completely in solid solution after solution annealing.
2. At 900°C, Nb and V precipitates at undissolved TiN. These precipitates have a core–shell structure, with a TiN rich core and a shell consisting of V and Nb. N is the dominant interstitial atom in these precipitates.
3. After the deformation, strain induced (Ti, Nb, V) (C, N) precipitates occur.
4. Nb is the main element in the strain induced precipitates after the isothermal heat treatment at 900°C for 5 min. The formation of the precipitates is facilitated by N, however the growing process is facilitated by C.
5. The (Ti, Nb, V) (C, N) precipitates have MX stoichiometry.

Received: September 25, 2012

Keywords: micro-alloyed; strain-induced precipitates; atom probe; transmission electron microscopy

References

[1] T. Gladman, *The Physical Metallurgy of Microalloyed Steels*, The Institute Of Materials, The University Press, London **1997**.
[2] S. G. Hong, H. J. Jun, K. B. Kang, C. G. Park, *Scr. Mater.* **2003**, *48*, 1201.
[3] S. Yannacopoulos, M. C. Chaturvedi, *Can. Metall. Q.* **1988**, *27*, 163.
[4] S. F. Medina, M. I. Vega, M. Gómez, P. P. Gómez, *ISIJ Int.* **2005**, *45*, 1307.
[5] E. V. Pereloma, B. R. Crawford, P. D. Hodgson, *Mater. Sci. Eng. A* **2001**, *299*, 27.

[6] S. W. Thompson, G. Krauss, *Metall. Trans. A* **1989**, *20A*, 2279.
[7] K. Banks, A. Koursaris, F. Verdoorn, A. Tuling, *Mater. Sci. Technol.* **2001**, *17*, 1596.
[8] N. Maruyama, R. Uemori, M. Sugiyama, *Mater. Sci. Eng. A* **1998**, *250*, 2.
[9] S. Vervynckt, K. Verbeken, P. Thibaux, Y. Houbaert, *Mater. Sci. Eng. A* **2011**, *528*, 5519.
[10] L. Bäcke, *ISIJ Int.* **2010**, *50*, 239.
[11] A. Bakkaloglu, *Mater. Lett.* **2002**, *56*, 200.
[12] S. C. Hong, S. H. Lim, H. S. Hong, K. J. Lee, D. H. Shin, K. S. Lee, *Mater. Sci. Eng. A* **2003**, *355*, 241.
[13] M. Charleux, W. J. Poole, M. Militzer, A. Deschamps, *Metall. Mater. Trans. A* **2001**, *32A*, 1635.
[14] R. W. K. Honeycombe, in: *Fundamental Aspects of Precipitation in Microalloyed Steels* (Eds: J. M. Gray, T. Ko, Z. Shouhua, W. Baorong, X. Xishan), ASM, China **1985**, p. 243.
[15] M. Cabbibo, A. Fabrizi, M. Merlin, G. L. Garagnani, *J. Mater. Sci.* **2008**, *43*, 6857.
[16] M. D. C. Sobral, P. R. Mei, H.-J. Kestenbach, *Mater. Sci. Eng. A* **2004**, *367*, 317.
[17] M. Hillert, L. I. Staffansson, *Acta Chem. Scand.* **1970**, *24*, 3618.
[18] A. Pandit, A. Murugaiyan, A. S. Podder, A. Haldar, D. Bhattacharjee, S. Chandra, R. K. Ray, *Scr. Mater.* **2005**, *53*, 1309.
[19] H. R. Wang, W. Wang, *J. Mater. Sci.* **2008**, *44*, 591.
[20] R. M. Poths, R. L. Higginson, E. J. Palmiere, *Scr. Mater.* **2001**, *44*, 147.
[21] S. Q. Yuan, G. L. Liang, *Mater. Lett.* **2009**, *63*, 2324.
[22] S. G. Hong, K. B. Kang, C. G. Park, *Scr. Mater.* **2002**, *46*, 163.
[23] H. J. Jun, K. B. Kang, C. G. Park, *Scr. Mater.* **2003**, *49*, 1081.
[24] A. I. Fernández, P. Uranga, B. López, J. M. Rodriguez-Ibabe, *Mater. Sci. Eng. A* **2003**, *361*, 367.
[25] M. Balart, C. L. Davis, M. Strangwood, *Scr. Mater.* **2004**, *50*, 371.
[26] M. Prikryl, A. Kroupa, G. C. Weatherly, S. V. Subramanian, *Metall. Mater. Trans. A* **1996**, *27A*, 1149.
[27] B. Dutta, E. Valdes, C. M. Sellars, *Acta Metall. Mater.* **1992**, *40*, 653.
[28] S. Shanmugam, M. Tanniru, R. D. K. Misra, D. Panda, S. Jansto, *Mater. Sci. Technol.* **2005**, *21*, 165.
[29] Y. Li, J. A. Wilson, D. N. Crowther, P. S. Mitchell, A. J. Craven, T. N. Baker, *ISIJ Int.* **2004**, *44*, 1093.
[30] C. P. Reip, S. Shanmugam, R. D. K. Misra, *Mater. Sci. Eng. A* **2006**, *424*, 307.
[31] R. D. Fu, T. S. Wang, W. H. Zhou, W. H. Zhang, F. C. Zhang, *Mater. Charact.* **2007**, *58*, 968.
[32] M. K. Miller, A. Cerezo, M. G. Hetherington, G. D. W. Smith, *Atom Probe Field Ion Microscopy*, Oxford University Press, Inc., Oxford **1996**.
[33] M. P. Moody, L. T. Stephenson, A. V. Ceguerra, S. P. Ringer, *Microsc. Res. Tech.* **2008**, *71*, 542.
[34] T. N. Baker, Y. Li, J. A. Wilson, A. J. Craven, D. N. Crowther, *Mater. Sci. Technol.* **2004**, *20*, 720.
[35] S. F. Medina, *J. Mater. Sci.* **1997**, *32*, 1487.
[36] Z. Wang, X. Mao, Z. Yang, X. Sun, Q. Yong, Z. Li, Y. Weng, *Mater. Sci. Eng. A* **2011**, *529*, 459.
[37] K. Inoue, N. Ishikawa, I. Ohnuma, H. Ohtani, K. Ishida, *ISIJ Int.* **2001**, *41*, 175.
[38] H. Zou, J. S. Kirkaldy, *Metall. Trans. A* **1992**, *23A*, 651.

8. Paper B

Influence of deformation on the precipitation behavior of Nb(CN) in austenite and ferrite

M. Nöhrer, W. Mayer, S. Zamberger, E. Kozeschnik, H. Leitner

Submitted to **Metallurgical and Materials Transactions A**, April 2013

Influence of deformation on the precipitation behavior of Nb(CN) in austenite and ferrite

M. Nöhrer[1], W. Mayer[2], S. Zamberger[3], E. Kozeschnik[2] and H. Leitner[1]

[1]Christian Doppler Laboratory for Early Stages of Precipitation, Department of Physical Metallurgy and Materials Testing, Montanuniversität Leoben, Franz-Josef-Straße 18, A-8700 Leoben, Austria

[2]Christian Doppler Laboratory for Early Stages of Precipitation, Vienna University of Technology, Favoritenstrasse 9-11, A-1040 Vienna, Austria

[3]voestalpine Stahl Donawitz GmbH, Kerpelystraße 199, A-8700 Leoben, Austria

Email: matthias.noehrer@unileoben.ac.at

Keywords: strain induced precipitates, niobium, precipitation evolution, atom probe

Abstract

The evolution of Nb precipitates in low-alloy steel at 700°C, influenced by different deformation strains, is studied via atom probe tomography (APT) and transmission electron microscopy (TEM). The results show that, with increasing accumulated deformation, also the volume fraction of the precipitates increases. The deformation-induced dislocations act as nucleation sites for the Nb precipitates. The chemistry of the Nb carbonitrides changes with longer dwell times after the deformation step. The larger the precipitates grow, the higher is their C fraction. The precipitation analysis in austenite and ferrite delivers the observation that Nb precipitates grown in ferrite are larger with a higher C fraction compared to the precipitates growing in the austenite at the same condition. The investigations also show that the volume fraction of Nb carbonitrides grown in ferrite is higher than that in the austenite phase.

Introduction

Micro-alloyed steels play an important role in the automotive and pipeline industry. A key micro-alloying element is Nb. By adding small amounts of less than 0.1 wt%, a significant improvement of the mechanical properties can be achieved. [1,2] At temperatures, where Nb is in solid solution, it retards austenite recrystallization and grain growth by the solute drag

effect. [3–5] Nb precipitates, i.e. carbides, nitrides or carbonitrides, also retard recrystallization and grain growth. [2,5–8] However, investigations showed that precipitates are more effective than Nb in solid solution [5] and the most effective retardation is obtained with a fine dispersion of Nb precipitates with a diameter of about 20 nm. [9]

The formation of Nb precipitates in austenite can be facilitated by deformation processes. [10–13] While austenite grain boundaries act as nucleation sites without deformation [14], deformation-induced nucleation occurs at dislocation networks, which develop during deformation. [10–12,15,16] Due to the generation of dislocations, the number of nucleation sites and, thus, the ultimate number of precipitates increases. The diffusion of Nb is accelerated by pipe diffusion along dislocations. [10–12] Due to deformation, the incubation time for nucleation and the growth and coarsening kinetics are influenced. The higher the accumulated strain is, the shorter is the incubation time [6,13,14] and the higher is the coarsening rate. [7,12] Nb precipitates formed in austenite do not have the pronounced strengthening impact compared to the particles formed in ferrite, since they become incoherent when austenite transforms into ferrite. [12,17]

Nb also shows a strong influence on ferrite formation. Nb precipitates delay the ferrite formation by constraining the migration of the α/γ-interface. [18,19] On the other hand, the formation is supported by coarse Nb precipitates formed in austenite, as they act as ferrite nucleation sites. [18,20] This leads to finer ferrite grains, being the main strengthening effect of Nb in low and medium C steels.

Nb precipitates can also be formed in the ferrite phase. Nb precipitation is even benefited due to the lower solubility of Nb, C and N in ferrite compared to austenite. [7] Like in austenite, precipitation in ferrite is supported and accelerated by deformation. [7,17] The Nb precipitates, which nucleate heterogeneously at dislocations, have an f.c.c. structure. [21] They exhibit an orientation relationship to the matrix of Baker Nutting type $(001)_{\alpha}$ // $(001)_{Nb(C, N)}$, $[001]_{\alpha}$ // $[011]_{Nb(C, N)}$. [22] In contrast to austenite, Nb precipitates can also nucleate homogenously in ferrite. When Nb precipitates are formed homogenously, Nb atoms are arranged in monatomic platelets or in “GP” zones in the early stages. [21] Maugis et al. [23] reported that Nb precipitates in ferrite are C-rich in the early stages and, with longer annealing time, the N-content of the precipitates increases. This compositional development depends on the contents of N and C of the alloy, though.

Numerous models exist, dealing with the formation of Nb precipitates in austenite as well as in ferrite.[10,11,15,17,21,23] These models capture the effect of deformation on the formation of precipitates in different phases. The heterogeneous and homogenous nucleation of precipitates is extensively discussed. A lack of information exists in the development of the chemistry of such precipitates in austenite as well as in ferrite. The aim of the current work is to investigate the effect of strain on the precipitate chemistry during nucleation and growth in austenite and in ferrite. The investigations are performed on industrially produced 0.2 wt% C steel alloyed with 0.029 wt% Nb. Transmission electron microscopy (TEM) and atom probe tomography (APT) are used for the analysis. To aid the interpretation of the Nb precipitation behavior, the driving forces for NbN, NbC and NbCN in austenite and ferrite were determined by MatCalc calculations.

Experimental

Table 1: Chemical composition of the investigated steel.

	C	Si	Mn	Nb	Cr	Ni	Al	Cu	P	Mo	N
wt%	0.20	0.27	1.29	0.029	0.031	0.015	0.035	0.015	0.018	0.003	0.004
at%	0.92	0.53	1.30	0.017	0.033	0.014	0.072	0.013	0.032	0.002	0.016

Table 1 shows the chemical composition of the investigated steel. Figure 1 schematically illustrates the thermo-mechanical treatment. The samples were solution annealed at 1250°C for 30min. After solution annealing, the samples were cooled down to the deformation temperature of 700°C, which is in the austenite ferrite two-phase field. The samples were held at 700°C for 7 min, in order to transform austenite partially into ferrite. After this dwell time the samples were deformed to different true strains φ= 0.7 / 0.2 / 0.05. The strain rate was $\dot{\varphi}$=0.1 s^{-1}. After this, isothermal holding for 5 respectively 10 min at 700°C is performed following the deformation process. At the end of the heat treatment, the samples were quenched to room temperature within 5 s. The as-quenched condition was used for the investigation of the precipitation behavior.

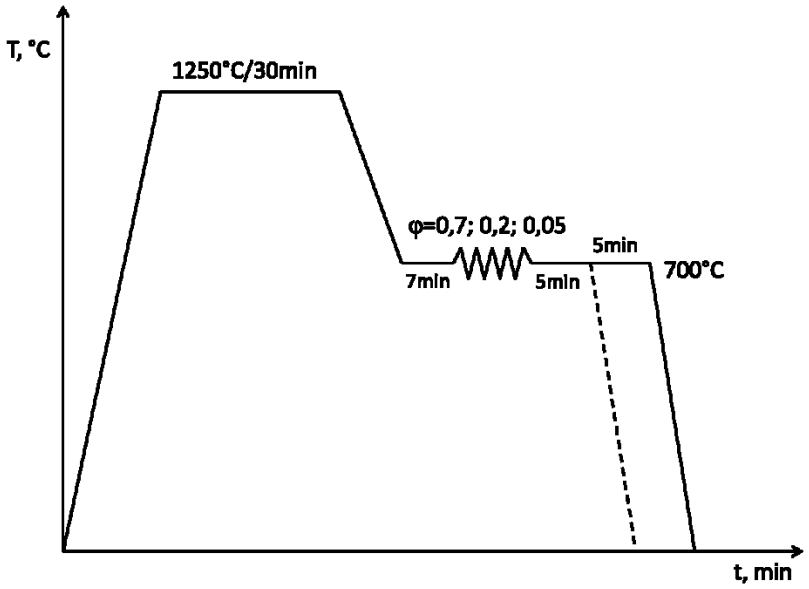

Figure 1: Scheme of the thermo-mechanical treatment used for the study of precipitation in micro-alloyed steel.

The thermo-mechanical treatment was carried out on a quenching dilatometer DIL 805 A/D from Bähr-Thermoanalyse GmbH. The deformation process was done with silicon nitride stamps. The cylindrical samples were 5 mm in diameter and 10 mm in length. For temperature control, a type S thermocouple was spot welded onto the surface of the sample. The samples for the microstructural characterization were cut parallel to the deformation direction. For determination of the microstructure after the heat treatment, light optical microscope investigations were carried out with a Polyvar Met. To analyze the development of the precipitates during the thermo-mechanical treatment, the material was investigated using transmission electron microscopy (TEM) and atom probe tomography (APT). The samples for the TEM investigations were prepared by mechanical thinning to a thickness of 0.1 mm and then electro-polished in a Tenu-Pol 5 using the electrolyte, Struers trade name, A2. The TEM investigations were conducted on a TEM Philips CM12. For the preparation of the APT samples, small rods with a cross-section of 0.3 x 0.3 mm^2 were cut out of the heat-treated samples. The tips were prepared by the standard two-stage electro polishing procedure. [24] The APT measurements were carried out on a LEAP 3000X HR from Cameca, using voltage mode with a pulse fraction of 20% and a pulse repetition of 200 kHz at a sample temperature of 60K. Data reconstruction was conducted using the software package IVAS 3.4.3 from Cameca. Size and chemistry of the precipitates were determined with the double maximum separation method with erosion [25], implemented in the software package IVAS 3.4.3. The evaluation of the searching parameters for the clusters of the different APT measurements indicated that the same could be used. The separation-, surrounding- and erosion-distance

were chosen with 1 nm. A minimum of 8 atoms was used to define a cluster and to eliminate random fluctuations.

The driving forces for NbC, NbN and NbCN precipitation in austenite and ferrite were calculated in the software package MatCalc (Version 5.51, rel. 1.003).[26,27] The Gibbs energies of matrix and precipitate phases used for evaluation of the driving forces are stored in a CALPHAD-assessed database.[27] The diffusion data of substitutional elements in Fe-alloys are taken from ref [26]. For the calculations in austenite, a C-content of 0.92 at% and an N-content of 0.016 at% were used. In the ferrite phase, the driving force was evaluated using a C-content of 0.12 at% and an N-content of 0.016 at%.

Results

Microstructure

After deformation to different true strains and with different dwell times, the microstructure consists of different phases, as shown in figure 2. In all conditions, the microstructure of the steel contains regions with ferrite, bainite and martensite structure. The amount of the individual phases depends on the applied thermo-mechanical treatment procedure. Generally, the longer the isothermal heat treatment at 700°C is, the more austenite is transformed into ferrite. The so-formed ferrite nucleates at the austenite grain boundaries. Also, by increasing the true strain, the formation of ferrite is promoted. The evolution of these phases will not be discussed in the present paper, because this work focuses on the precipitation behavior of Nb particles in ferrite and austenite. It should be noted that a differentiation of precipitates, which were found in either bainite or martensite, can be disregarded because, in both cases, the particles were formed in austenite at 700°C.

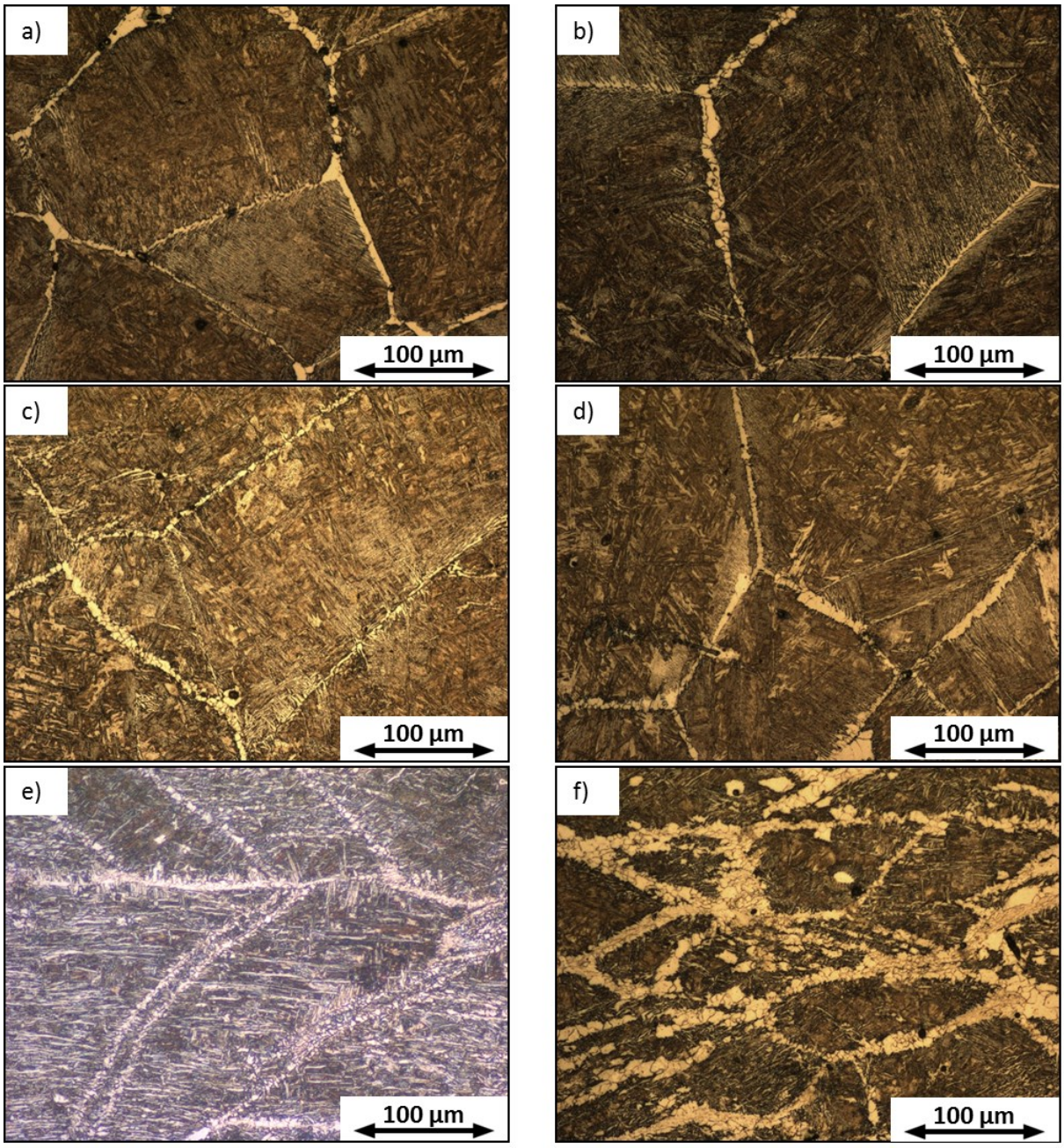

Figure 2: Optical micrograph for the material deformed at 700°C and a strain rate of 0.1 s^{-1} with different strains and isothermal sequences: a) φ=0.05 / 5min, b) φ=0.05 / 10min, c) φ=0.2 / 5min, d) φ=0.2 / 10min, e) φ=0.7 / 5min, f) φ=0.7 / 10min.

Important for the description of the precipitation behavior in austenite and ferrite is the chemistry of the matrix phase in which the precipitates grow. In the present work, the different phases were distinguished by the C content, based on APT measurements. Table 2 shows the composition of the different phases after different true strains and dwell times as determined by APT. The values were determined by several APT measurements per condition. To identify the ferrite phase, a C content of lower than 0.12 at% in the APT measurement was used. The C content in ferrite varies from 0.04 to 0.12 at% as can be seen from Table 2. Compared to the C content in ferrite, C in the martensite/bainite phase is much

higher than 0.12 at%. The martensite/bainite phase exhibit a C content from 0.57 to 1.718 at%. Due to the small volume of the APT measurements, the chemical composition of the phases varies strongly, especially the values of the C content in the martensite and bainite. Table 2 suggests that Nb is mainly in solid solution, because its matrix content is close to the nominal composition. All other elements, such as Mn, Si and N, show minor partitioning.

Table 2: Composition of the different phases in the steel after different deformations and dwell times determined by APT.

φ	Time [min]	Phase	Mn [at%]	Si [at%]	Nb [at%]	C [at%]	N [at%]
0.05	5	ferrite	1.22±0.032	0.61 ±0.015	0.020±0.004	0.040±0.008	0.032±0.011
		martensite or bainite	1.28±0.023	0.61±0.018	0.029±0.005	0.584±0.152	0.041±0.018
	10	ferrite	Could not be detected				
		martensite or bainite	1.34±0.033	0.64±0.016	0.044±0.004	0.691±0.100	0.043±0.015
0.2	5	ferrite	1.29±0.025	0.60±0.013	0.038±0.003	0.085±0.006	0.029±0.007
		martensite or bainite	1.46±0.028	0.69±0.013	0.045±0.004	1.718±0.273	0.048±0.018
	10	ferrite	1.28±0.031	0.59±0.014	0.028±0.002	0.110±0.011	0.052±0.015
		martensite or bainite	1.31±0.029	0.63±0.012	0.033±0.003	0.570±0.108	0.035±0.011
0.7	5	ferrite	1.19±0.021	0.56±0.016	0.027±0.004	0.066±0.007	0.027±0.001
		martensite or bainite	1.34±0.033	0.64±0.012	0.035±0.002	0.789±0.141	0.034±0.008
	10	ferrite	1.30±0.035	0.63±0.015	0.038±0.004	0.120±0.009	0.029±0.010
		martensite or bainite	1.39±0.034	0.68±0.016	0.037±0.003	1.305±0.212	0.040±0.016

Precipitates

The composition, the size, the distribution and the structure of the precipitates were studied by TEM and APT. Figure 3 shows, representative for all conditions, how the precipitates were characterized and identified by TEM. The images correspond to the material condition after a true strain of φ=0.7 at 700°C and a dwell time of 10 min. Figure 3a depicts a TEM bright field image of the ferrite phase containing small particles, which appear as dark points. Figure 3b is the corresponding dark field image in a lower magnification. To create the dark field image, the marked precipitate diffraction reflex $(0\bar{2}0)$ in figure 3c was used. The bright appearing dots, in figure 3b, typify the precipitates. Based on the diffraction pattern, the structure of the precipitates and an orientation relationship is observed. The ferrite has a bcc structure and the precipitates a NaCl type f.c.c structure, indicating that the precipitates are Nb carbonitrides. Figure 3c also describes the orientation relationship between the ferrite phase and the Nb precipitates. In this case, the orientation relationship $[001]_{\alpha}$ // $[011]_{Nb(C, N)}$ is found. In addition to this particle characterization, EDX-measurements were carried out. Figure 3d shows a representative EDX-spectrum of the precipitates in ferrite. In the spectrum, Nb is

clearly detected, the dominant Fe peak stems from the surrounding ferritic matrix. Estimation about the C and N fraction is not possible.

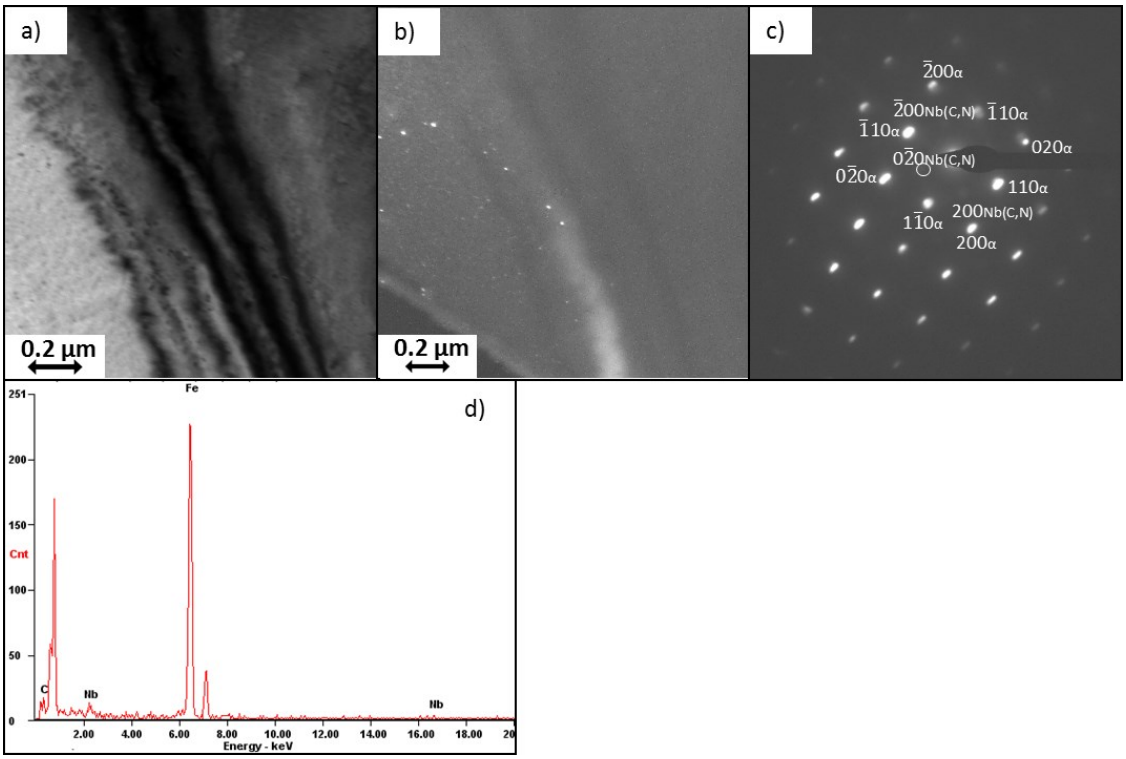

Figure 3: TEM bright field image (a), TEM dark field image (b) of the ferrite phase in the material after deformation of φ=0.7 at 700°C and a dwell time of 10min. (c) shows the selected area diffraction pattern of the ferrite phase and the Nb precipitates in (a) with the orientation relationship $[001]_\alpha$ // $[011]_{Nb(C,N)}$, (d) is representative energy dispersive X-ray spectrum from the particles.

The analysis of the precipitates in martensite or bainite were mainly done by EDX measurements in TEM, because of the less significant results obtained by diffraction analysis. Summing up the identification of the Nb precipitates in the different conditions leads to the assumption that the Nb precipitates in the ferrite showed $[001]_\alpha$ // $[011]_{Nb(C,N)}$ orientation relationship. The EDX measurements of the Nb precipitates in the other conditions correspond to the spectrum in figure 3d. In the different conditions, the Nb precipitates have a maximum diameter of 25 nm and an elliptical shape. Nucleation and growth of the precipitates is facilitated by deformation, where strain-induced precipitates can form easily at dislocations.

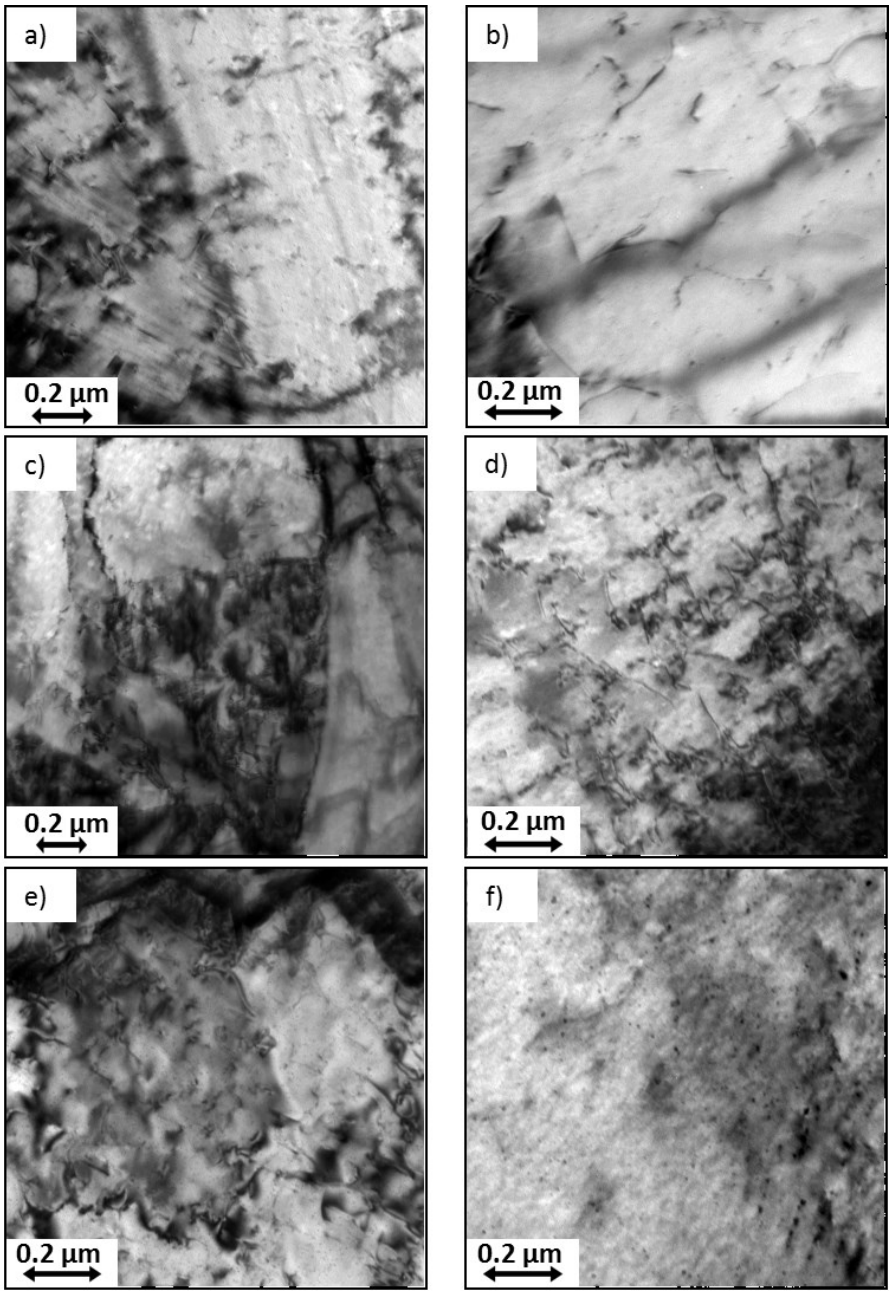

Figure 4: TEM bright field image for the material deformed at 700°C at a strain rate of 0.1 s^{-1} with different strains and isothermal holding: a) φ=0.05 / 5min, b) φ=0.05 / 10min, c) φ=0.2 / 5min, d) φ=0.2 / 10min, e) φ=0.7 / 5min, f) φ=0.7 / 10min.

Figure 4 illustrates the ferrite phase at different conditions. The figures show a dislocation precipitate network. By visual inspection it is obvious that the dislocation density increases with the deformation. Furthermore it is visible that dislocations are not homogenously distributed. In the martensite or bainite phase this relationship could not be shown clearly because of the formation of dislocations during the quenching process.

From the APT measurements, the chemistry and the size of the precipitates were determined. Figure 5 shows typical APT elemental maps of the Nb atoms in martensite/bainite and ferrite after deformation to different true strains and a subsequent dwell time of 5 min. As mentioned

before, the distinction between phases was done by the C content in the APT measurement. The image in figure 5 reveals that the Nb particles in martensite/bainite (figure 5a-5c) and ferrite (figure 5d-5f) are not homogenously distributed. The detected particles have an elliptical shape and, by visual comparison of the particle size in martensite/bainite and ferrite with identical deformation (figure a and d, b and e and c and f), it seems that the particles in ferrite are larger than in the martensite/bainite. The 3D atom maps also reveal that the precipitates are arranged in chains, which leads to the assumption that they nucleated at dislocations.

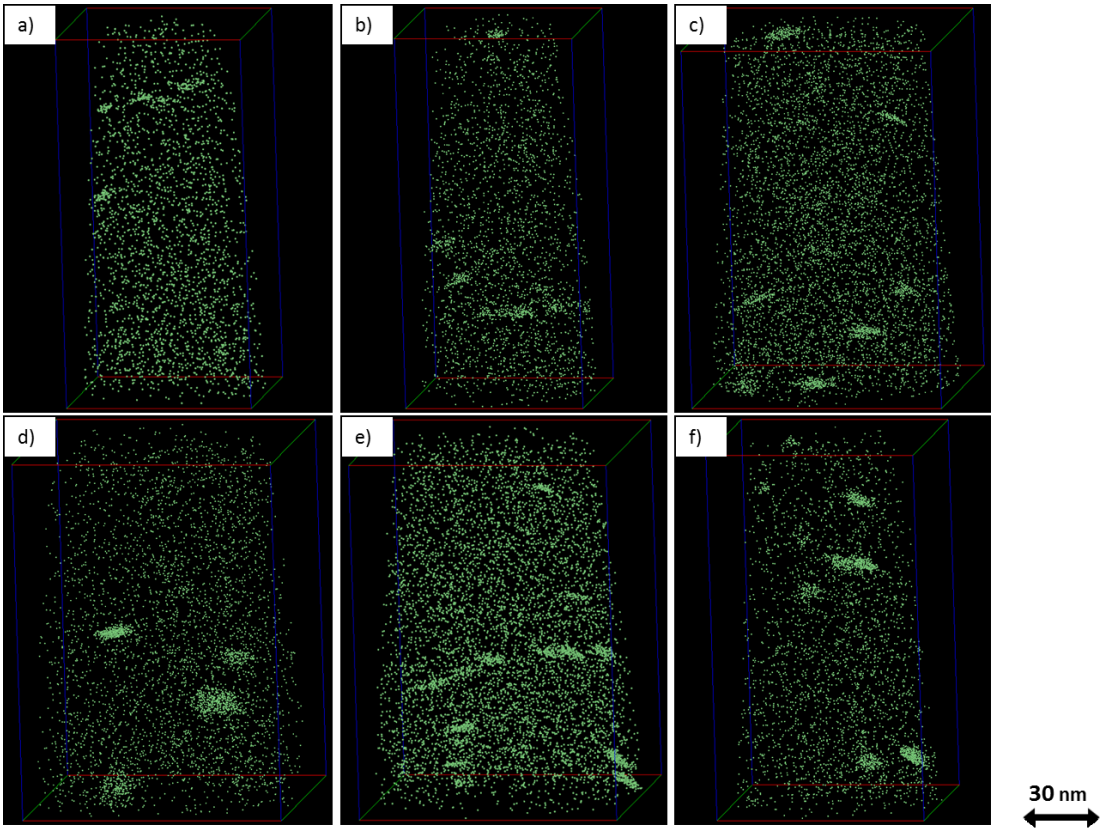

Figure 5: Three dimensional elemental map of the particles in ferrite and martensite or bainite after deformation and a dwell time of 5min, showing the distribution of the Nb atoms. a) φ=0.05 / martensite or bainite, b) φ=0.2 / martensite or bainite, c) φ=0.7 / martensite or bainite, d) φ=0.05 / ferrite, e) φ=0.2 / ferrite, f) φ=0.7 / ferrite.

The results of the precipitation analysis in the different conditions, using the double maximum separation method with erosion, are shown in table 3. The table exhibits the size of the particles as radius of gyration (Rg), because of their elliptic shape, the composition of the precipitates and the C/N ratio. Despite the difficulty that the distribution of Nb precipitates is inhomogeneous, the volume fraction was still determined and is reported in Table 3. The values should be treated with caution, therefore. The results were ascertained by several APT measurements per condition. Table 3 confirms the visual impression of the different size of the precipitates in ferrite and in martensite/bainite. At the same condition, the Rg of the

precipitates in ferrite is larger than that in martensite/bainite. By comparing the C/N ratio of each condition, it is apparent that the C fraction of precipitates in ferrite is higher than that of the precipitates formed in austenite (martensite/bainite). This tendency is most pronounced at dwell times of 10 min. After deformation to a true strain of 0.7 and a dwell time of 10 min, the precipitates in ferrite have a C/N ratio of 1.41 and in martensite/bainite of 0.89. Table 3 also shows that the C fraction increases with longer dwell time, especially within the Nb precipitates in ferrite. This tendency is clearly visible for both applied true strains. In the case of the true strain 0.2, the C/N ratio increases from 0.55 to 1.57 when the dwell time is prolonged from 5 to 10 min. After a true strain of 0.7, the ratio increases from 0.93 at 5 min to 1.41 at 10 min. The APT results also indicate that, at lower true strains, the content of N is higher than that of C. Table 3 reveals that higher true strains lead to higher phase fractions of Nb precipitates. For example, after a true strain of 0.05 and a dwell time of 5 min the Nb precipitate phase fraction in ferrite is 2.6 x 10^{-4}% and in martensite/bainite 1.5 x 10^{-4}%. Compared with the condition after a true strain of 0.7 and the same dwell time (5 min), the Nb precipitate phase fraction in ferrite is more than 3 times higher, with 10 x 10^{-4}% and in martensite/bainite 2 times higher with 3.4 x 10^{-4}%. By comparing the phase fractions of Nb precipitates in ferrite and in martensite/bainite at the same condition it is obvious that precipitation in ferrite is favored. The Nb precipitate phase fraction is more than 2 times higher. The most significant difference is found in the condition after a true strain of 0.2 and a dwell time of 10 min, where the Nb precipitate phase fraction in ferrite is 4.4 x 10^{-4}% and in martensite/bainite 0.64 x 10^{-4}%.

Table 3: Average radius of gyration, composition of the particles, the C/N ratio and the phase fraction of the particles in the different phases in the steel after different deformations and dwell times determined using the double maximum separation method with erosion from APT data.

φ	Time [min]	Phase	Rg [nm]	Nb [at%]	C [at%]	N [at%]	Fe [at%]	C/N	Phase fraction [10^{-4}%]
0.05	5	ferrite	1.01±0.66	24.6±0.68	7.15±0.17	8.44±0.56	56.56±0.75	0.85	2.6
		martensite or bainite	0.72±0.16	35.49±2.40	2.11±0.28	8.90±0.39	52.19±2.23	0.24	1.5
	10	ferrite	Could not be detected						
		martensite or bainite	0.84±0.43	22.45±0.56	5.34±0.37	5.01±0.19	64.88±0.59	1.07	3.4
0.2	5	ferrite	0.86±0.39	22.13±0.36	3.32±0.13	6.03±0.36	65.70±0.38	0.55	5.6
		martensite or bainite	0.57±0.17	32.46±2.05	3.66±0.55	6.95±0.09	55.58±1.59	0.53	1.9
	10	ferrite	0.8±0.22	17.18±0.54	8.46±0.27	5.38±.37	67.11±0.64	1.57	4.4
		martensite or bainite	1.02±0.35	38.22±2.06	5.69±0.73	11.43±0.46	42.43±1.46	0.50	0.64
0.7	5	ferrite	1.02±0.47	15.99±0.57	4.46±0.22	4.81±0.28	72.22±0.76	0.93	7.5
		martensite or bainite	0.75±0.35	27.10±0.57	6.54±0.20	6.93±.25	57.50±0.75	0.94	3.4
	10	ferrite	1.99±0.68	10.36±0.21	5.24±0.13	3.71±0.16	78.12±0.30	1.41	10
		martensite or bainite	0.68±0.25	31.87±0.53	4.25±0.30	4.80±0.22	56.91±0.73	0.89	3.4

Discussion

In this work, the influence of strain on the formation of Nb precipitates in the two phase field was investigated by means of APT and TEM. After the whole thermo-mechanical treatment (figure 1), independent from dwell time and true strain, a ferritic, martensitic, bainitic structure exists (figure 2). The fraction of the different phase changes with the applied thermo-mechanical process. Basically, the longer the isothermal sequence is, the more ferrite is formed and, also by deformation, the austenite-ferrite transformation is promoted. Plastic deformation forms a substructure, which provides new favorable nucleation sites for ferrite and polygonal ferrite can form inside the austenite grains and not only at austenite grain boundaries. [28–30]

The quenching process after the thermo-mechanical treatment at 700°C triggers the transformation from austenite into martensite or bainite. The precipitates, which were found in martensite or bainite, were formed at 700°C in austenite. In all these different microstructures, Nb precipitates were detected (figure 4, 5). The investigations revealed that the precipitates were formed in combination at dislocations (figure 4, 5). In literature, it is well known that dislocations act as heterogeneous nucleation sites for precipitates. [4,15,31] The preferred nucleation at dislocations implies that, due to the heterogeneous dislocation substructure during deformation, the precipitate distribution is heterogeneous as well. [4] Consequently, the volume fraction values in table 3 should be considered with caution, because the volume fractions were obtained by analyzing a small volume measured by atom probe. A trend of the volume fraction behavior by true strain and dwell time can be determined, though, because at every condition several atom probe measurements were done. The size and chemistry of precipitates are not affected by their heterogeneous distribution. At this point, it is important to mention that the identification of the exact nature of these particles by APT is subjective and depends on the parameters, which were used for the determination with the double maximum separation method with erosion.

The further analysis of experiments revealed that, in every microstructure condition, the identified particles are Nb carbonitrides (table 3). Depending on true strain, dwell time and the phase, in which the precipitates were formed, the precipitates have different sizes and chemistry. Precipitates investigated at the same thermo-mechanical condition are larger in ferrite than in austenite (martensite or bainite) and they have a higher C fraction in ferrite than in austenite (table 3). This is mainly caused by two effects. On one hand, the diffusivity of the

precipitate forming elements is widely different in austenite and ferrite. On the other hand, the solubility of NbC and NbN varies strongly between ferrite and austenite.

Table 4: Diffusion coefficients of C, N, and Nb at 700°C in ferrite and austenite. [1,21]

	D_0 [m^2s^{-1}]	Q [kJ mol^{-1}]	D (700°C) [m^2s^{-1}]
C_α [1]	6.2×10^{-7}	80.4	2.99×10^{-11}
C_γ [1]	1.0×10^{-5}	135.7	5.18×10^{-13}
N_α [1]	5.0×10^{-7}	77.0	3.67×10^{-11}
N_γ [1]	9.1×10^{-5}	168.6	8.08×10^{-14}
Nb_α [41]	1.7×10^{-4}	252.0	5.03×10^{-18}
Nb_γ [11]	1.4×10^{-4}	270.0	4.47×10^{-19}

To specify the influence of diffusivity, table 4 summarizes the diffusion data for Nb, C and N in ferrite and austenite. From these data it is obvious that Nb, C and N are more mobile in ferrite than in austenite at 700°C. As a consequence of the 5 to 6 orders of magnitude slower diffusion of Nb compared to C and N, Nb is mainly responsible for the precipitate growth kinetics. The second reason for the larger and C-richer Nb carbonitrides is the solubility of the Nb precipitates. It is well known from literature that Nb precipitates in ferrite have a lower solubility than in austenite and that NbN has a lower solubility than NbC in both phases. [1] These characteristics of the Nb precipitates suggest that NbN in ferrite should have the highest driving force, whereas the driving force for NbC precipitation in austenite is expected to be the lowest. Based on this behavior, the formation of NbN in ferrite and austenite is favored. To aid this interpretation, the driving forces for NbN, NbC and NbCN were calculated, based on the chemical composition of the matrix phases, using the software MatCalc with the mc_fe database. Table 5 shows the driving forces for NbC, NbN and NbCN at 700°C in austenite and ferrite. The calculations reveal that the driving force for Nb precipitates in ferrite is higher than that in austenite. This is caused by the lower solubility of the different Nb precipitates in ferrite compared to austenite. The results indicated that the driving force for NbCN is the highest in ferrite with 40.6 kJ/mol and in austenite with 34.8 kJ/mol. From literature, it is expected that NbN should have the highest driving force but the lowest was calculated. This effect is ascribed to the chemical composition of the material, especially the C and N content. In literature, a lot of different solubilities for NbC and NbN in

austenite and ferrite are reported. [1,10,11,23,32,33] These different solubilities exist because the solubility of the precipitates depends on the amount of Nb, C and N in the alloy and, of course, on the composition of the steel. That means, the higher the amounts of the different precipitate forming elements are (Nb, C and N), the lower is the solubility of NbC, NbN, NbCN. The thermodynamic background to this is that the driving force for precipitation increases. In ferrite, the maximum C content is 0.12 at% and the N content was measured to be 0.052 at% (table 2). Hence, for the Nb precipitates, C is, at least, twice as much available than N. For the C content in austenite, at least an amount of 0.92 at% is expected, because this is the nominal composition of the steel (table 1). The measured C content of the former austenite varies from 0.284 to 1.718 at% (table 2). The reason for this strong variation of the C content is its heterogeneous distribution, which occurs during the formation of martensite and bainite. [34,35] This fact is clearly reflected in the analyses because of the small volume analyzed in APT. The important point for the precipitate formation in austenite is that the maximum N content (0.048 at%) is much lower than the available C content.

Table 5: Driving force for NbN, NbC and NbCN in ferrite and austenite at 700°C.

	Driving force (kJ/mol) in ferrite	Driving force (kJ/mol) in austenite
NbN	39.1	29.1
NbC	39.7	34.6
NbCN	40.6	34.8

Investigations of the dwell time influence on precipitation showed that the C fraction increases with longer dwell times. It is expected that, during the growth of the NbCN precipitates, the N content in solid solution decreases rapidly. Due to this depletion, N is not available for further precipitation and only C continues to accumulate at existing NbCN precipitates. Therefore, the C content of the precipitates increases at longer dwell times. For V micro-alloyed steel, similar processes and influences on the precipitation formation, as described in this section, were reported. [36–40]

By estimation of the volume fraction, the atom probe measurements indicate that, with increasing true strain, the volume fraction of precipitates increases. This tendency is a consequence of the accelerated formation of more precipitates per volume. In literature, it is reported that, by increasing the true strain, the incubation time is reduced, the diffusion is accelerated by pipe diffusion and the precipitates grow faster. [6,10,11,14] Such a similar trend

could not be observed in this study. An increase in the precipitate phase fraction with increasing true strain was apparent, but not by accelerated precipitate growth. In our experiments, we show that, the higher the true strain is, the more deformation-induced dislocations were formed (figure 4), which act as nucleation sites for precipitates. [15,31] In the presence of more nucleation sites, the number density of precipitates increases and the volume fraction of precipitates increases faster than at lower true strains. [13,14] At higher true strains, more precipitates were formed, while the measured size is similar to that of the precipitates formed at lower true strains (table 3). It is assumed that a higher dislocation density at higher true strains causes this effect. Nb diffusion is accelerated by the higher dislocation density (pipe diffusion) and sufficient Nb is available after shorter times for the growth of the larger number of precipitates, compared to the conditions deformed with lower true strains.

Conclusion

In this work, the influence of deformation in the α/γ region on the precipitation behavior of Nb carbonitrides was studied. It is shown that the conditions for precipitate formation are different in the microstructural regions observed after quenching. Also, the amount of strain has a strong effect on the precipitation behavior. The analysis of our APT and TEM investigations leads to the following conclusions:

Nb nucleates as carbonitride. Since more C is available compared to N, the N content of the matrix decreases rapidly. After a significant portion of the available N has already moved into the Nb carbonitride, C is still available to accumulate at existing precipitates. This mechanism leads to a higher C fraction in the precipitates with increasing dwell time after deformation.

Nb precipitates have a lower solubility in ferrite than in austenite and the diffusivity of Nb in ferrite is higher than in austenite. As a result, the precipitates in ferrite are larger than in austenite at the same condition.

By APT, we find that the precipitates have a higher C fraction in ferrite than in the austenite, which is due to the low N content in solid solution and the lower solubility of NbC in ferrite when compared to austenite.

APT and TEM show that, with higher true strain, the dislocation density increases. This results in an increase of the volume fraction of the Nb precipitates due to the formation of more precipitates at these dislocations.

Due to the inhomogeneous nature of the deformation-induced dislocation network, also, the distribution of precipitates in ferrite and austenite becomes inhomogeneous.

References

[1] T. Gladman: *The Physical Metallurgy of Microalloyed Steels*, The Institute of Materials, The University Press, London, 1997.

[2] A. Bakkaloglu: *Mater. Lett.*, 2002, vol. 56, pp. 200 – 209.

[3] L. Bäcke: *ISIJ Int.*, 2010, vol. 50, pp. 239–247.

[4] S. S. Hansen, L. B. Vander Sande, and M. Cohen: *Metall. Trans. A*, 1980, vol. 11, pp. 387–402.

[5] S. Vervynckt, K. Verbeken, P. Thibaux, M. Liebeherr, and Y. Houbaert: *ISIJ Int.*, 2009, vol. 49, pp. 911–920.

[6] S. F. Medina, A. Quispe, P. Valles, and J. L. Banos: *ISIJ Int.*, 1999, vol. 39, pp. 913–922.

[7] M. G. Burke, L. J. Cuddy, J. Piller, and M. K. Miller: *Mater. Sci. Technol.*, 1988, vol. 4, pp. 113–116.

[8] S. Vervynckt, K. Verbeken, P. Thibaux, and Y. Houbaert: *Mater. Sci. Eng., A*, 2011, vol. 528, pp. 5519–5528.

[9] Y. Cao, F. Xiao, G. Qiao, C. Huang, X. Zhang, Z. Wu, and B. Liao: *Mater. Sci. Eng., A*, 2012, vol. 552, pp. 502–513.

[10] B. Dutta and C. M. Sellars: *Mater. Sci. Technol.*, 1987, vol. 3, pp. 197–206.

[11] B. Dutta, E. J. Palmiere, and C. M. Sellars: *Acta Mater.*, 2001, vol. 49, pp. 785–794.

[12] E. V. Pereloma, B. R. Crawford, and P. D. Hodgson: *Mater. Sci. Eng., A*, 2001, vol. 299, pp. 27 – 37.

[13] S. F. Medina and A. Quispe: *ISIJ Int.*, 1996, vol. 36, pp. 1295–1300.

[14] J. S. Park, Y. S. Ha, S. J. Lee, and Y. K. Lee: *Metall. Mater. Trans. A*, 2009, vol. 40, pp. 560–568.

[15] B. Dutta, E. Valdes, and C. M. Sellars: *Acta Metall. Mater.*, 1992, vol. 40, pp. 653–662.

[16] A. J. Craven, K. He, L. A. J. Garvie, and T. N. Baker: *Acta Mater.*, 2000, vol. 48, pp. 3857–3868.

[17] J C Herman, B Donnay, and V Leroy: *ISIJ Int.*, 1992, vol. 32, pp. 779–785.

[18] S. C. Hong, S. H. Lim, H. S. Hong, K. J. Lee, D. H. Shin, and K. S. Lee: *Mater. Sci. Eng., A*, 2003, vol. 355, pp. 241–248.

[19] G. Chen, W. Yang, S. Guo, and Z. Sun: *J. Univ. Sci. Technol. Beijing*, 2007, vol. 14, pp. 36–40.

[20] M. Cabbibo, A. Fabrizi, M. Merlin, and G. L. Garagnani: *J. Mater. Sci.*, 2008, vol. 43, pp. 6857–6865.

[21] M. Perez, E. Courtois, D. Acevedo, T. Epicier, and P. Maugis: *Philos. Mag. Lett.*, 2007, vol. 87, pp. 645–656.

[22] R. G. Baker, D. G. Brandon, and J. Nutting: *Philos. Mag.*, 1959, vol. 4, pp. 1339–1345.

[23] P. Maugis, M. Goune, P. Barges, D. Dougnac, D. Ravaine, M. Lamberigts, T. Siwecki, and Y. Bi: *Mater. Sci. Forum*, 2003, vol. 426-432, pp. 1313–1318.

[24] M. K. Miller, A. Cerezo, M. G. Hetherington, and G. D. W. Smith: *Atom Probe Field Ion Microscopy*, Oxford University Press Inc., Oxford, 1996, p. 532.

[25] L. T. Stephenson, M. P. Moody, P. V. Liddicoat, and S. P. Ringer: *Microsc. Microanal.*, 2007, vol. 13, pp. 448–463.

[26] Thermodynamic database for Fe-systems, (mc_fe_v1.030.tdb), Institute of Materials Science and Technology, Vienna University of Technology, Austria

[27] Mobility database for Fe-systems, (mc_fe_v1.001.ddb), Institute of Materials Science and Technology, Vienna University of Technology, Austria

[28] H. Beladi, I. B. Timokhina, S. Mukherjee, and P. D. Hodgson: *Acta Mater.*, 2011, vol. 59, pp. 4186–4196.

[29] S C Hong and K S Lee: *Mater. Sci. Eng., A*, 2002, vol. 323, pp. 148–159.

[30] M. Zhao, K. Yang, F. Xiao, and Y. Shan: *Mater. Sci. Eng., A*, 2003, vol. 355, pp. 126–136.

[31] W. J. Liu: *Metall. Mater. Trans. A*, 1995, vol. 26, pp. 1641–1657.

[32] R. Radis and E. Kozeschnik: *Modell. Simul. Mater. Sci. Eng.*, 2012, vol. 20, pp. 1–15.

[33] R. C. Sharma, V. K. Lakshmanan, and J. S. Kirkaldy: *Metall. Trans. A*, 1984, vol. 15, pp. 545–553.

[34] M. Peet, S. S. Babu, M. K. Miller, and H. K. D. H. Bhadeshia: *Scripta Mater.*, 2004, vol. 50, pp. 1277–1281.

[35] C. Lerchbacher, S. Zinner, and H. Leitner: *Micron*, 2012, vol. 43, pp. 818–826.

[36] F. Perrard and C. Scott: *ISIJ Int.*, 2007, vol. 47, pp. 1168–1177.

[37] Y Li, J A Wilson, A J Craven, P S Mitchell, D N Crowther, and T N Baker: *Mater. Sci. Technol.*, 2007, vol. 23, pp. 509–518.

[38] P. Maugis and M. Goune: *Acta Mater.*, 2005, vol. 53, pp. 3359–3367.

[39] M. M. A. Bepari: *Metall. Trans. A*, 1990, vol. 21A, pp. 2839–2855.

[40] Y. Li, J. A. Wilson, D. N. Crowther, P. S. Mitchell, A. J. Craven, and T. N. Baker: *ISIJ Int.*, 2004, vol. 44, pp. 1093–1102.

[41] M. Perez, M. Dumont, and D. Acevedo-Reyes: *Acta Mater.*, 2008, vol. 56, pp. 2119–2132.

9. Paper C

Atom probe study of V interphase precipitates and randomly formed V precipitates in ferrite

M. Nöhrer, S. Zamberger, S. Primig, H. Leitner

Submitted to **Micron**, May 2013

Atom probe study of V interphase precipitates and randomly distributed V precipitates in ferrite

M. Nöhrer[1], S. Zamberger[2], S. Primig[1], H. Leitner[1]

[1]Christian Doppler Laboratory for Early Stages of Precipitation, Department of Physical Metallurgy and Materials Testing, Montanuniversität Leoben, Franz-Josef-Straße 18, A-8700 Leoben, Austria

[2]voestalpine Stahl Donawitz GmbH, Kerpelystraße 199, A-8700 Leoben, Austria

Email: matthias.noehrer@unileoben.ac.at

Keywords: steel, micro-alloyed, vanadium, interphase precipitates, atom probe tomography

Abstract

Atom probe tomography and transmission electron microscopy were used to examine the precipitation reaction in V micro-alloyed steel after a thermo-mechanical process in the austenite and the ferrite phase. It was observed that only in the ferrite phase precipitates could be found, whereupon two different types were detected. Thus, the aim was to reveal the difference between these two types. The first type was randomly distributed precipitates from V supersaturated ferrite and the second type V interphase precipitates. Not only the arrangement of the particles was different also the chemical composition. The randomly distributed precipitates were enriched in C and N, in contrast to that the interphase precipitates showed an enrichment of C and Mn. It was assumed that the reason for these differences is caused by the site in which they were formed. The randomly distributed precipitates were formed in a matrix consisting mainly of 0.05 at% C, 0.68 at% Si, 0.03 at% N, 0.145 at% V and 1.51 at% Mn. The interphase precipitates were formed in a region with a much higher C, Mn and V content.

Introduction

Low and medium carbon steels in automotive and pipeline industry have to meet the increasing requirements of the industry. An easy way to improve the mechanical properties of such steels without influencing the technological properties is to alloy with micro-alloying elements such as V, Nb and Ti. Micro-alloying elements are added in small amounts of less than 0.1 wt%. They can form precipitates in the austenite, which impede the austenite

recrystallization and also the grain growth. In solution the micro-alloying elements act as austenite grain growth inhibitor by the so-called solute drag effect (Bäcke, 2010). Due to the inhibition of the austenitic recrystallization and grain growth, fine ferrite grains are formed during cooling, which results in a higher strength and toughness (Yannacopoulos and Chaturvedi, 1988; Pereloma et al., 2006; Stasko et al., 2006). Micro-alloying elements can also affect the strength of ferrite by forming nm-sized precipitates (Gladman, 1997). Here, the most effective element is V, due to the higher solubility of V in austenite compared to Nb and Ti. Thus, V remains mainly in solution while Nb and Ti already form precipitates in the austenite (Gladman, 1997). At the early stages the precipitates have a coherent V(C, N)/α-interface, which becomes semi-coherent during growth (Baker, 2009). Their orientation relationship to the ferritic matrix is of the Baker-Nutting ($(001)_{\alpha}$ // $(001)_{V(C, N)}$, $(001)_{\alpha}$ // $(001)_{V(C, N)}$) type (Baker and Nutting, 1959). The nucleation of these precipitates can occur in different ways. Either they precipitate homogeneously from the supersaturated ferrite or they nucleate heterogeneously on dislocations and subgrain boundaries (Furuhara and Maki, 2001; Gündüz and Cochrane, 2005). These kinds of precipitates occur mainly at temperatures below 973 K. At temperatures above 973 K mainly interphase precipitates are formed (Smith and Dunne, 1988). They precipitate at the austenite/ferrite (γ/α) interface during the austenite-ferrite (γ-α) transformation. These precipitates are arranged in sheets which occur periodically (Smith and Dunne, 1988). The sheet structure can be curved and regular as well as irregular and planar (Smith and Dunne, 1988). In literature different kinds of formation processes for the interphase precipitates are described. Honeycombe et al. (Honeycombe, 1985; Honeycombe and Mehl Medalist, 1976) and Aaronson et al. (Aaronson et al., 1978) described the interphase formation process by the so-called ledge mechanism. They assume that particles form heterogeneously at planar, low energy, immobile γ/α-interfaces, while the γ-α-transformation takes place by lateral, high energy mobile steps. The intersheet spacing depends on the step height of the lateral steps. To explain the formation of interphase precipitates at incoherent and often curved γ/α-interfaces, Ricks and Howell proposed a new concept (Ricks and Howell, 1983). This model has been termed the quasi ledge mechanism or bowing mechanism (Ricks and Howell, 1983). Another model for the interphase precipitate formation is based on the diffusion control of V in solution, it was firstly suggested by Roberts (Roberts, 1978). He proposed that V carbonitrides were formed directly behind a migrating interface. The growth of the carbonitrides happens through the depletion of V in ferrite. Further investigations by Khalid and Edmonds (Khalid and Edmonds, 1993) refused the idea that the precipitates occur behind the migration interface. They showed that the

particles occur at the interface. Further studies on this mechanism were done by Li and Todd (Todd et al., 1988; Todd and Su, 1989; Li and Todd, 1988a), Lagneborg et al. (Lagneborg and Zajac, 2001) and Okamoto et al. (Okamoto and Ågren, 2010). Li and Todd (Todd et al., 1988) developed a model that proposes the formation of a V depletion zone due to the V diffusion to the γ/α-interface. After reaching a critical concentration of V at the interface, V(C, N) nucleates. They also found out that the nucleation process does not influence the migration of the interface and that the incubation time is very short. Lagneborg et al. (Lagneborg and Zajac, 2001) and Okamoto et al. (Okamoto and Ågren, 2010) combined the model based on diffusion with the ledge model to explain the larger intersheet spacing because the diffusion data of V opposes to the larger spacing. They suggested that at lateral mobile steps V could diffuse easier than by volume diffusion. Further investigations showed that the formation process of the interphase precipitates depends on the amount of V, C and N in the material as well as on the forming temperature (Todd et al., 1988; Lagneborg and Zajac, 2001; Murakami et al., 2012). These parameters also influence the intersheet spacing. With lower temperatures and also with increasing V content the intersheet spacing decreases (Miyamoto et al., 2011). By decreasing the migration velocity of the γ/α-interface also fibrous precipitates which are aligned perpendicular to the interface occur (Khalid and Edmonds, 1993).

In the past a number of models were developed with different theories. The main focus in the past was to explain the intersheet spacing between the precipitation rows. Investigations of the processes at the interface during the precipitate formation as well differences in the chemistry of precipitates formed in V supersaturated ferrite and interphase precipitates are missing in literature. In this study, the difference in the chemical composition of the differently formed precipitates and the circumstances under which they were formed were investigated by atom probe tomography (APT). This method was chosen to analyze the processes in nano scale and also to detect minor changes of chemical composition which is not possible with other investigation methods.

Experimental

Table 1: Chemical composition of the investigated steel.

	C	Si	Mn	V	Cr	Ni	Al	Cu	P	Mo	N
wt%	0.18	0.31	1.55	0.145	0.038	0.047	0.033	0.019	0.027	0.014	0.01
at%	0.83	0.61	1.56	0.157	0.040	0.044	0.068	0.017	0.027	0.008	0.039

The composition of the micro-alloyed steel is shown in Table 1, denoted in wt% and at%. The heat treatment was carried out on a quenching dilatometer DIL 805 A/D from Bähr-Thermoanalyse GmbH. The sample had a diameter of 5 mm and a length of 10 mm. The temperature control was done by using a type S thermocouple, which was spot welded on the surface of the sample. For the deformation process, silicon nitride stamps were used. The applied thermo-mechanical treatment is illustrated in Figure 1. The samples were solution annealed at 1323 K for 1800 s. After austenitisation, the material was cooled down to the deformation temperature of 1173K with a cooling rate of 1.7 K/s. It should be noted that this temperature is in the γ-phase field. After a dwell time of 480 s at 1173 K, the samples were deformed to a true strain of φ=0.7 with a strain rate $\dot{\varphi}$=0.1. After this, an isothermal sequence of 300 s in the γ-region followed the deformation process. To transform the austenite into ferrite, the samples were cooled down to a temperature of 973 K with a cooling rate of 1 K/s, at which a further isothermal sequence of 300 s was applied. Finally, each sample was quenched to room temperature within 30 s.

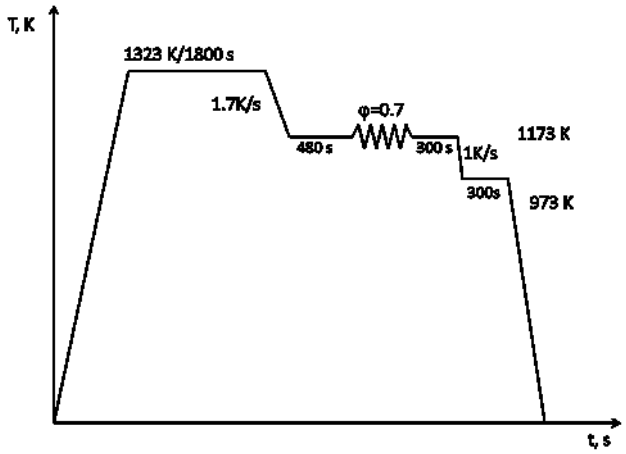

Figure 1: Scheme of the thermo-mechanical treatment used for the study of the behavior of the micro-alloying elements.

For the investigation of the γ/α-interface the as-quenched condition was used. The samples for the TEM investigations were prepared by mechanical thinning to a thickness of 0.1 mm and they were electro-polished in a Tenu-Pol 5 using the electrolyte, Struers trade name, A2. The TEM investigations were conducted on a TEM Philips CM12. For the APT investigations small rods with a cross-section of 0.3 x 0.3 mm² were cut out of the heat treated samples. The tips were prepared by the standard two-stage electro polishing procedure (Miller et al., 1996). For the measurements, a LEAP 3000X HR from Cameca was used. The measurements were performed in voltage mode with a pulse fraction of 20%, a pulse rate of 200 kHz and a

temperature of 60 K. Data reconstructions were conducted using the software package IVAS 3.4.3. from Cameca. For the identification of the precipitates by APT the following peaks were used $^{50}V^{2+}$, $^{51}V^{2+}$, $^{51}V^{3+}$, $^{64}VN^{2+}$, $^{65}VN^{2+}$, $^{14}N^{2+}$, $^{12}C^{2+}$, $^{13}C^{2+}$, $^{12}C^{+}$, $^{13}C^{+}$, $^{12}C_2^{+}$, $^{12}C_3^{2+}$ and $^{55}Mn^{2+}$. By the investigation of the precipitates an enrichment of Si was detected, which was due to the $^{28}Si^{2+}$peak. This enrichment results from the overlap of the $^{14}N^{+}$ and the $^{28}Si^{2+}$ peak. In a first step, this peak was identified as $^{28}Si^{2+}$. However, an erroneous increase of Si content in the precipitates was caused by this procedure. To determine the N fraction of the $^{28}Si^{2+}$ peak of the precipitates, they were extracted by isolating regions with a V content higher than 1.2 at%. For this isolated regions a peak decomposition of $^{14}N^{+}$ and $^{28}Si^{2+}$ was done. Due to the isotopic abundance of $^{29}Si^{2+}$ and $^{30}Si^{2+}$ it was possible to calculate the N fraction from the $^{28}Si^{2+}$ peak. This calculation is also implemented in the software package IVAS 3.4.3. Due to the fact that that the Si amount was 30 times higher than the N content the peak decomposition was only done when the precipitates were extracted, because otherwise the N content was overestimated. The precipitates were studied by proximity histograms (Hellman et al., 2000) based on V isosurfaces (Hellman et al., 2003) to get significant differences when comparing the different types of precipitates. A proximity histogram shows the concentration over the proximity normal to the isosurface. The different kinds of precipitates were investigated by several APT measurements, except the analyzed grain boundary which could only be detected once.

Results

Figure 2 shows a TEM bright field image of ferrite and martensite. The dark appearing region is martensite and the bright appearing region is ferrite. The analysis of the martensite did not show any indications for V precipitates. As figure 2 shows, the ferrite phase contains dark appearing dots, which are randomly distributed and have a diameter of maximum 20 nm and smaller. The diffraction pattern in figure 2 corresponds to the illustrated ferrite phase and reveals that these dots are V precipitates with a NaCl f.c.c structure. Furthermore, the diffraction pattern shows a ferrite-precipitate orientation relationship of $[001]_{\alpha}//[011]_{V,(C, N)}$.

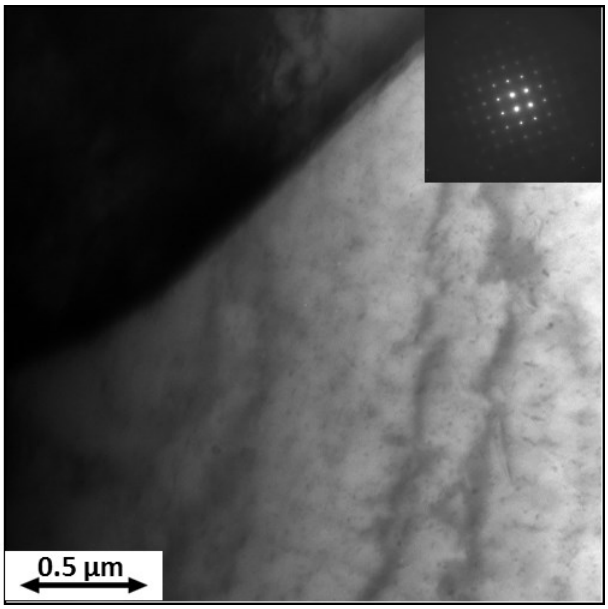

Figure 2: TEM bright field image of the material after the thermo-mechanical treatment (figure 1) showing martensite (dark) and ferrite (light). The corresponding diffraction pattern of the ferrite is shown in the inset.

Due to the limited information of the chemistry and the different types of precipitates by TEM, APT measurements were performed. Applying APT different types of V precipitates in ferrite could be found, but in martensite no precipitates were detected. The nature of the different phases could be defined based on the chemical composition, measured by APT in combination with the TEM investigations. For the distinction of the ferrite and martensite the C-content was the decisive factor and thus the C-content was measured. Table 2 shows the chemical compositions of the two phases determined by APT. The average measured C content in ferrite is 0.048 at% and in martensite the determined C content is 3.24 at% which is higher than the nominal composition (table 1). The higher amount was expected because C diffuses from ferrite into austenite during the austenite-ferrite transformation, therefore C enriches in austenite. Table 2 further reveals that the alloying element contents are higher in martensite than in ferrite. The content of the precipitate formatting element V in martensite is about 0.07 at% higher than in ferrite. The interstitial elements C and N are approximately 3.2 at% and 0.013 at% higher in the martensitic region. It should also be mentioned that the Mn and the Si contents in martensite are higher than in austenite.

Table 2: Chemical composition of the martensitic and ferrite phase determined by APT, given in at%.

	C	Si	Mn	V	Cr	Ni	Al	Cu	P	Mo	N
Martensite	3.24±0.790	0.77±0.100	1.81±0.230	0.213±0.040	0.051±0.006	0.038±0.011	0.055±0.009	0.050±0.011	0.022±0.009	0,018±0.002	0,044±0.013
Ferrite	0.048±0.003	0.68±0.080	1.51±0.120	0.145±0.006	0.031±0.004	0.021±0.001	0.050±0.001	0.034±0.004	0.036±0.009	0.050±0.070	0.031±0.019

APT measurements of the ferritic phase reveal that different types of particles exist. Figure 3a shows a representative three-dimensional elemental map of the V atoms in ferrite including isoconcentration surfaces with a concentration of 1.2 at% V. Visual inspection of this volume shows randomly distributed V particles with a diameter of 5 – 20 nm and an elliptical shape. For a closer examination, a proximity histogram was calculated based on 1.2 at% V isosurfaces, shown in figure 3b. This diagram contains the most significant elements which are used to compare the different types of precipitates in this condition, namely C, N, Mn and V. Additionally, the Si content is illustrated because of the overlap of the Si and N peak. The peak decomposition indicates that approximately 25% of ions in the $^{28}Si^{2+}$ peak are in fact N. It was calculated that approximately 30% of the detected N in the precipitates stem from the $^{28}Si^{2+}$ peak. Hence, the Si increase in the precipitates results from the N content in the $^{28}Si^{2+}$ peak. Further elements are not shown, because they are not enriched in the particles. Figure 3b reveals that in the V enriched regions also the C and N contents are increased, whereas the C content is higher than the N content. The enrichment of Si depends on the N fraction of the overlapping peak, which was explained before. The N curve can be seen as the sum of N and Si and, thus, this interpretation should be treated with caution. A differentiation between the position of Si and N ions is not possible by peak decomposition. Mn does not show enrichments in these regions and seems to be constant.

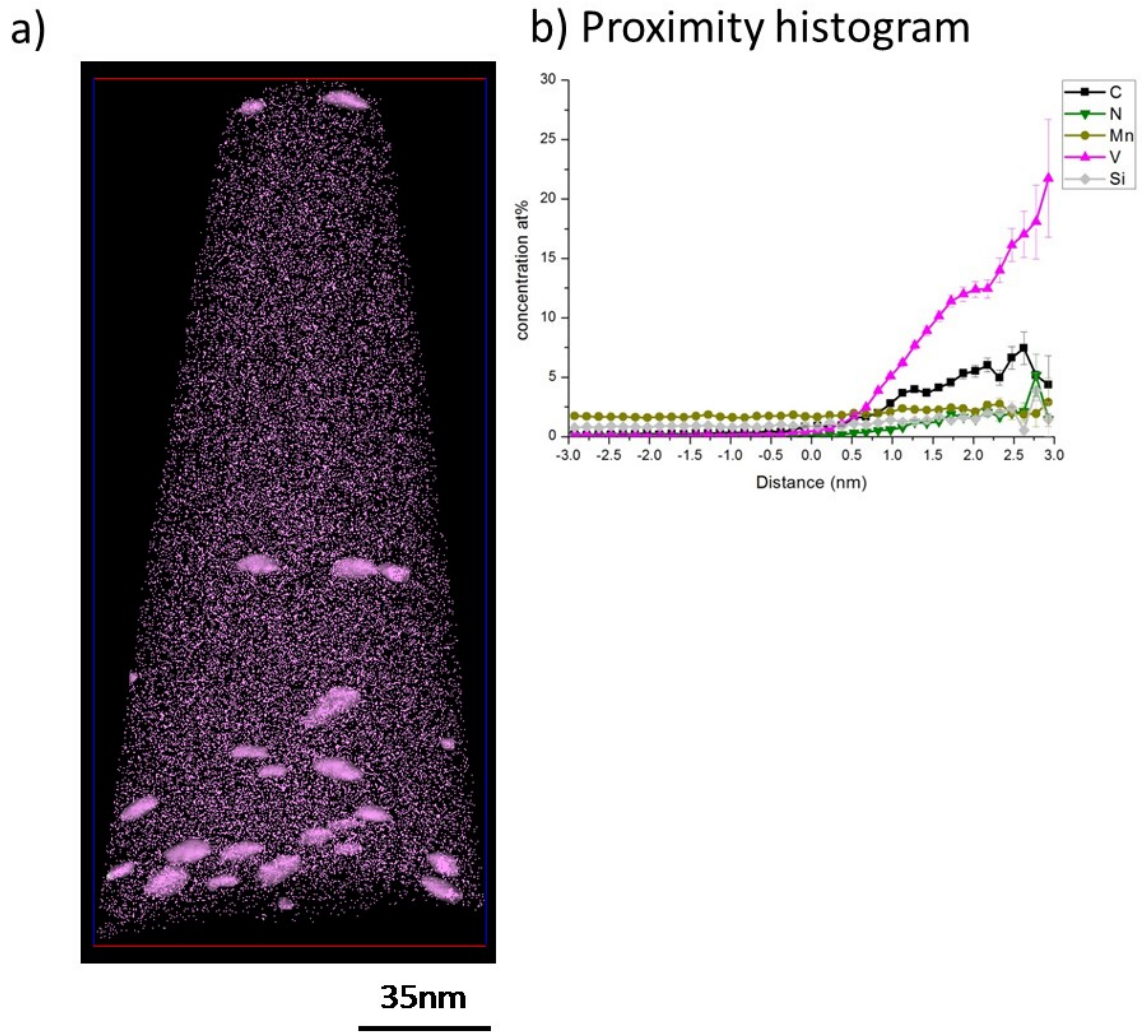

Figure 3: a) Three dimensional elemental map of the particles in the ferrite after the heat treatment, showing the V atoms and isoconcentration surfaces with 1.2 at% V, b) Proximity histogram of C, Mn, V, N and Si.

Figure 4a and b depicts a second representative three-dimensional elemental map of the V atoms in ferrite including isoconcentration surfaces with a concentration of 1.2 at% V. By visual inspection V enriched planes are visible. In the lateral illustration of the planes (Figure 4a) it is visible that the planes have a periodical distance of approximately 20 nm. In Figure 4b one representing plain was extracted and the top view is illustrated. It can be clearly seen that the plane consists of V particles with elongated shape and a length of 5 - 15 nm. For a closer examination again a proximity histogram was calculated based on the 1.2 at% V isosurfaces, which is shown in Figure 4c. The proximity histogram shows that in the V enriched regions also C and Mn are significantly increased, the N and Si contents are slightly increased. The apparent Si enrichment results from the N part of the $^{28}Si^{2+}$ peak which was explained before. In this case the $^{28}Si^{2+}$ peak contains approximately 20% N ions.

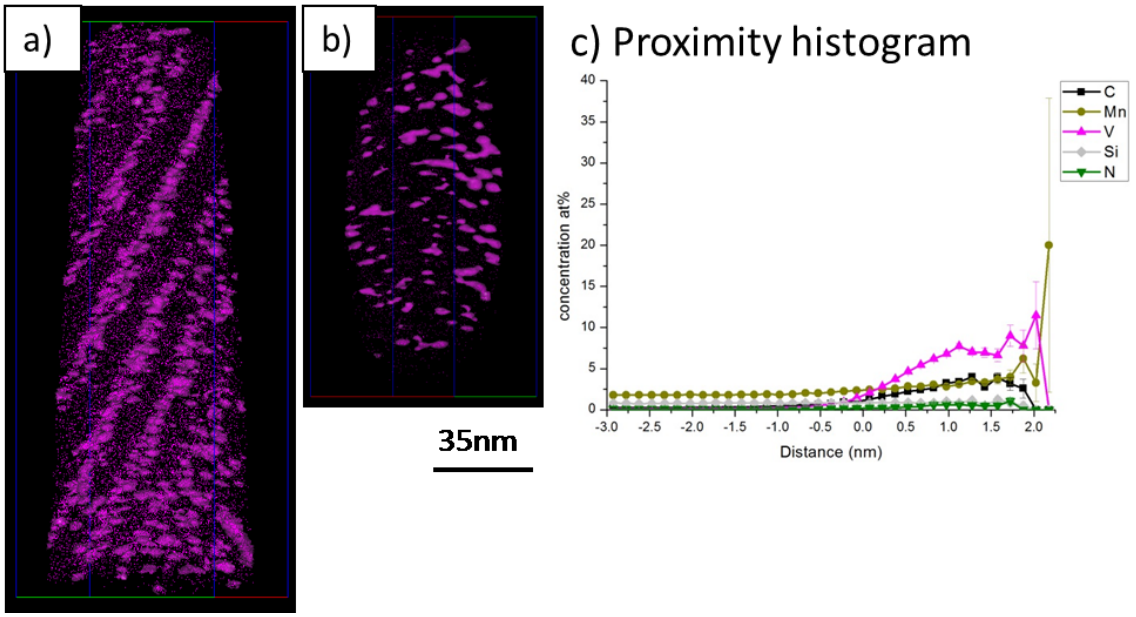

Figure 4: a) Three dimensional elemental map of the interphase precipitates in ferrite after the heat treatment showing the V atoms and isoconcentration surfaces with 1.2 at% V which show the interphase precipitates laterally, b) top view of one interphase plane front. c) Proximity histogram of C, Mn, V, N and Si.

Figure 5 shows a third representative three dimensional elemental map of the V atoms. As mentioned before, table 2 exhibits the chemical composition of the different phases and reveals that the alloying elements have higher concentrations in martensite than in ferrite. Due to the different chemical compositions of the phases, it is suggested that a redistribution of the elements took place. Due to the inhomogeneous V distribution (figure 5) it is apparent that the APT volume consists of 2 different phases which are separated by an interface. The chemical compositions of the different regions reveal that in the upper part the C content amounts 0.05 at% which means that this region is ferrite and that in the lower part the C content amounts 3.5 at% and this region is martensite. Thus, the interface, which separates these regions, can be related to a γ/α-interface before quenching from 973 K. For a detailed examination of the element distribution a 1D concentration profile from ferrite across the interface into the martensite was generated, as can be seen in Figure 5a. The 1D concentration profiles for C, Mn, V, Si and N are shown in Figure 5b. The γ/α-interface is marked in Figure 5b by an arrow and labeled as “Interface”. Figure 5b reveals that Mn and V are strongly enriched at the interface. Furthermore, it can be seen that V and Mn are depleted above the interface. C is also enriched at the interface, but not as strong as Mn and V. Si did not show any enrichment at the interface.

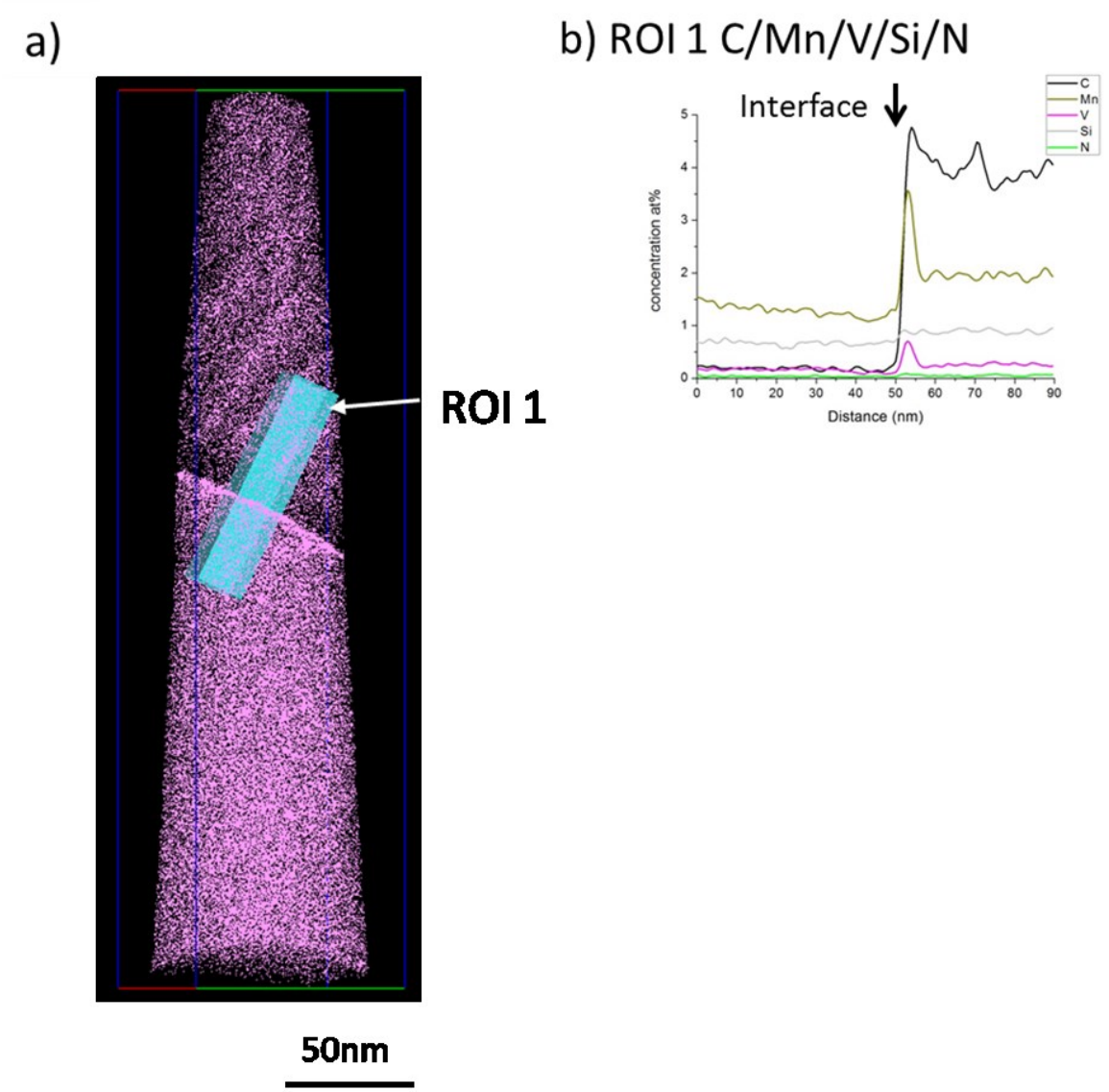

Figure 5: a) Three-dimensional elemental map of an interface after the heat treatment, showing the V distribution. For a detailed investigation of the interface by a concentration profile a box (ROI 1, box size of 20 x 20 x 90 nm^3, marked by an arrow) was positioned. b) one-dimensional concentration profile of C, Mn, V, Si and N.

In order to investigate the interface more closely, the V enrichments at the interface were analyzed by creating isoconcentration surfaces. For an illustration of the V arrangements the isosurface was constructed with a V concentration of 1.2 at% in Figure 6. This illustration shows that the V enrichment is not homogenously distributed at the interface. Figures 6a and c show the interface from a side-view, whereas figure 6b represents the top view. Here the string-like arrangement of V at the interface is revealed. The average distance between the individual strings is approximately 15 - 20 nm. In these strings spherical and elongated particles are visible. It seems that the elongated particles split into spherical particles during growth. For a detailed investigation of the fibers a proximity histogram was calculated based on the isosurface. The proximity histogram in Figure 6d shows that in the V enriched regions also Mn is strongly enriched. Compared to the Mn enrichment C is less enriched. A

significant enrichment of N or Si in the V particles was not detected. By investigating the extracted V enriched regions the decomposition of the $^{28}Si^{2+}$ peak revealed that less than 10% of the ions in the peak belong to N.

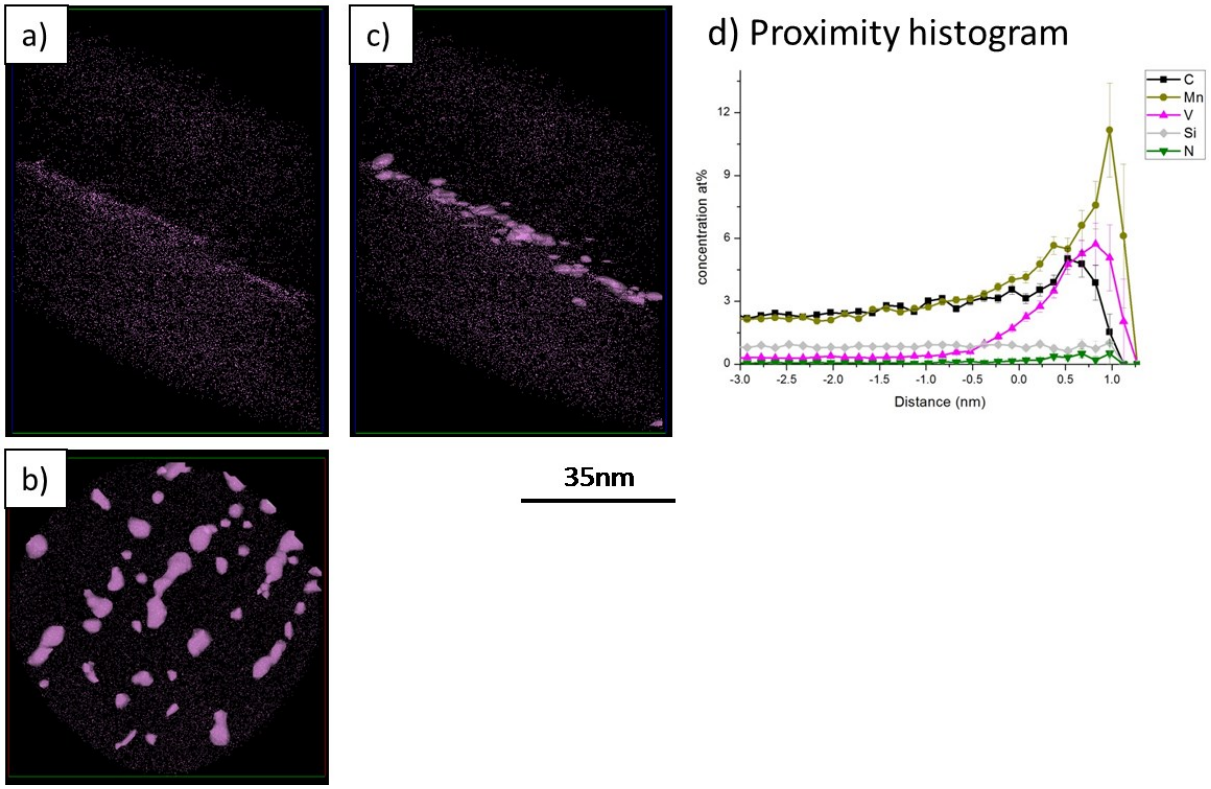

Figure 6: a) b) c) Three-dimensional elemental map of an interface after the heat treatment, showing the V distribution. a) side view of the interface lateral, b) top view of the interface including isoconcentration surfaces with 1.2 at% V, c) side view of the interface including isoconcentration surfaces with 1.2 at% V. d) Proximity histogram of C, Mn, V, N and Si.

Discussion

During the cooling from 1173 K to 973 K the austenite was transformed into ferrite. Due to the transformation and the isothermal sequence of 300s at 973 K two types of V precipitates were formed by different precipitation mechanisms. TEM and APT investigations did not show the existence of V precipitates in martensite. The martensite phase was formed by quenching and was therefore, at higher temperatures austenite. This leads to the assumption that in the austenite phase no precipitate formation took place. However, by TEM it was possible to show that V precipitates were formed in the ferrite phase exhibiting a NaCl f.c.c structure and a ferrite-precipitate orientation relationship of $[001]_{\alpha}//[011]_{V,(C,\ N)}$ (Figure 2). A differentiation of the precipitates was not possible by TEM. Further investigations by APT revealed that two types of precipitates were found in ferrite. Due to their different

arrangements, the precipitate types were distinguished, on the one hand as randomly distributed precipitates (Figure 3), which were formed homogenously from V supersaturated ferrite (Baker, 2009; Lagneborg et al., 1999; Epicier et al., 2008; Bepari, 1990). On the other hand as planar arrangement of interphase precipitates (Figure 4) (Davenport and Honeycombe, 1971; Miyamoto et al., 2011; Li and Todd, 1988b; Khalid and Edmonds, 1993; Lagneborg and Zajac, 2001; Honeycombe, 1985; Aaronson et al., 1978).

In other studies it is reported that interphase precipitation is incomplete at a temperature of 973 K and the formation of randomly distributed precipitates from supersaturated ferrite takes over (Lagneborg et al., 1999; Honeycombe, 1985). This is also the case in this work. The existence of interphase precipitates or randomly distributed V precipitates or both of them depends on the interaction of the diffusivity of V and the velocity of the γ/α-interface. It is essential that V has to be enriched at the γ/α-interface to form interphase precipitates. That means, the velocity of the γ/α-interface should correspond to the V diffusivity, thereby the γ/α-interface can get V enriched by V diffusion or by V dragging by the γ/α-interface. These effects are most pronounced at temperatures above 973 K for V micro-alloyed steels. Consequently, at higher temperatures complete interphase precipitation can occur (Davenport and Honeycombe, 1971; Barbacki and Honeycombe, 1976; Lagneborg and Zajac, 2001; Murakami et al., 2012).

The two identified precipitate types did not only have different arrangements also the chemical composition, the shape and the size was different. At this point it should be mentioned that the different types were analyzed by several APT measurements. In this article representative results are shown which reflect the general trend of further APT measurements. However, the randomly distributed precipitates had a size of 5 – 20 nm and an elliptical shape, the interphase precipitates a size of 5-15 nm and elliptical to elongated shape. The difference in the chemical composition was obvious by comparing the proximity histogram for the randomly distributed precipitates from V supersaturated ferrite (Figure 3b) to the proximity histogram for the interphase precipitates (Figure 4c). This revealed that the V interphase precipitates were enriched in C and Mn. In contrast, the randomly distributed V precipitates were enriched in C and V, Mn enrichment or depletion was not detected. The analysis of the N content was influenced by the peak overlap with Si, but by peak decomposition it was possible to estimate the N content in the precipitates and to assume that the Si enrichment in the precipitates actually stem from the N fraction of this peak. By consideration of this it was obvious that in the randomly distributed V precipitates the N

content was significantly increased and in the interphase precipitates N was only slightly enriched.

It is supposed that the difference in the chemistry of the precipitates depends on the chemistry of the area in which these precipitates were formed. The randomly distributed V carbonitrides nucleated homogenously or heterogeneously from a V supersaturated ferrite. Table 2 showed the chemistry of ferrite. V, C and N were available to form V carbonitrides. The thermo-dynamical background for the formation of the precipitates is the low solubility of VC and VN in ferrite (Gladman, 1997). The nucleation and growth of this type of V precipitate is well described in literature and will be explained only shortly (Lagneborg et al., 1999; Epicier et al., 2008; Bepari, 1990). Due to the lower solubility of VN than VC in ferrite, the early stages of the precipitates are N rich. By limited availability of N this element depletes in ferrite and C accumulates at existing precipitates, whereby carbonitrides are formed.

In contrast, interphase precipitates are formed directly at the γ/α-interface. To explain the conditions under which the interphase precipitates were formed, it is important to understand what happened during the γ-α-transformation. The rearrangement and the activities during γ/α-transformation could be seen in the APT measurements in Figure 5 and Table 2. Table 2 showed that especially C, V, Mn and Si were enriched in the martensitic phase compared to the ferrite phase, which means that mainly these elements were rearranged during the γ/α–transformation. Honeycombe et al. (Honeycombe, 1980; Honeycombe and Mehl Medalist, 1976) reported that the transformation from austenite into ferrite depends mainly on C. Because of the much higher solubility in austenite than in ferrite, C diffuses into the austenite region. However, in this work the chemical composition of the different phases (Table 2) revealed that beside the C redistribution also other elements (V, Mn and Si) were redistributed. This rearrangement seems to be important for the formation of interphase precipitates, because the γ/α–transformation rate and the migration velocity of the γ/α-interface is also influenced by the different solubilities of the elements in the ferrite- and austenite phase (Murakami et al., 2012; Lagneborg and Zajac, 2001; Wilyman and Honeycombe, 1982).

In the present study a significant enrichment of V, Mn and C at the interface was detected. It is assumed that during the γ/α–transformation at the moving γ/α-interface these elements did not only diffuse into the remaining austenite, they also accumulated at the interface by solute drag (Figure 5). The solute drag effect leads to a Mn and V enrichment at the interface

because a depletion of Mn and V was detected in ferrite after the γ/α-interface. As a consequence of this rearrangement and element dragging, at the interface an area mainly enriched in V, Mn and C was created where the interphase precipitates were formed. Figure 6 shows that the V precipitates which were formed directly at the interface were enriched in Mn and slightly in C. Craven et al. (Craven et al., 2008) showed by APT measurements that Mn is enriched in V precipitates in randomly distributed V precipitates which was not detected in this work. Furthermore, it is known from literature that $V_{0.82}Mn_{0.18}C_{0.74}$ carbides with a NaCl structure can exist (Telegus and Kuz'ma, 1971). In previous works about V interphase precipitates it is also reported that V_4C_3 and VC are formed without mentioning a Mn increase (Davenport and R W K Honeycombe, 1971; Davenport et al., 1968; Murakami et al., 2012; Khalid and Edmonds, 1993; Barbacki and Honeycombe, 1976), but this studies were mainly done by TEM and specific investigations of the V interphase precipitates were not conducted. This work deals with the influence of the nucleation site on the chemical composition of the different types of precipitates and shows that enrichments at the γ/α-interface influence the precipitates chemical composition. However, to understand the formation of interphase precipitates more work on the activities at the γ/α-interface is required.

Conclusion

In the present work the differences between randomly distributed V precipitates from V supersaturated ferrite and V interphase precipitates were investigated by APT. The main conclusions are listed below:

After the isothermal heat treatment, i.e. isothermal aging at 973K for 300s, V interphase precipitates and randomly distributed V precipitates were formed.

APT measurements showed that the two types have different chemical compositions, sizes and shapes. The randomly distributed precipitates are enriched in C and N and they have a diameter of 5 – 20 nm and an elliptical shape. The interphase precipitates are enriched in C and Mn and have a length of 5 – 15 nm and an elongated shape.

By APT investigations it was revealed that the chemical composition depends on the area in which they were formed. The randomly distributed precipitates occur in ferrite. Whereas, the interphase precipitates were formed at the γ/α-interface. By rearrangement of the alloying elements during the austenite-ferrite transformation and the solute drag of them the γ/α-interface got enriched in Mn, V and C. That means the interphase precipitates were formed in this enriched area and therefore the particles consist mainly of these elements.

References

Bäcke, L., Modeling the Effect of Solute Drag on Recovery and Recrystallization during Hot Deformation of Nb Microalloyed Steels, ISIJ Int.. 50 (2010) 239–247.

Yannacopoulos, S., Chaturvedi, M.C., Thermomechanical Treatment of a Titanium bearing HSLA steel, Can. Metall. Q.. 27 (1988) 163–168.

Pereloma, E.V., Timokhina, I.B., Russell, K.F., Miller, M.K., Characterization of clusters and ultrafine precipitates in Nb-containing C–Mn–Si steels, Scripta Mater.. 54 (2006) 471–476.

Stasko, R., Adrian, H., Adrian, A., Effect of nitrogen and vanadium on austenite grain growth kinetics of a low alloy steel, Mater. Charact.. 56 (2006) 340 – 347.

Gladman, T., The Physical Metallurgy of Microalloyed Steels, The Institute of Materials, The University Press, London, 1997.

Baker, T.N., Processes, microstructure and properties of vanadium microalloyed steels, Mater. Sci. Technol.. 25 (2009) 1083–1107.

Baker, R.G., Nutting, J., Precipitation processes in steels, London, 1959.

Furuhara, T., Maki, T., Variant selection in heterogeneous nucleation on defects in diffusional phase transformation and precipitation, Mater. Sci. Eng., A. 312 (2001) 145– 154.

Gündüz, S., Cochrane, R.C., Influence of cooling rate and tempering on precipitation and hardness of vanadium microalloyed steel, Mater. Des.. 26 (2005) 486–492.

Smith, R.M., Dunne, D.P., Structural Aspects of Alloy Carbonitride Precipitation in Microalloyed Steels, Mater. Forum. 11 (1988) 166–181.

Honeycombe, R.W.K., Fundamental aspects of precipitation in microalloyed steels, in: International Conference on HSLA Steels 1985, 1985: pp. 243–250.

Honeycombe, R.W.K., Mehl Medalist, R.F., Transformation from Austenite in Alloy Steels, Metall. Trans. A. 7 (1976) 915–936.

Aaronson, H.I., Plichta, M.R., Franti, G.W., Russell, K.C., Precipitation at Interphase boundaries, Metall. Trans. A. 9A (1978) 363–371.

Ricks, R.A., Howell, P.R., The formation of discrete precipitate dispersions on mobile interphase boundaries in iron- base alloys, Acta Metall.. 31 (1983) 853–861.

Roberts, W., Hot deformation studies on a V-microalloyed steel, Stockholm, 1978.

Khalid, F.A., Edmonds, D.V., Interphase precipitation in microalloyed engineering steels and model alloy, Mater. Sci. Technol.. 9 (1993) 384–396.

Todd, J.A., Li, P., Copley, S.M., A New Model for Precipitation at Moving Interphase Boundaries, Metall. Trans. A. 19A (1988) 2133–2138.

Todd, J.A., Su, Y.J., A Mass Transport Theory for Interphase Precipitation with Application to Vanadium Steels, Metall. Trans. A. 20A (1989) 1647–1655.

Li, P., Todd, J.A., A new model for precipitation at moving interphase boundaries, Metall. Trans. A. 19A (1988) 2139–2151.

Lagneborg, R., Zajac, S., A Model for Interphase Precipitation in V-Microalloyed Structural Steels, Metall. Mater.Trans. A. 32A (2001) 39–50.

Okamoto, R., Ågren, J., A model for interphase precipitation based on finite interface solute drag theory, Acta Mater.. 58 (2010) 4791–4803.

Murakami, T., Hatano, H., Miyamoto, G., Furuhara, T., Effects of Ferrite Growth Rate on Interphase Boundary Precipitation in V Microalloyed Steels, ISIJ Int.. 52 (2012) 616–625.

Miyamoto, G., Hori, R., Poorganji, B., Furuhara, T., Interphase Precipitation of VC and Resultant Hardening in V-added Medium Carbon Steels, ISIJ Int.. 51 (2011) 1733–1739.

Miller, M.K., Cerezo, A., Hetherington, M.G., Smith, G.D.W., Atom Probe Field Ion Microscopy, Oxford University Press Inc., Oxford, 1996.

Hellman, O.C., Vandenbroucke, J.A., Isheim, D., Seidman, D.N., Analysis of Three-dimensional Atom-probe Data by the Proximity Histogram, Microsc. Microanal.. 6 (2000) 437–444.

Hellman, O.C., du Rivage, J.B., Seidman, D.N., Efficient sampling for three-dimensional atom probe microscopy data, Ultramicroscopy. 95 (2003) 199–205.

Lagneborg, R., Siwecki, T., Zajac, S., Hutchinson, B., The Role Of Vanadium In Microalloyed Steels, The Scand. J. Metall.. (1999).

Epicier, T., Acevedo, D., Perez, M., Crystallographic structure of vanadium carbide precipitates in a model Fe-C-V steel, Philos. Mag.. 88 (2008) 31–45.

Bepari, M.M.A., Effects of precipitates on strength and toughness of vanadium structural steels, Mater. Sci. Technol.. 6 (1990) 338–348.

Davenport, A.T., Honeycombe, R.W.K., Precipitation of carbides at gamma-ferrite boundaries in alloy steels, Proceedings of the Royal Society of London A. 322 (1971) 191–205.

Li, P., Todd, J.A., Application of a New Model to the Interphase Precipitation Reaction in Vanadium Steels, Metall. Trans. A. 19A (1988) 2139–2151.

Barbacki, A., Honeycombe, R.W.K., Transition in Carbide Morphology in Molybdenum and Vanadium Steels, Metallography. 9 (1976) 277–291.

Honeycombe, R.W.K., Ferrite, Metal Science. 29th Hatfield memorial lecture (1980) 201–214.

Wilyman, P.R., Honeycombe, R.W.K., Relation between austenite-ferrite transformation kinetics and mechanical properties of vanadium steels, Met. Sci.. 16 (1982) 295–303.

Craven, A.J., MacKenzie, M., Cerezo, A., Godfrey, T., Clifton, P.H., Spectrum imaging and three-dimensional atom probe studies of fine particles in a vanadium micro-alloyed steel, Mater. Sci. Technol.. 24 (2008) 641–650.

Telegus, V.S., Kuz'ma, Y.B., The investigation of the transition metals of the fourth with carbon, Visn. L'viv. Derzh. Univ., Ser. Khim. 12 (1971) 28–33.

Davenport, A.T., Berry, F.G., Honeycombe, R.W.K., Interphase precipitation in iron alloys, Met. Sci. J.. 2 (1968) 104–106.

10. Paper D

Precipitation behavior of strain-induced V precipitates in ferrite at different temperatures in a 0.2 wt% carbon steel

M. Nöhrer, W. Mayer, S. Zamberger, E. Kozeschnik, H. Leitner

Submitted to **Steel research international**, May 2013

Precipitation behavior of strain-induced V precipitates in ferrite at different temperatures in a 0.2 wt% carbon steel

M. Nöhrer[1], W. Mayer[2], S. Zamberger[3], E. Kozeschnik[2], H. Leitner[1]

[1]Christian Doppler Laboratory for Early Stages of Precipitation, Department of Physical Metallurgy and Materials Testing, Montanuniversität Leoben, Franz-Josef-Straße 18, A-8700 Leoben, Austria

[2]Christian Doppler Laboratory for Early Stages of Precipitation, Institute of Materials Science and Technology, Vienna University of Technology, Favoritenstrasse 9-11, A-1040 Vienna, Austria

[3]voestalpine Stahl Donawitz GmbH, Kerpelystraße 199, A-8700 Leoben, Austria

Email: matthias.noehrer@unileoben.ac.at

Keywords: micro-alloyed, vanadium, strain induced precipitates, ferrite

Abstract

The evolution of strain-induced V precipitates at two different temperatures (600°C and 700°C) in ferrite was studied via atom probe tomography and transmission electron microscopy. The interpretation of experimental results is supported by simulation data, which was calculated by means of MatCalc. The study reveals that V carbonitrides are formed independently from the formation temperature. Initially, the precipitates have a higher N content than C. With longer dwell times, the C to N ratio changes from N-rich to C-rich V carbonitrides. At 700°C formation temperature, the growth of precipitates and the change from higher N to higher C occurs faster than at 600°C. Due to the faster growth, the V content in solid solution decreases earlier. The precipitates exhibit an elliptical shape and have NaCl type f.c.c structure. A [012] $_{\alpha}$ // [011] $_{V(C, N)}$ and a [001] $_{\alpha}$ // [011] $_{V(C, N)}$ orientation relationship with the ferrite matrix were detected.

Introduction

Several demands are made on low and medium carbon steels in the automotive industry and in pipeline applications. They are required to have good technological properties like weldability and formability and also high strength and toughness. In plain carbon steels, the

strength is increased by higher carbon contents, but an increase in carbon content has a negative influence on the toughness. To avoid this, micro-alloying elements, such as Nb, V and Ti, are added to low and medium carbon steels. The amounts are small, in the order of 0.1 wt% and less. These elements influence the microstructure of the steel in several ways, either by precipitation or in solid solution (solute drag effect).[1] The latter effect impedes recrystallization and austenite grain growth.[2, 8]

Micro-alloying elements also contribute to the strength of the ferrite by precipitate formation. The most effective element is V, which forms VN, V(C, N) and VC.[2, 8–11] There are several mechanisms by which V can precipitate in ferrite. Particles can precipitate on a migrating γ/α-interface during the austenite-ferrite (γ-α) transformation.[12–17] In literature this formation process is ambiguously interpreted and discussed. On one hand, it is reported that the precipitates are formed via the so-called ledge mechanism, where the precipitates emerge at low energy, semi-coherent immobile interfaces. The γ-α transformation proceeds by the passage of high energy ledges, which do not act as nucleation sites because of their high mobility.[12, 18] On the other hand, the solute drag nucleation model is proposed, where γ/α-interfaces get enriched by C and V. By dragging C and V, the movement of the interfaces is decreased and VC can nucleate.[15, 17] This process is repeated continuously. With decreasing γ-α transformation temperatures, these interphase precipitates are more infrequently found. At lower temperatures, V precipitates are formed randomly in a supersaturated ferrite.[19–21] This can happen homogenously or heterogeneously. The heterogeneous nucleation is facilitated mainly by dislocations, which are generated by metal forming processes.[22, 23] However, V can form carbides, nitrides and carbonitrides with an f.c.c. structure. All these precipitates exhibit a Baker-Nutting orientation relationship $(001)_{\alpha} // (001)_{V(C, N)}$, $[001]_{\alpha} // [011]_{V(C, N)}$ [24] with the ferritic matrix. In the early stages of precipitation, the V(C, N)/α-interface is coherent and becomes semi-coherent during growth.[19] In case of V(C, N), the early stage precipitates are N-rich and remain N-rich until the entire N is consumed. After that, C will be incorporated and, also, VC precipitates can be formed.[11, 25]

N has a strong influence on the precipitate formation process and on the strengthening effect. Most of the previous studies were carried out focusing on the precipitation behavior due to V supersaturated ferrite.[9, 21, 25–27] Less understood is the precipitation behavior due the deformation process in ferrite. There are no detailed studies about the chemistry change from N to C-rich carbonitrides. Thus, this work focuses on the precipitation behavior of V in a 0.2 wt% C-steel after deformation at different temperatures in ferrite. The characterization of the

precipitates was done by means of transmission electron microscopy (TEM) and atom probe tomography (APT). To support the experimental results and to aid the interpretation, thermo-kinetic calculations with the software MatCalc were performed.

Experimental

Table 1: Chemical composition of the investigated steel.

	C	Si	Mn	Cr	Ni	Cu	Al	Ti	V	Nb	P	Co	N
at%	0.823	0.602	1.554	0.040	0.047	0.017	0.067	0.002	0.157	0	0.027	0.002	0.087
wt%	0.18	0.31	1.55	0.038	0.047	0.019	0.033	0.002	0.145	0	0.015	0.002	0.01

The nominal composition of the V alloyed steel is listed in Table 1 (wt% and at%). The thermo-mechanical treatments were carried out on a quenching dilatometer DIL 805 A/D by BÄHR – Thermoanalyse GmbH. The deformation process was done with silicon nitride stamps. The samples were cylindrical and had a diameter of 5 mm and a length of 10 mm. The experiments were temperature controlled with a type S thermocouple, which was fixed on the sample by a spot welding process. Figure 1 schematically illustrates the thermo-mechanical treatment. After austenitisation at 1050°C for 1800 s, the specimens were cooled with a cooling rate of 3°C/s to 700° or 600°C. After a holding time of 420 s at 700°C or at 600°C, the specimens were deformed to a true strain of $\varphi = 0.7$ with a strain rate of $\dot{\varphi} = 0.1$. Subsequently, the samples were held at 700°C or 600°C for 60, 300 or 7200 s. Finally, the material was quenched to room temperature within less than 5 s.

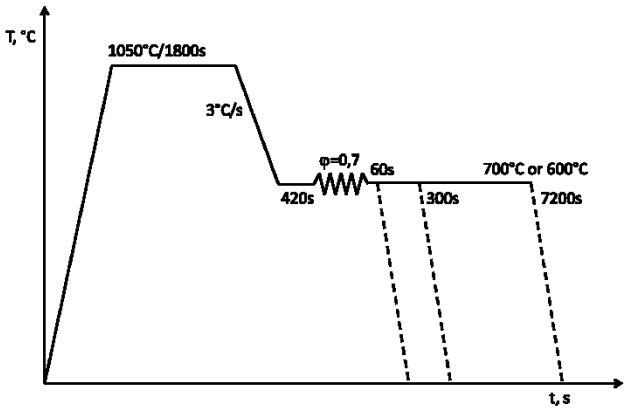

Figure 1: Scheme of the thermo-mechanical treatment used for the study of precipitation in V micro-alloyed steel.

The as-quenched conditions were investigated after deformation and the different isothermal holding sequences. The microstructural characterization was carried out by conventional transmission electron microscopy (TEM) and atom probe tomography (APT). The samples for the TEM and atom probe investigations were cut parallel to the loading direction from the center of each dilatometer specimen. For TEM investigations, samples of 3 mm diameter were mechanically thinned to a thickness of 100 µm. The subsequent electro-polishing was carried out with a Tenu-Pol 5 using the electrolyte Struers trade name A2. For the TEM investigations, a Philips CM12 was used. For preparation of the APT samples, small rods with a cross-section of 0.3 x 0.3 mm^2 were cut out of the dilatometer samples. Preparation of the tips was done by the standard two-stage electro polishing procedure.[28] A LEAP 3000X HR from Cameca in voltage mode was used for the atom probe measurements. The sample temperature was 60 K, a pulse fraction of 20% and a pulse repetition rate of 200 kHz were applied. The data reconstruction was carried out using the software package IVAS 3.4.3 from Cameca. For the determination of size and chemistry of the precipitates from APT data, the double maximum separation method with erosion, implemented in the software package IVAS 3.4.3, was used.[29] The searching parameters evaluation for the double maximum separation method with erosion of the different APT measurements indicated that the same set of parameters could be used for all conditions examined. The separation, surrounding and erosion distances were chosen as 0.65 nm. A minimum of 8 atoms was used for the particles to eliminate random fluctuations.

The thermodynamic and kinetic simulations for the V precipitation in ferrite were performed using multi-component classical nucleation theory and mean-field evolution equations, as implemented in the software package MatCalc (Version 5.52, rel. 0.019).[30–32] The thermodynamic data required for the thermo kinetic simulation, i.e. Gibbs energies of matrix and precipitate phases, are stored in a CALPHAD-assessed database.[33] The diffusion data were taken from the MatCalc mobility database.[34] For the calculations, the chemical composition of the ferrite phase in table 2 was used. This composition was calculated at 600°C and 700°C, where 12.5% and 27.5% austenite are stable, respectively, in the austenite and ferrite phase equilibrium.

Table 2: Composition of the ferrite, directly after transformation from austenite into ferrite at 600 and 700°C calculated by MatCalc.

Temp [°C]	Mn [at%]	Si [at%]	Al [at%]	V [at%]	C [at%]	N [at%]
700	0.880	0.651	0.069	0.165	0.051	0.006
600	0.870	0.640	0.064	0.140	0.054	0.005

Results

Isothermal heat treatment at 700°C

Deformation facilitates nucleation of precipitates due to the generation of strain-induced excess dislocations. These provide accelerated diffusion kinetics as well as an increased density of heterogeneous nucleation sites for precipitation. Figures 2a, b and c show TEM bright field images of the microstructure after deformation at 700°C and 3 different dwell times 60, 300 and 7200 s, respectively. At this point, it should be noted that these TEM images were taken at different magnifications. In Figure 2a, the ferritic grains with dislocations are visible. The images also show dark grey dots, which are marked by arrows. These are precipitates, which are only infrequently found in ferrite. The precipitates have a diameter of about 25 nm and an elliptical shape. Figure 2b illustrates the ferrite after a dwell time of 300 s in a higher magnification than figure 2a. It shows dislocations and particles. Several precipitates are marked by arrows. From this figure, it is obvious that the observed particles are mainly located at the dislocations. They have a diameter of about 5 nm and appear spherical in the TEM. Figure 2c is representative for the ferrite phase after a dwell time of 7200 s. The magnification of this figure is similar to figure 2a. Again, dislocations and particles are observed. Several of these precipitates are marked by arrows. The more frequently found precipitates are spherical and have a diameter of 5 to 50 nm. The type of precipitate was identified via diffraction patterns. Figure 2d shows a representative pattern of the ferrite microstructure containing precipitates. Based on these patterns, the precipitates can be identified as V precipitates, which have a NaCl type f.c.c structure. The diffraction pattern reveals that the precipitates and the ferrite have a $[001]_{\alpha}$ // $[011]_{V(C, N)}$ orientation relationship.[21] The weakly appearing reflexes for the V precipitates are marked in figure 2d by the symbol x.

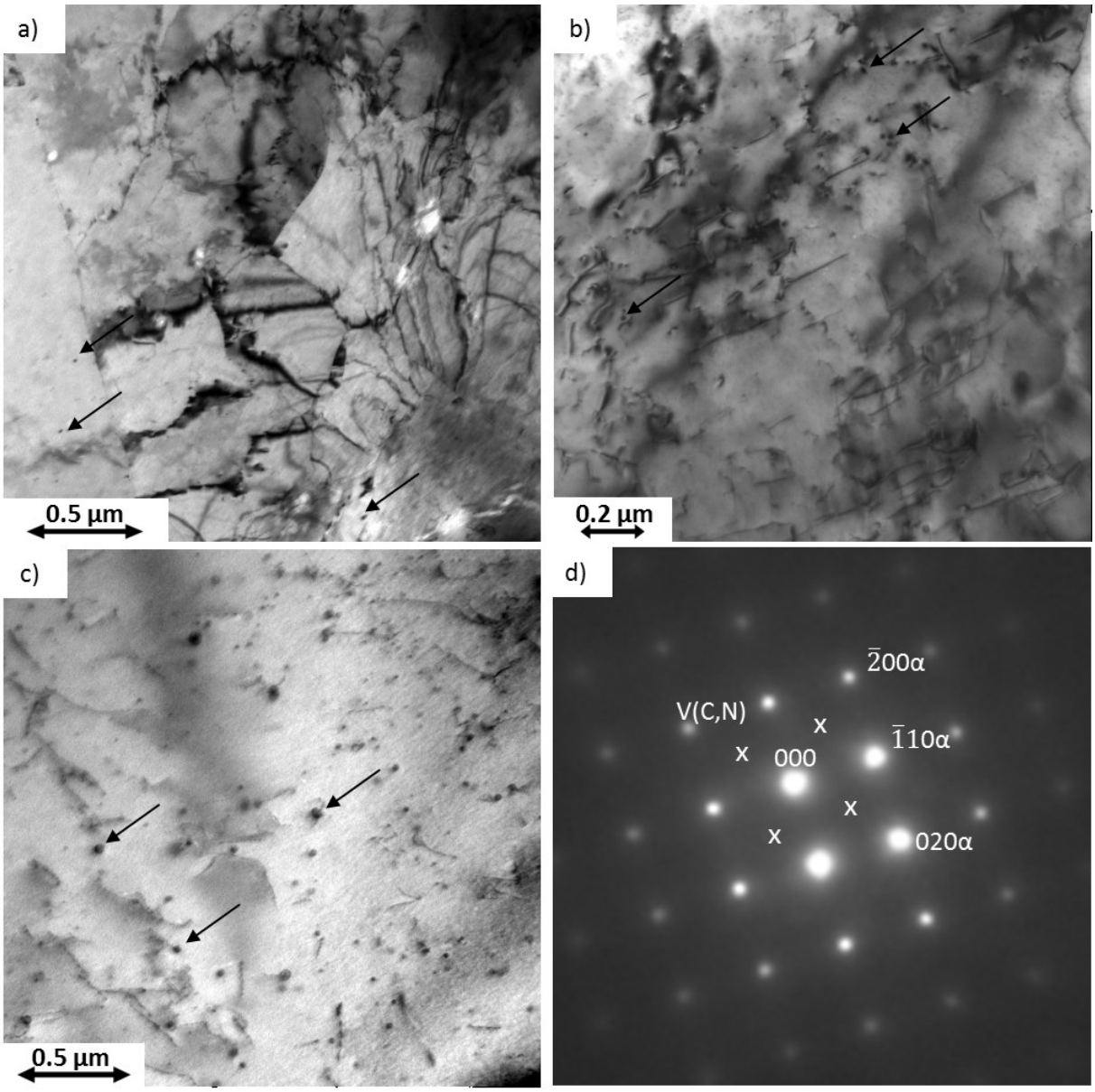

Figure 2: TEM bright field images for the material after a deformation of φ=0.7, a temperature of 700°C and different dwell times: a) after 60 s, b) after 300 s, c) after 7200 s, d) representative diffraction pattern of the ferrite phase with precipitates, several precipitates are marked by an arrow. The marked spots in d) represent the V(C, N) reflexes.

Figure 3 shows typical APT elemental maps of the V atoms in ferrite after deformation at 700°C and at the three different dwell times. Visual inspection indicates that there are regions enriched in V, which can be associated with V precipitates. Most of them have elliptical shape, some of them are elongated precipitates, which indicates that they are formed at dislocation lines. It is apparent that the size of the precipitates increases with longer dwell times, but the number of precipitates decreases when the dwell time goes from 300 to 7200 s.

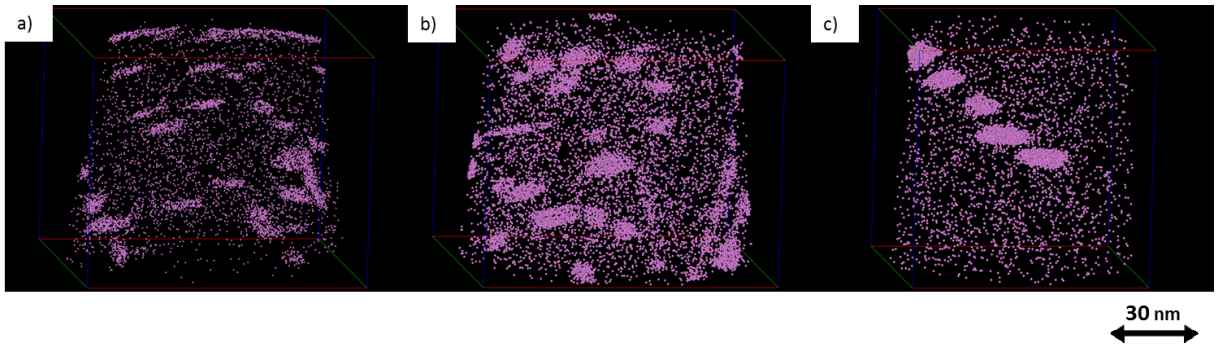

Figure 3: Three dimensional reconstructions of the particles in ferrite after a deformation of φ=0.7 at 700°C for different dwell times, showing the distribution of the V atoms. a) 60 s, b) 300 s, c) 7200 s.

Based on several APT measurements per condition, the chemistry and size of the particles, as well as the chemistry of ferrite, were determined (Table 3). From Table 3, it is obvious that the remaining V content in solid solution decreases with longer dwell times. After a dwell time of 60 s, the V content is 0.112 at% and decreases to 0.059 at % after 7200 s. All other elements show only marginal changes.

Table 3: Composition of the ferrite after a deformation of φ=0.7 and different dwell times and temperatures determined by APT.

Temp [°C]	time [s]	Mn [at%]	Si [at%]	V [at%]	C [at%]	N [at%]
700	60	1.49±0.15	0.60±0.02	0.112±0.023	0.068±0.009	0.016±0.003
	300	1.43±0.08	0.62±0.01	0.095±0.010	0.078±0.006	0.034±0.018
	7200	1.43±0.01	0.64±0.01	0.059±0.003	0.040±0.051	0.015±0.001
600	60	1.35±0.09	0.62±0.03	0.123±0.034	0.090±0.040	0.014±0.004
	300	1.49±0.19	0.65±0.10	0.091±0.008	0.106±0.036	0.019±0.002
	7200	1.25±0.19	0.68±0.03	0.083±0.004	0.118±0.037	0.016±0.003

The results of the precipitate analysis of the different dwell times at 700°C using the double maximum separation method with erosion are listed in Table 4. At this point, it is important to mention that these values should be considered critically, because the exact nature of the precipitates is subjective and depends on the parameters, which were used for their identification. In Table 4, the size of the precipitates is described by the radius of gyration (R_g) because of their elliptical shape. In case of spherical precipitates, the radius r is displayed to be able to compare the simulation data with the experimental data. Furthermore, Table 4 shows the chemical composition, the C/N ratio of the precipitates and the V precipitate

volume fraction. Table 4 confirms the visual impression that the size of the V precipitates increases with increasing dwell time after deformation. After 60 s, the R_g of the precipitates is 0.39 nm and increases to 0.63 nm after 7200 s. The precipitates consist of V, C, N and Fe. All other elements are only present in trace amounts, only for Mn a slight increase is observed.

To understand how the chemistry of the precipitates changes, the C/N ratio is shown. When the precipitates are small, the N content is significantly higher than the C content, e.g. after 60 s, a C/N ratio of 0.5 is obtained. At longer dwell times, the C/N ratio of the precipitates changes from N- to C-rich. After a dwell time of 7200 s, the C/N ratio is 3.75. Table 4 also shows that the precipitate phase fraction increases with longer dwell times. After a dwell time of 60 s, the phase fraction is 0.0650 % and it increases to 0.1294 % when the material is isothermally aged for 7200 s.

Table 4: Average radius of gyration Rg, average radius (spherical particles), composition of the particles, the C/N ratio and the phase fraction of the particles in ferrite after a deformation of φ=0.7 and different dwell times and temperatures determined using the double maximum separation method with erosion from APT data.

Temp [°C]	Time [s]	Rg [nm]	r [nm]	V [at%]	C [at%]	N [at%]	Fe [at%]	Mn [at%]	C/N	Phasefr. [%]
700	60	0.39±0,11	0.98±0.29	59.34±8.74	2.10±1.40	4.24±1.43	39.12±14.59	1.76±0.30	0.50	0.0650
	300	0.45±0,20	1.34±0.58	37.49±5.67	4.41±0.35	3.37±0.10	52.87±5.37	1.42±0.31	1.31	0.0908
	7200	0.63±0,20	3.13±1.76	25.92±6.20	9.44±2.47	2.52±0.52	60.04±9.81	1.52±0.21	3.75	0.1294
600	60	0.35±0,10	0.69±0.29	52.00±6.80	1.28±0.17	5.66±1.46	39.40±11.60	1.70±0.40	0.23	0.0080
	300	0.45±0,16	1.02±0.49	35.97±6.29	2.84±1.43	5.44±0.98	53.22±7.75	1.99±0.52	0.52	0.1192
	7200	0.46±0,18	1.24±0.53	43.97±9.31	3.31±0.11	3.38±0.52	47.31±10.02	1.52±0.29	0.98	0.1034

Isothermal heat treatment at 600°C

The evolution of precipitates at 600°C was examined in analogy to 700°C. Figures 4a, b and c show TEM bright field images of the ferrite after deformation at 600°C and subsequent dwell times of 60, 300 or 7200 s at different magnifications. The condition after a dwell time of 60 s, which is shown in Figure 4a, exhibits only ferrite with dislocations. Large precipitates, with a diameter of 25 nm, such as in the condition at 700°C and 60 s were not detected. After 300 s (Figure 4b) dark appearing dots in ferrite are visible, several of these dots are marked by arrows. These dots are particles, which are frequently found in ferrite in all grains. The particles have a diameter of maximum 5 nm and appear spherical in the TEM. Figure 4c shows the condition of the microstructure after a dwell time of 7200 s. Spherically shaped

particles are visible within the ferrite matrix. They exhibit a diameter of 5 to 20 nm (precipitates are marked by arrows). In the TEM images of the conditions after a dwell time of 300 s and 7200 s, individual dislocations are hardly visible, but dislocation networks are present in this condition. Similar to the conditions at 700°C, the precipitates are connected with the dislocations, which suggest that the dislocations are preferred heterogeneous nucleation sites. Figure 4d illustrates a representative diffraction pattern of the ferrite. The diffraction pattern reveals that, again, the particles have NaCl type f.c.c structure and constitute a [012] $_{\alpha}$ // [011] $_{V(C, N)}$ ferrite-precipitate orientation relationship.[35] Again, the weakly visible reflexes for the V precipitates are marked in Figure 4d by the symbol x.

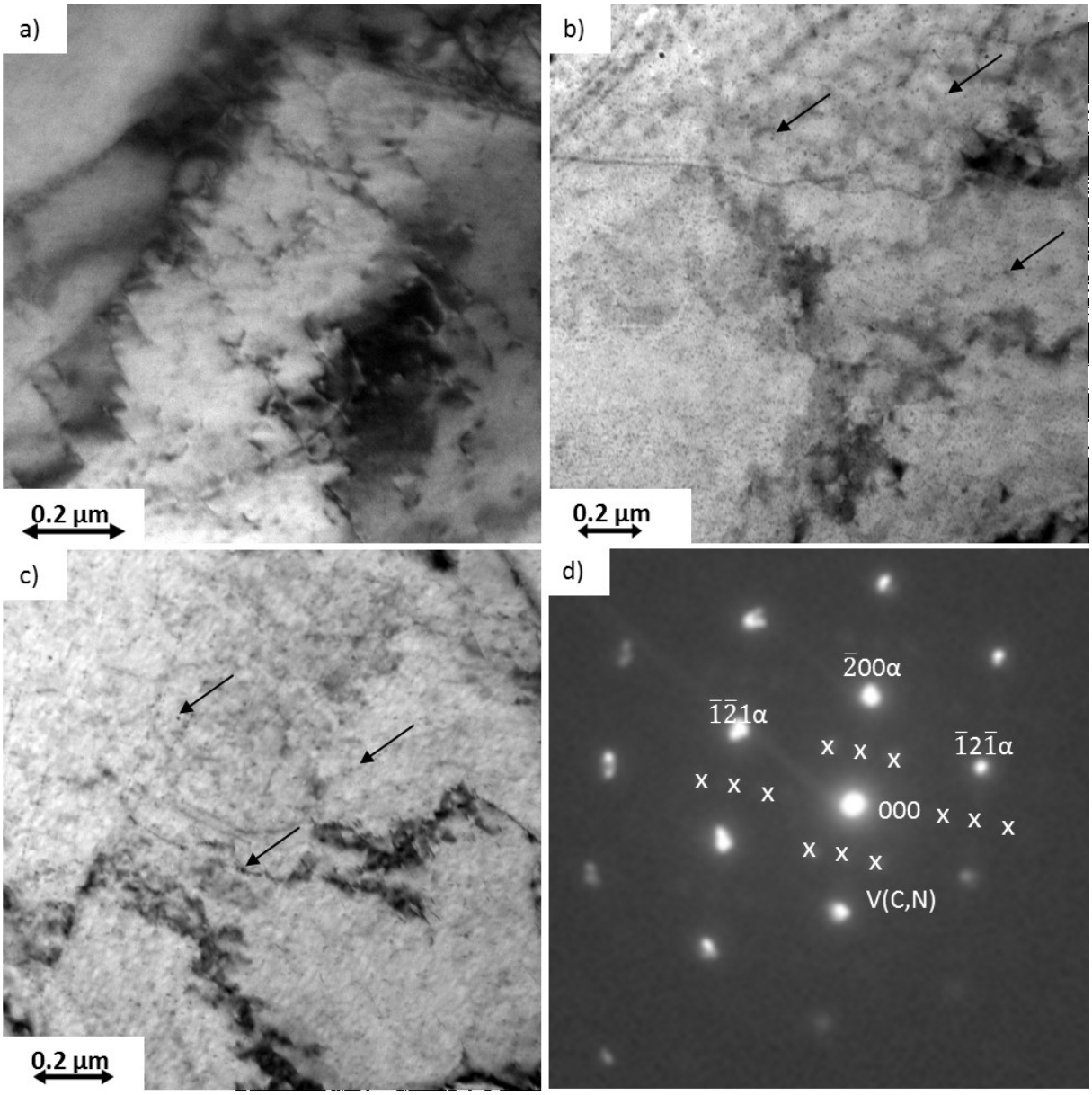

Figure 4: TEM bright field images for the material after a deformation of φ=0.7, a temperature of 600°C and different dwell times: a) after 60 s, b) after 300 s, c) after 7200 s, d) representative diffraction pattern of the ferrite phase with precipitates, several precipitates are marked by an arrow. The marked spots represent the V(C, N) reflexes.

In Figure 5, representative APT elemental maps of V atoms in ferrite after deformation and different dwell times at 600°C are illustrated. By visual inspection, regions with V enrichment are visible, which indicates the presence of V precipitates. After 60 s, the particles at 700°C are more pronounced but, also in this condition (600°C/60s), solute enrichments are visible. The APT reconstruction reveals that they have a spherical and elliptical shape and that their size increases with longer dwell times. The influence of the dwell time is also reflected in the number density. The number of precipitates decreases with longer dwell time, which is most obvious by comparing the conditions after 300 s and 7200 s dwell time. By several APT measurements of each condition, the chemistry of ferrite and the size and chemistry of the particles were determined (Table 3 and Table 4). Table 3 reveals that the V content in solid solution decreases continuously with longer dwell times. The V content is 0.123 at % after a dwell time of 60 s and only 0.083 at % after 7200 s. The other alloying element contents are almost constant during isothermal annealing after deformation.

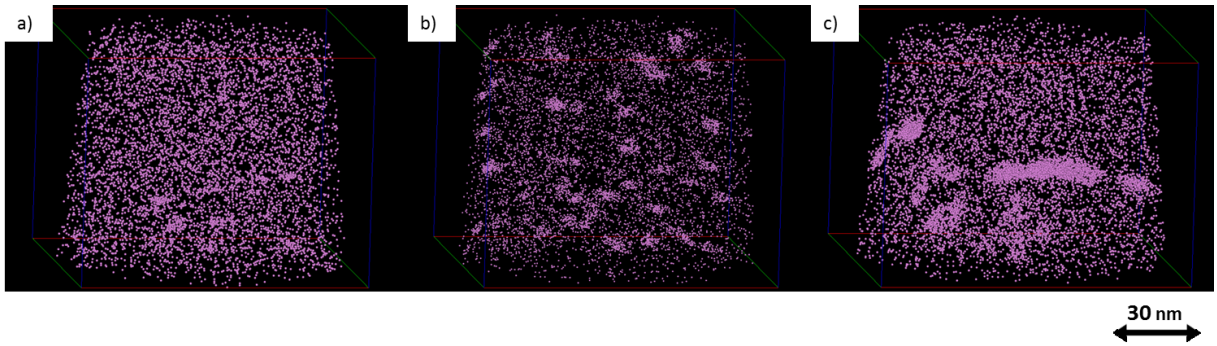

Figure 5: Three dimensional reconstructions of the particles in ferrite after a deformation of φ=0.7 at 600°C for different dwell times, showing the distribution of the V atoms. a) 60 s, b) 300 s, c) 7200 s.

The analysis of precipitate parameters at the different dwell times at 600°C are listed in Table 4. The results were determined similar to the conditions at 700°C using the double maximum separation method with erosion. In Table 4, the size of the precipitates is described by R_g in the case of elliptical precipitates and by r in the case of spherical precipitates. As indicated by the visual inspection (Figure 5), the size of the precipitates increases with longer dwell times. After a dwell time of 60s, R_g is 0.35 nm and increases to 0.46 nm after 7200s. In case of the spherical precipitates, the increase is more obvious. After 60s, r is 0.69 nm and, after 7200s dwell time, r is 1.24 nm. The growth of precipitates is apparent but, compared to 700°C, the growth is less distinct.

In addition to the chemical composition, the C/N ratio of the precipitates and the V precipitate phase fractions are shown. The precipitates are V carbonitrides at every condition, which

consist mainly of V, C, N and Fe. Mn is slightly enriched in the precipitates, the other available elements are found only in trace amounts. The C/N ratio reveals that, in the early stages of precipitation, the V carbonitrides are richer in N and, with longer dwell time, the C content increases. It was measured that, after short dwell time (60 s), the C/N ratio is 0.23 and changes to 0.98 (7200 s). The V precipitate phase fraction increases from 0.008% at 60 s to 0.1192 % at 300 s dwell time. A further phase fraction increase from 300s to 7200s was not examined, but it is assumed that the lower amount after a dwell time of 7200 s (0.1034 %) compared to that at 300 s (0.1192 %) is ascribed to the small volumes examined during the determination of the phase fraction by APT.

Discussion

In this study, we show by APT and TEM investigation that, due to deformation, strain-induced V carbonitrides were formed in a V micro-alloyed steel. The formation of these precipitates took place at both investigated temperatures of 700 and 600°C, but the precipitate evolution as a function of time is different at each temperature. To gain information and to aid the interpretation of the experimental data, thermodynamic and kinetic calculations of the V precipitates mean size, chemistry and the depletion of V in solid solution in the ferrite matrix were performed. The experimental data, i.e. particle size, chemical composition and V in solid solution in the ferrite are compared to values obtained by the MatCalc simulations.

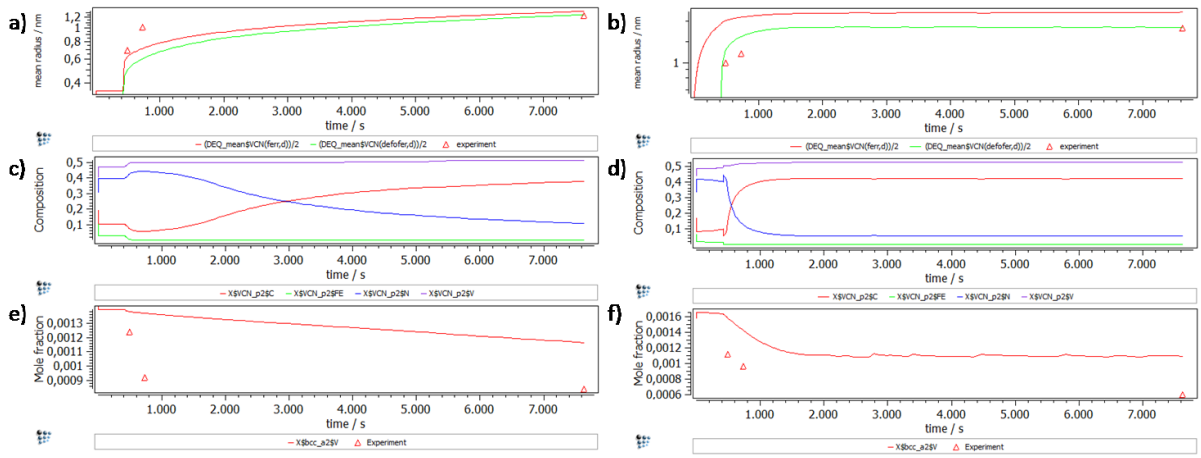

Figure 6: Calculated and experimental data of the precipitation kinetics of V-precipitates in ferrite: development of the mean radius of the precipitates at 600°C (a) and at 700°C (b), the development of the composition of the precipitates at 600°C (c) and at 700°C (d). e) shows the decrease of the V-content in solid solution in ferrite at 600°C, for 700°C it is shown in f).

In the calculation, V carbonitrides were assumed to nucleate heterogeneously at dislocations. Since the interfaces of the precipitates are coherent in the early stages of precipitation [19] and we observe some dilution of the interface in the APT analysis, the value of the interfacial

energy was taken as 90% of the value of the sharp interface as calculated from the generalized broken-bond model (GBB model).[36, 37] The APT measurements showed that the precipitates are non-spherical, which was accounted for with a shape factor of 2. The calculations for the thermo-mechanical treatment (Figure 1) used in the experiments are shown in Figure 6.

During the isothermal aging at 600°C and 700°C, V carbonitrides were obtained in the simulation. For both temperatures, with longer dwell times, the size of the precipitates increases. For the sample isothermally aged at 600°C after a dwell time of 60 s, precipitates with a size of *r* equal to 0.69 nm (Figure 5a, Table 4) could be found. The experimental results showed that, at 700 °C after a dwell time of 60 s, larger precipitates with a size of 25 nm diameter (Figure 2b) were only rarely found but precipitates in a size of a few nm (Figure 3a, Table 4) could be identified. The simulations at 700°C indicate that the larger precipitates were formed during the isothermal aging prior to deformation. For this reason, we assume that the larger precipitates are formed at dislocations prior to deformation, whereas the nm-sized precipitates are formed because of deformation. This observation is confirmed in Figures 6a and 6b. The diagrams show the evolution of the precipitate mean size depending on time for 600°C (Figure 6a) and 700°C (Figure 6b) starting with the isothermal heat treatment prior to deformation. In these diagrams, the deformation process takes place after 420 s, hence the diagram for 700°C shows that some precipitates are already formed prior to this step. Despite the formation of precipitates before deformation, still, considerable nucleation and growth of strain-induced precipitates is observed.[22] As Figure 6a reveals at 600°C the precipitate formation and growth is strongly supported by the deformation process. The strain induced precipitates grow faster at 700°C than at 600°C (Table 4). This behavior is well reflected by the simulation showing that, at 700°C after 1500 s, a constant precipitate mean radius is reached (Figure 6b). For 600°C, this is not the case. Here the size of the precipitates is still increasing after 7200 s dwell time. The faster growth of the precipitates at 700°C is mainly caused by the higher diffusion rate of V.[2] Other influences, like a lower solubility of VC and VN at lower temperatures, seemed to have a minor influence. Another effect at 700 and 600°C is that the V diffusivity is additionally enhanced by deformation-induced dislocation networks, which promote pipe diffusion.[2, 19, 20, 37]

APT measurements of the V carbonitrides revealed for both temperatures that the V carbonitrides contain more N than C in the early stages but, during the growth of the particles, the C content increases (Table 4). The evolution of the C/N ratio of the carbonitrides at 700°C shows C-rich precipitates after 300 s dwell time. At 600°C after a dwell time of 7200 s, the

precipitates are still N-rich (Table 4). The simulated chemical composition of the precipitates, which is illustrated for 600°C in Figure 6c and for 700°C in Figure 6d, confirm the experimentally observed trend. Figure 6c shows that, at 600°C, the change from N-rich into C-rich occurs after longer dwell times than for 700°C (Figure 6d). C-richer carbonitrides were not detected at 600°C (Table 4) but the calculated data describes the C/N behavior well, especially the later change from N to C rich. The calculations of the compositions of the V carbonitrides at 700°C in Figure 6d also show the change of the C/N ratio well. At this point, it should be mentioned that substantial Fe enrichment was found in the precipitates at every condition (table 4), which has already been observed in earlier work.[38, 39]

Finally, the shift from N-rich to C-rich carbonitrides can be explained by the higher driving force for the formation of nitrides compared to carbides, which stems from the lower solubility of VN in ferrite than VC.[2, 25] Despite the fact that the early stages of the precipitates are N-rich, due to limited N availability and N depletion in solid solution, C accumulates at already existing precipitates. A similar behavior is known from V precipitates formed from super-saturated ferrite.[25] At 700°C, the change from N-rich carbonitrides into C-rich happens earlier caused by two effects. On one hand, during the isothermal aging prior to deformation, some precipitates were already formed, which consume part of the N in solid solution. On the other hand, by the faster V diffusion at 700°C, the precipitates grow faster and the C/N ratio changes earlier.

During the growth of the precipitates, V in solid solution is reduced, which was investigated by APT measurements and calculated by MatCalc. The V depletion in solution is also an indication for the increase of the precipitate phase fraction because V is used for precipitate formation. Figure 6e shows the V solid solution depletion in ferrite for 600°C. The simulation data reveals that the V content in solid solution decreases after the deformation and still after 7200 s dwell time. A similar trend is obvious at 700°C which is shown in figure 6f. In this case after 2000 s dwell time a constant amount of V in solid solution is calculated. APT also confirmed this trend. The corresponding data (Table 3) shows that the V content in solid solution decreases during the entire dwell time. The observed discrepancy between simulation and APT measurement in terms of the V content is attributed to the fact that APT measures the V evolution very locally around the precipitates, whereas the simulations are based on a mean-field representation of the precipitation process. The latter can therefore reproduce the V evolution in the close vicinity of the precipitates only qualitatively correct. Quantitatively, we see the expected deviations, which we do not consider as being critical for this reason.

Conclusion

The characterization and investigation of the evolution of strain-induced V precipitates at different temperatures in ferrite by TEM and APT lead to the following conclusions:

APT measurements showed that, at 700°C and 600°C, only V carbonitrides were formed. During the precipitate growth, the C/N ratio changes from N-rich into C-rich composition. At 700°C, this change takes place earlier than at 600°C.

Both characterization methods depict that the incubation time for precipitation at 700°C is lower than at 600°C. Especially, even without a deformation process, the incubation time is smaller at 700°C. In this case, precipitation occurred already prior the deformation. At 600°C, it was not possible to detect such early precipitates.

Experimental data and simulations showed that, at 700°C, the precipitates grow faster and, also, the V depletion in solid solution occurs faster. That happens because the limiting factor for the formation of the precipitates is the diffusivity of V. The higher undercooling and the higher chemical driving force for precipitation at lower temperature seem less important.

References

[1] L. Bäcke, *ISIJ Int.* **2010**, *50*, 239.

[2] T. Gladman, *The Physical Metallurgy of Microalloyed Steels*, The Institute Of Materials, The University Press, London **1997**.

[3] S.F. Medina, *J. Mater. Sci.* **1997**, *32*, 1487.

[4] S. Vervynckt, K. Verbeken, P. Thibaux, Y. Houbaert, *Mater. Sci. Eng., A* **2011**, *528*, 5519.

[5] J. Fernández, S. Illescas, J.M. Guilemany, *Mater. Lett.* **2007**, *61*, 2389.

[6] L. Ma, Z. Liu, S. Jiao, X.-Q. Yuan, D. Wu, *J. Iron Steel Res., Int.* **2008**, *15*, 31.

[7] N. Maruyama, G.D.W. Smith, *Mater. Sci. Eng., A* **2002**, *327*, 34.

[8] R. Stasko, H. Adrian, A. Adrian, *Mater. Charact.* **2006**, *56*, 340.

[9] M.M.A. Bepari, *Mater. Sci. Technol.* **1990**, *6*, 338.

[10] Y. Li, J.A. Wilson, D.N. Crowther, P.S. Mitchell, A.J. Craven, T.N. Baker, *ISIJ Int.* **2004**, *44*, 1093.

[11] Y. Li, J.A. Wilson, A.J. Craven, P.S. Mitchell, D.N. Crowther, T.N. Baker, *Mater. Sci. Technol.* **2007**, *23*, 509.

[12] P. Li, J.A. Todd, *Metall. Trans. A* **1988**, *19A*, 2139.

[13] R. Lagneborg, S. Zajac, *Metall. Mater. Trans. A* **2001**, *32A*, 39.

[14] R. Okamoto, J. Ågren, *Acta Mater.* **2010**, *58*, 4791.

[15] W. Roberts, *Hot Deformation Studies on a V-microalloyed Steel*, Stockholm **1978**.

[16] R.A. Ricks, P.R. Howell, *Acta Metall.* **1983**, *31*, 853.

[17] H.I. Aaronson, M.R. Plichta, G.W. Franti, K.C. Russell, *Metall. Trans. A* **1978**, *9A*, 363.

[18] P. Li, J.A. Todd, *Metall. Trans. A* **1988**, *19A*, 2139.

[19] T.N. Baker, *Mater. Sci. Technol.* **2009**, *25*, 1083.

[20] R.W.K. Honeycombe, *Metal Sci.* **1980**, *29th Hatfi*, 201.

[21] S. Yan, X. Liu, W. Tian, *J. Univ. Sci. Technol. Beijing* **2006**, *13*, 420.

[22] T. Furuhara, T. Maki, *Mater. Sci. and Eng., A* **2001**, *312*, 145.

[23] M.M.A. Bepari, *Metall. Trans. A* **1990**, *21A*, 2839.

[24] R.G. Baker, J. Nutting, *Precipitation Processes in Steels*, London **1959**.

[25] R. Lagneborg, T. Siwecki, S. Zajac, B. Hutchinson, *Scand. J. Metall.* **1999**.

[26] T. Epicier, D. Acevedo, M. Perez, *Philos. Mag.* **2008**, *88*, 31.

[27] G.L. Dunlop, C.-J. Carlsson, G. Frimodig, *Metall. Trans. A* **1978**, *9*, 261.

[28] M.K. Miller, A. Cerezo, M.G. Hetherington, G.D.W. Smith, *Atom Probe Field Ion Microscopy*, Oxford University Press Inc., Oxford **1996**.

[29] L.T. Stephenson, M.P. Moody, P.V. Liddicoat, S.P. Ringer, *Microsc. Microanal.* **2007**, *13*, 448.

[30] J. Svoboda, F.D. Fischer, P. Fratzl, E. Kozeschnik, *Mater. Sci. Eng., A* **2004**, *385*, 166.

[31] E. Kozeschnik, J. Svoboda, P. Fratzl, F.D. Fischer, *Mater. Sci. Eng., A* **2004**, *385*, 157.

[32] E. Kozeschnik, J. Svoboda, F.D. Fischer, *Calphad* **2005**, *28*, 379.

[33] Thermodynamic database for Fe-systems, (mc_fe_v1.030.tdb), Institute of Materials Science and Technology, Vienna University of Technology, Austria

[34] Mobility database for Fe-systems, (mc_fe_v1.001.ddb), Institute of Materials Science and Technology, Vienna University of Technology, Austria

[35] K.A. Padmanabhan, S. Sankaran, *J. Mater. Process. Technol.* **2008**, *207*, 293.

[36] B. Sonderegger, E. Kozeschnik, *Metall. Mater. Trans. A* **2009**, *40*, 499.

[37] B. Sonderegger, E. Kozeschnik, *Scripta Mater.* **2009**, *60*, 635.

[38] A. Pandit, A. Murugaiyan, A.S. Podder, A. Haldar, D. Bhattacharjee, S. Chandra, R.K. Ray, *Scripta Mater.* **2005**, *53*, 1309.

[39] A.J. Craven, M. MacKenzie, A. Cerezo, T. Godfrey, P.H. Clifton, *Mater. Sci. Technol.* **2008**, *24*, 641.

[40] E.V. Pereloma, I.B. Timokhina, K.F. Russell, M.K. Miller, *Scripta Mater.* **2006**, *54*, 471.